

A technique for solving the polygon inclusion problems

Kai Jin, Taikun Zhu, Ruixi Luo

Abstract

We propose a technique called Rotate-and-Kill for solving the polygon inclusion and circumscribing problems. By applying this technique, we obtain $O(n)$ time algorithms for computing (1) the maximum area triangle in a given n -sided convex polygon P , (2) the minimum area triangle enclosing P , (3) the minimum area triangle enclosing P touching edge-to-edge, i.e. the minimum area triangle that is the intersection of three half-planes out of the n half-planes defining P , and (4) the minimum perimeter triangle enclosing P touching edge-to-edge.

Our algorithm for computing the maximum area triangle is simpler than the alternatives given in [Chandran and Mount, IJCGA'92] and [Kallus, arXiv'17]. Our algorithms for computing the minimum area or perimeter triangle enclosing P touching edge-to-edge improve the $O(n \log n)$ or $O(n \log^2 n)$ time algorithms given in [Boyce *et al.*, STOC'82], [Aggarwal *et al.*, Algorithmica'87], [Aggarwal and J. Park., FOCS'88], [Aggarwal *et al.*, DCG'94], and [Schieber, SODA'95].

keywords. Polygon inclusion problem, Convex Polygon, Geometric Optimization.

1 Introduction

The problems of computing extremal figures inside or outside a polygon region introduced in [24, 6, 9, 11] have been studied extensively over the past four decades due to their enormous applications in operation research, shape recognition, and shape approximation [31, 12, 10, 14, 13, 25]. The most typical and fundamental problems in this category include: computing (1) the maximum (area / perimeter) k -gon inside a given convex polygon P ; (2) the minimum (area / perimeter) k -gon enclosing P ; and (3) the minimum (area / perimeter) k -gon that is the intersection of k half-planes out of the half-planes defining P , which is also known as the minimum *all-flush* k -gon enclosing P , where all-flush means that each edge of the k -gon contains an edge of P as a subregion.

Boyce *et al.* [6] showed how to find the maximum k -gon in two phases: In phase 1, choose a vertex v of P and find the maximum k -gon Q in P that is rooted at v (which means that it admits v as one of its corner). Assume v_1, \dots, v_n are the n vertices of P in clockwise order, and assume $Q = (v_{i_1} = v, v_{i_2}, \dots, v_{i_k})$. Let $Q_{v'} = (v_{j_1} = v', v_{j_2}, \dots, v_{j_k})$ denote the maximum k -gon rooted at v' for vertex v' between v_{i_1} and v_{i_2} . It is proved in [6] that $Q_{v'}$ *interleaves* Q_v , namely, v_{j_x} lies between v_{i_x} and $v_{i_{x+1}}$ for every x . In Phase 2, based on the interleaving property and by a binary search, compute $Q_{v'}$ for each v' between v_{i_1} and v_{i_2} ; the largest among these rooted k -gons is the maximum k -gon in P . This method also works in computing the minimum all-flush k -gon [6].

The two phases were solved in $O(kn \log n)$ and $O(n \log^2 n)$ time respectively in [6], and were later solved in $O(kn)$ and $O(n \log n)$ time respectively by Aggarwal *et al.* [1], as applications of their *Matrix-Searching technique*. Moreover, Aggarwal *et al.* [3] solved phase 1 in $O(n\sqrt{k \log n})$ time using their technique for computing the *minimum weight k -link path*, and this bound was further improved by Schieber [23] who optimized the k -link path technique. These bounds on phase 1 are

better than $O(kn)$ when $k = \Omega(\log n)$, but the $O(kn)$ time algorithm is optimal for $k = O(1)$. To our best, there is no improvement on phase 2 over the $O(n \log n)$ bound even for $k = 3$.

Other approaches were proposed for solving the maximum area k -gon problem, and the problem was solved in $O(n)$ time for $k \leq 4$. Observe that each diagonal of the maximum area 4-gon connects an antipodal pair (pair v_i, v_j is an *antipodal pair* if it admits parallel lines of support). It is not difficult to compute the maximum area 4-gon in $O(n)$ time after preprocessing the antipodal pairs (which takes $O(n)$ time [24, 26]). Chandran and Mount [8] gave the first (correct) linear time algorithm (*Alg-CM*) for finding the maximum area triangle, which actually computes the maximum triangle in P and the minimum triangle enclosing P simultaneously. Kallus [16] recently posted another linear time algorithm (*Alg-K*) for the maximum triangle problem. Both Alg-CM and Alg-K are clever applications of the well-known *Rotating-Caliper technique* [26]. However, neither of them extend to the perimeter case, nor to the case of finding the minimum area all-flush triangle. As a side note, Alg-K turns out to be essentially equivalent to Alg-CM; we discuss this in section 7.

Before Chandran and Mount [8], Dobkin and Snyder [11] gave an algorithm (*Alg-DS*) for computing the maximum area triangle, which has been found incorrect by Hoog *et al.* [28].

O'Rourke *et al.* [21] gave the first linear time algorithm for computing the minimum area triangle enclosing P , which improves over an $O(n \log^2 n)$ time algorithm of [18]. Alg-CM is an extension of this linear algorithm. The minimum perimeter enclosing triangle is also solved in $O(n)$ time [5]. For general k , [2] computed the minimum area k -gon in $O(kn + n \log n)$ time, whereas [20] computed the minimum perimeter k -gon in much larger polynomial time.

In this paper, we propose a unified technique (which we call Rotate-and-Kill) for solving all the three problems (1) – (3) for the case $k = 3$. As its prototype applications, we design linear time algorithms for finding the maximum area triangle in P , the minimum area triangle enclosing P , the minimum area all-flush triangle, and the minimum perimeter all-flush triangle. We remark that the previously best known algorithms for finding the minimum area / perimeter all-flush triangle take nearly linear time [6, 1, 2, 3, 23], that is, $O(n \log n)$ or $O(n \log^2 n)$ time.

Subsection 1.2 presents a technique overview of Rotate-and-Kill, from which we can see this technique is different from the Rotating-Caliper technique (see discussions in subsection 1.2.3). One major difference is that the Rotating-Caliper uses only one parameter (e.g. some angle θ), whereas the Rotate-and-Kill uses two (which are not functions of some hidden θ).

In fact, the Rotate-and-Kill technique is powerful in solving other polygon inclusion / circumscribing problems, but the running time is sometimes more than $O(n)$. The reason is as follows. The inclusion / circumscribing problems usually admit the property that the set of locally optimal solutions are pairwise interleaving [6]. Once this property is admitted and $k = 3$, we show that an iteration process (also referred to as *Rotate-and-Kill*) can be applied for searching all the locally optimal solutions, and thus find the optimum solution. The mentioned iteration process will be conducted by a specialized function Kill (which we call the *killing function*), and the running time of the iteration process is $O(n \cdot t_{\text{Kill}})$, where t_{Kill} denotes the expected running time of the function Kill. It is usually not too difficult to give a killing function that runs in $O(\log n)$ time. Toward a linear time algorithm, however, we need a killing function with $t_{\text{Kill}} = O(1)$, which becomes challenging.

There seems to be no unified way for designing such a constant time killing function.

Other related work. Melissaratos and Souvaine [19] computed the maximum area triangle in a simple polygon. Zhou and Suri [31] and Vivien and Wicker [30] computed extremal polytopes in three dimensional space. Brass and Na [7] computes the maximum intersection of k half-planes

out n half-planes in arbitrary position. Computing extremal equilateral triangles, squares, rectangles, parallelograms, disks, and ellipses in or outside a given region received attention from many researchers; see references in [15].

The extremal triangle problems have found applications in collision detection [6, 31], shape approximation and convexity measuring, [31, 12, 10], and shape classification [14, 13]. In particular, computing the maximum area triangle serves as a subroutine in [12, 14, 13].

These problems have also found applications in operation design (VLSI design / robot motion plan), Earth science [31], and bioinformatics [25].

It is shown in [15] that the simplest case of the Heilbronn triangle problem reduces to finding the maximum area triangle and the maximum area parallelogram inside a polygon P .

1.1 Preliminary: 3-stable, G-3-stable, and F-3-stable triangles

Let v_1, \dots, v_n be a *clockwise* enumeration of the *vertices* of P . Assume that any three vertices are not collinear. Denote by e_1, \dots, e_n the n *edges* of P , such that e_i is the line segment connecting v_i and v_{i+1} (where $v_{n+1} = v_1$). Throughout, regard P as a polygon region which contains its interior and boundary. Denote by ∂P the boundary of P . Denote by p_i the (closed) half-plane delimited by the extended line ℓ_i of e_i and contains P . Denote by $\text{area}(\phi)$ the area of any region ϕ . For distinct points X and Y , denote by \overleftrightarrow{XY} and \overrightarrow{XY} the *line* connecting X and Y and the *directed line segment* from X to Y , respectively. Given points X, X' on the boundary of P , denote by $[X \circ X']$ the boundary portion of P that starts from X and clockwise to X' which contains its two endpoints X and X' ($[X \circ X] = X$).

Consider any triangle $T = \triangle X_1 X_2 X_3$ with X_1, X_2, X_3 lying in ∂P and lying in clockwise order. For $i \in \{1, 2, 3\}$, corner X_i is *stable* in T if X_i has the largest distance to $\overrightarrow{X_{i+1} X_{i-1}}$ among all points in P that lie on the right of $\overrightarrow{X_{i+1} X_{i-1}}$ (subscripts taken modulo 3). Throughout, when we write $\triangle X_1 X_2 X_3$, we assume that X_1, X_2, X_3 *lie in clockwise order*.

3-stable. Consider three vertices v_i, v_j, v_k of P in clockwise order, which forms a triangle $T = \triangle v_i v_j v_k$. This triangle is *3-stable* if all its three corners v_i, v_j, v_k are stable in T .

G-3-stable. Consider any triangle $T = \triangle X_1 X_2 X_3$ with X_1, X_2, X_3 lying in ∂P and lying in clockwise order. It is *G-3-stable* if all its three corners X_1, X_2, X_3 are stable in T .

All-flush. For distinct edges e_i, e_j, e_k that are in clockwise order, the intersecting region $p_i \cap p_j \cap p_k$ is denoted by $\triangle e_i e_j e_k$ and is called an *all-flush triangle*. Throughout, when we write $\triangle e_i e_j e_k$, we assume that e_i, e_j, e_k *are distinct and lie in clockwise order*.

F-3-stable. For triangle $T = \triangle e_i e_j e_k$ with a finite area, e_i is *stable* in T if no all-flush triangle $\triangle e_{i'} e_j e_k$ has a smaller area than T ; e_j is *stable* in T if no all-flush triangle $\triangle e_i e_{j'} e_k$ has a smaller area than T ; and e_k is *stable* in T if no all-flush triangle $\triangle e_i e_j e_{k'}$ has a smaller area than T . Moreover, T is *F-3-stable* if e_i, e_j, e_k are all stable in T .

Definition 1 ([6]). Triangles $\triangle A_1 A_2 A_3$ and $\triangle B_1 B_2 B_3$ with all corners lying in ∂P are *interleaving* if we can permute $A_1, A_2, A_3, B_1, B_2, B_3$ to Z_1, \dots, Z_6 so that Z_1, \dots, Z_6 lie in clockwise order (in a non-strict manner; so neighbors may be identical), in which $\{Z_1, Z_3, Z_5\} = \{A_1, A_2, A_3\}$ and $\{Z_2, Z_4, Z_6\} = \{B_1, B_2, B_3\}$. Two all-flush triangles $\triangle e_r e_s e_t$ and $\triangle e_i e_j e_k$ are *interleaving* if we can permute r, s, t, i, j, k to z_1, \dots, z_6 so that e_{z_1}, \dots, e_{z_6} lie in clockwise order (in a non-strict manner; so neighbors may be identical), in which $\{z_1, z_3, z_5\} = \{r, s, t\}$ and $\{z_2, z_4, z_6\} = \{i, j, k\}$.

Lemma 2. 1. [28] The 3-stable triangles are pairwise interleaving.

2. The F-3-stable triangles are pairwise interleaving.

3. The G-3-stable triangles are pairwise interleaving.

Corollary 3. The number of 3-stable or F-3-stable triangles is $O(n)$.

Easy proofs of Lemma 2 and Corollary 3 can be found in appendix A.

1.2 Technique overview

It is easy to compute one 3-stable triangle in $O(n)$ time; we show how to do this in section 4¹. Denote the computed 3-stable triangle by $\Delta v_r v_s v_t$ and assume r, s, t are given in the following.

Due to the interleaving property of 3-stable triangles (Lemma 2), these triangles can be listed as $\Delta v_{a_1} v_{b_1} v_{c_1}, \dots, \Delta v_{a_m} v_{b_m} v_{c_m}$, where $v_{a_1}, \dots, v_{a_m}, v_{b_1}, \dots, v_{b_m}, v_{c_1}, \dots, v_{c_m}$ lie in clockwise order (neighbors may be identical). Assume $(a_1, b_1, c_1) = (r, s, t)$ without loss of generality. Starting from the 3-stable triangle $\Delta v_r v_s v_t$, we search all the 3-stable triangles one by one by iterations. During this iteration process, maintain variables a, b, c , which are initially assigned to r, s, t respectively. At each iteration, select one of a, b, c and increase it (increasing x means that $x \leftarrow x \bmod n + 1$). By carefully selecting the variable to increase at each iteration, which will be elaborated right below, we make sure that $\Delta v_a v_b v_c$ arrives at each 3-stable triangle $\Delta v_{a_1} v_{b_1} v_{c_1}, \dots, \Delta v_{a_m} v_{b_m} v_{c_m}$ one after another, and that it takes $O(a_i - a_{i-1} + b_i - b_{i-1} + c_i - c_{i-1})$ iterations to arrive $\Delta v_{a_i} v_{b_i} v_{c_i}$ from $\Delta v_{a_{i-1}} v_{b_{i-1}} v_{c_{i-1}}$ for each $i > 1$. Applying the fact that $v_{a_1}, \dots, v_{a_m}, v_{b_1}, \dots, v_{b_m}, v_{c_1}, \dots, v_{c_m}$ lie in clockwise order, we see the searching process takes only $O(n)$ iterations. Furthermore, it takes $O(n)$ time if the selection at each iteration took amortized $O(1)$ time. By finding all the 3-stable triangles, we immediately obtain the maximum area triangle in P .

How to select among a, b, c to increase is essential to the algorithm. We must make decision rapidly yet make sure that no 3-stable triangle is missing. This is difficult. Two previous algorithms, Alg-DS (FOCS'79) and an algorithm given in [6] (STOC'82), were based on the above approach and they presented two simple methods for selection. Yet their selection methods would miss 3-stable triangles and even worse, sometimes they miss the largest 3-stable triangle, as shown by [28].

We come up with a different selection method which is sketched in the following. Above all, we state that a vertex pair (v_j, v_k) is *dead* if there is no v_i such that $\Delta v_i v_j v_k$ is 3-stable.

Assume $b \in \{s, \dots, t\}$ and $c \in \{t, \dots, r\}$. The interleaving property of 3-stable triangles implies that (I) $(v_b, v_{c+1}), \dots, (v_b, v_r)$ are dead **or** (II) $(v_{b+1}, v_c), \dots, (v_t, v_c)$ are dead. (Otherwise, there exist two 3-stable triangles that are not interleaving; see an easy proof below Observation 4.)

Suppose for the time being there is a function $\text{Kill}(b, c)$ defined for each (b, c) such that $b \in \{s, \dots, t\}$ and $c \in \{t, \dots, r\}$, which returns either 'b' or 'c' and which owns the following properties: ① it returns 'b' only if (I) hold and returns 'c' only if (II) hold. ② it costs amortized $O(1)$ time to compute.

By utilizing this function, we can select among a, b, c to increase at each iteration as follows. If $\text{Kill}(b, c) = \text{'b'}$, select b to increase; if $\text{Kill}(b, c) = \text{'c'}$, select c to increase. In the subsequent iterations, select a to increase until v_a has the largest distance to $\overleftrightarrow{v_b v_c}$. The running time is clearly $O(n)$ due to ②, and the correctness easily follows from property ①, as we will analyze in section 2.

¹Alg-DS fails to find one 3-stable triangle and so we introduce the algorithm in section 4. This algorithm in section 4 is not the same as and does not originate from Alg-DS (see appendix A.2).

The process for searching the 3-stable triangles as above is referred to as a *Rotate-and-Kill process*. Obviously, its kernel lies in the function Kill, which we call the *killing function*.

Design of killing function Kill. There exists an surprisingly simple design of $\text{Kill}(b, c)$. Assume the line parallel to e_c at v_b and the line parallel to e_b at v_c intersect at $I_{b,c}$. Make a parallel line $\ell_{b,c}$ of $v_b v_c$ at $I_{b,c}$, as shown in Figure 1 (1). Define $\text{Kill}(b, c) = \text{'b'}$ if v_a is below $\ell_{b,c}$ and $\text{Kill}(b, c) = \text{'c'}$ otherwise, where v_a denotes the vertex of P on the right of $\overrightarrow{v_b v_c}$ furthest to $\overrightarrow{v_b v_c}$. The proof that this definition of $\text{Kill}(b, c)$ does satisfy ① and ② will be presented in subsection 2.1.

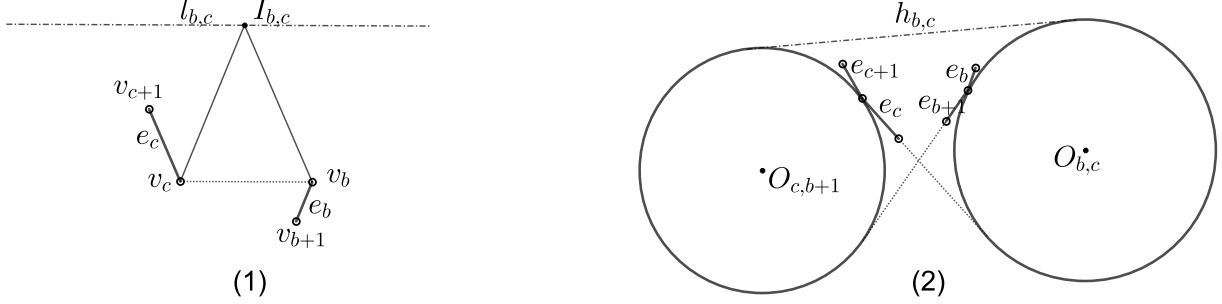


Figure 1: Illustration of the killing functions.

1.2.1 Minimum perimeter all-flush triangle (technique overview)

In the following, we sketch how to apply the Rotate-and-Kill process to solve a polygon circumscribing problem, that is, finding the all-flush triangle with the minimum perimeter. The details are given in section 6.

We say e_i is *stable* in $\triangle e_i e_j e_k$ if $\text{perimeter}(\triangle e_i e_j e_k)$ cannot be reduced by changing e_i to other edges. We state that $\triangle e_i e_j e_k$ is *3-stable*, if e_i, e_j, e_k are all stable in $\triangle e_i e_j e_k$. Pair (e_i, e_j) is *dead* if there is no e_k such that $\triangle e_i e_j e_k$ is 3-stable. A triangle refers to an all-flush triangle in the following. We first compute a 3-stable triangle $\triangle e_r e_s e_t$. This can be done using the ideas given in section 4.

All the 3-stable triangles are pairwise interleaving (see Lemma 40, which is similar to Lemma 2). As a corollary, for $b \in \{s, \dots, t\}$ and $c \in \{t, \dots, r\}$, at least one of the following holds: (I) $(e_b, e_{c+1}), \dots, (e_b, e_r)$ are dead **or** (II) $(e_{b+1}, e_c), \dots, (e_t, e_c)$ are dead.

To apply Rotate-and-Kill, the challenging part lies in designing a killing function $\text{Kill}(b, c)$ that satisfies ① and ②. Unfortunately, we do not know how to design such a function. Instead, we provide a function $\text{Kill}_p(b, c)$ satisfying some weaker properties to be elaborated below. This function is insufficient for finding all 3-stable triangles, yet sufficient for finding the minimum perimeter (all-flush) triangle.

Design of killing function Kill_p . See Figure 1 (2). Make a circle $O_{c,b+1}$ tangent to $\ell_c, \ell_{c+1}, \ell_{b+1}$ on the right of e_{b+1} and left of e_c, e_{c+1} , and a circle $O_{b,c}$ tangent to $\ell_b, \ell_{b+1}, \ell_c$ on the right of e_c and left of e_b, e_{b+1} . Moreover, find their common tangent $h_{b,c}$ (that intersects the ray $\overrightarrow{v_c v_{c+1}}$) as shown in the picture. We define $\text{Kill}_p(b, c) = \text{'b'}$ if e_a is (entirely) below $h_{b,c}$, and $\text{Kill}_p(b, c) = \text{'c'}$ otherwise, where a denotes the index in $\{a \mid e_a \prec e_b, e_c \prec e_a\}$ that minimizes $\text{perimeter}(\triangle e_a e_b e_c)$.

We say (e_i, e_j) is *DEAD* if there is no e_k such that $\triangle e_i e_j e_k$ is the minimum perimeter triangle (among all all-flush triangles). Note that “dead” implies “DEAD” but the reverse is not true.

We prove (in Lemma 46) that if $\text{Kill}_p(b, c)$ returns ‘c’, (II) holds; and if $\text{Kill}_p(b, c)$ returns ‘b’, $(e_b, e_{c+1}), \dots, (e_b, e_r)$ are DEAD (this is weaker than (I)). Then, during the Rotate-and-Kill process, the pair (e_b, e_c) will meet all pairs that are not DEAD, which implies that the algorithm finds the minimum perimeter (all-flush) triangle. However, it is not guaranteed that all the pairs that are not dead will be meet, so the algorithm possibly misses some 3-stable triangles.

1.2.2 More applications of Rotate-and-Kill.

In section 3, we compute the F-3-stable triangles in linear time by a Rotate-and-Kill process, and thus find the minimum area all-flush triangle. In section 5, we compute the G-3-stable triangles in linear time by a Rotate-and-Kill process, and thus find the minimum area triangle enclosing P (see an explanation at the end of section 5).

As we will see, the killing functions in these problems are also simple. Nevertheless, it requires painstaking effort and creativity to derive the killing functions.

It remains to be investigated how to design killing functions for other related problems.

1.2.3 Rotate-and-Kill technique v.s. Rotating-Caliper technique

An application of Toussaint’s Rotating-Caliper (RC) [26] technique usually adopts the following framework: choose a variable θ (e.g., a direction over a discrete space), define some objects (e.g. A_θ, B_θ , and C_θ) as functions of θ , and prove that (i) each of $A_\theta, B_\theta, C_\theta$ has a monotonicity property with respect to θ , and then design an algorithm for updating $A_\theta, B_\theta, C_\theta$ after each change of θ . Updating $A_\theta, B_\theta, C_\theta$ should be taken care in amortized $O(1)$ time. Sometimes, however, this is not that easy, even if condition (i) holds. For example, Klee and Laskowski [18] spent $O(\log^2 n)$ time for updating B_θ or C_θ in finding the minimum area enclosing triangle based on RC. By using a nontrivial speedup technique, O’Rourke *et al.* [21] further showed that for the minimum area enclosing triangle problem, B_θ, C_θ effect each other and that (B_θ, C_θ) as a unity can be updated together in amortized $O(1)$ time. Nevertheless, O’Rourke *et al.* did not break the framework of RC.

In Rotate-and-Kill, a pair of variables (b, c) are maintained, which as a unity serves as a 2-dimensional variable. Unlike RC, b, c here are not functions of another variable θ . On the contrary, we may need to use a function θ of variable (b, c) ; see the description of Kill_F in subsection 3.1 for an example. As such, the flow of Rotate-and-Kill is different from RC.

1.2.4 Comparison to Alg-K and Alg-CM

We compare our algorithm (*Alg-A*) for finding the maximum area triangle with its two alternatives Alg-CM and Alg-K in section 7. We think Alg-A is better in almost every aspect. This is because it is essentially simpler. Among other merits, Alg-A is much **faster**, because it has a smaller constant behind the asymptotic complexity $O(n)$ than the others:

1. **Less candidates.** Alg-A computes at most n candidate triangles (proof is trivial and omitted) whereas Alg-CM computes at most $5n$ triangles (proved in [8]) and so as Alg-K. (by experiment, Alg-CM and Alg-K have to compute roughly $4.66n$ candidate triangles.)
2. **Simpler primitives.** Alg-A has simpler primitives because (1) the candidate triangles considered in it have all corners lying on P ’s vertices and (2) searching the next candidate from a given one is much easier – the code length for this is **1:7** in Alg-A and in Alg-CM.

More importantly, Alg-A is **more stable** and the brief reason is as follows. Alg-A has no accumulation of inaccuracy; it does not compute but reads the constant coordinates of the corners (which are on vertices) every iteration. See a detailed explanation in section 7.

We implement all algorithms by C++ programs and test them on random convex polygons [4]. Our experiment result shows that Alg-A is much faster and more stable than the others; see section 7.1. In particular, Alg-CM suffers from float-issue as it accumulates inaccuracy. If Alg-CM is implemented based on the original paper, it encounters problems when n arrives at 300. With optimizations such as avoiding trigonometric functions, it can merely handle $n = 10000$. The implementation of Alg-A easily handles n as large as 10000000.

2 Find all 3-stable triangles

In this section, assuming that we are given indices r, s, t so that $\triangle v_r v_s v_t$ is 3-stable, we show how to compute all the 3-stable triangles by a Rotate-and-Kill process.

Recall that a vertex pair (v_j, v_k) is *dead* if there is no 3-stable triangle $\triangle v_i v_j v_k$.

We start with an observation which is an immediate corollary of Lemma 2 part 1.

Observation 4. *Given (b, c) where $b \in \{s, \dots, t\}$, $c \in \{t, \dots, r\}$, at least one of the following holds.*

- (I) $(v_b, v_{c+1}), \dots, (v_b, v_r)$ are dead. (II) $(v_{b+1}, v_c), \dots, (v_t, v_c)$ are dead.

Proof. Suppose both (I) and (II) fail. This implies $(v_b, v_{c'})$ and $(v_{b'}, v_c)$ which are not dead, where $c' \in \{c+1, \dots, r\}$ and $b' \in \{b+1, \dots, t\}$, which implies 3-stable triangles $\triangle v_{a_1} v_b v_{c'}$ and $\triangle v_{a_2} v_{b'} v_c$ that are not interleaving (see Figure 2), contradicting Lemma 2 part 1. \square

Assume for the time being that we have a function (or oracle) Kill, which inputs parameters (b, c) , where $b \in \{s, \dots, t\}$ and $c \in \{t, \dots, r\}$, and which has the following two properties:

- ① It equals 'b' or 'c', and it equals 'b' only if (I) holds and equals 'c' only if (II) holds.
- ② It can be computed in amortized $O(1)$ time.

The Rotate-and-Kill process (sketch). Initially, set $(b, c) = (s, t)$. In each iteration, output all 3-stable triangles $\triangle XYZ$ with $Y = v_b$ and $Z = v_c$ (to be elaborated right below), and call Kill(b, c). If this function returns 'b', set $b \leftarrow b + 1$. If it returns 'c', set $c \leftarrow c + 1$. If $(b, c) \neq (t, r)$, go to the next iteration; otherwise, terminate the process. See Figure 3 for an illustration. (In this description of Rotate-and-Kill, the aforementioned variable a is hidden. But we will see it later.)

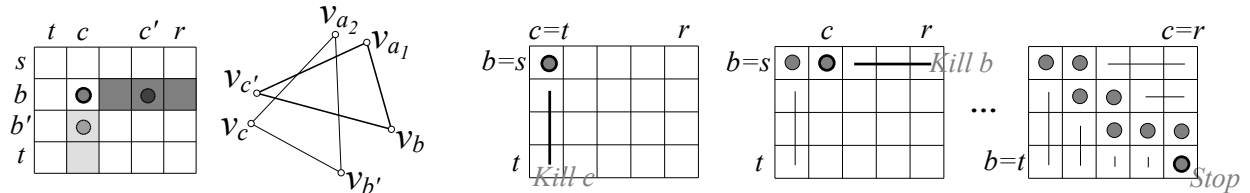


Figure 2: Proof of Observation 4.

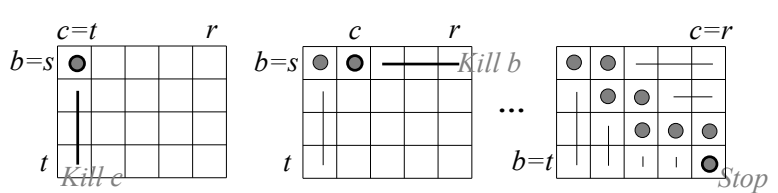


Figure 3: Illustration of the Rotate-and-Kill process.

Correctness. Since $\triangle v_s v_t v_r$ is 3-stable, (v_t, v_r) is not dead. Therefore, Kill(b, c) cannot return 'b' when $b = t$ and $c \neq r$, and cannot return 'c' when $c = r$ and $b \neq t$, due to property

①. This means (b, c) eventually reaches (t, r) . So the process terminates. Moreover, let $U = \{(v_j, v_k) \mid j \in \{s, \dots, t\}, k \in \{t, \dots, r\}\}$. As another corollary of property ①, for each pair (v_j, v_k) in U that is not dead, it holds that $(b, c) = (j, k)$ in some iteration. Consider an arbitrary 3-stable triangle $\triangle v_i v_j v_k$. By Lemma 2, it interleaves $\triangle v_r v_s v_t$. Therefore, without loss of generality we can assume $(v_j, v_k) \in U$. Since $\triangle v_i v_j v_k$ is 3-stable, (v_j, v_k) is not dead. In the iteration where $(b, c) = (j, k)$, the 3-stable triangle $\triangle v_i v_j v_k$ will be output.

It remains to be shown how do we compute 3-stable triangles $\triangle XYZ$ with $Y = v_b$ and $Z = v_c$ (for those (b, c) that will be visited by the Rotate-and-Kill process). This reduces to finding the vertex with the largest distance to $\overrightarrow{v_b v_c}$ on the right of $\overrightarrow{v_b v_c}$, which costs amortized $O(1)$ time since the direction of $\overrightarrow{v_b v_c}$ monotonously rotates in clockwise throughout the Rotate-and-Kill process.

Further according to property ②, the Rotate-and-Kill process runs in $O(n)$ time.

2.1 Description of the Kill function

The core of the above process lies in function Kill, which is yet to be described.

Above all, it is easy to find a function Kill that satisfies ①. Here are two candidates:

Candidate 1: determine whether (I) holds, and returns ‘b’ if (I) holds and ‘c’ otherwise.

Candidate 2: determine whether (II) holds, and returns ‘c’ if (II) holds and ‘b’ otherwise.

Because (I) or (II) holds, ① is satisfied by both candidates. Unfortunately, we do not know how to determine (I) (or (II)) efficiently in amortized $O(1)$ time. (In fact, this can be done in $O(\log n)$ time using a binary search, yet we cannot afford $O(\log n)$ time.)

To introduce our killing function Kill that satisfies both ① and ②, we need some notations.

Regard each edge e_i of P as *directed*. The direction of e_i is from v_i to v_{i+1} ($v_{n+1} = v_1$).

Definition 5. Assume v_j, v_k are distinct vertices of P . See Figure 4. Let r_1 and r_2 respectively denote the ray originating from v_j with the same direction as e_{k-1} and e_k . Let r'_1 and r'_2 respectively denote the ray originating from v_k with the opposite direction to e_{j-1} and e_j . The intersection of the wedge defined by r_1, r_2 and the wedge defined by r'_1, r'_2 defines a region, denoted by $\mathcal{R}_{j,k}$.

Denote by $H_{j,k}, I_{j,k}, J_{j,k}, K_{j,k}$ the intersecting points between r_1, r'_1 , between r_2, r'_2 , between r_1, r'_2 , and between r_2, r'_1 , respectively. When two rays do not intersect, their intersecting point is defined as ∞ . Therefore, $H_{j,k}, I_{j,k}, J_{j,k}, K_{j,k}$ are always defined for $v_j \neq v_k$.

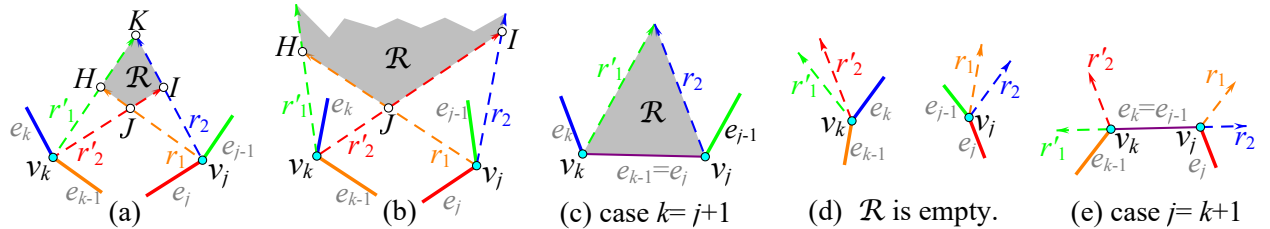


Figure 4: Illustration of Definition 5. Subscripts of \mathcal{R}, H, I, J, K are omitted for conciseness.

Our function Kill is as follows. Let v_a be the vertex on the right of $\overrightarrow{v_b v_c}$ furthest to $\overrightarrow{v_b v_c}$.

$$\text{Kill}(b, c) = \text{'b' if } v_a \leq I_{b,c} \text{ in the distance to } \overrightarrow{v_b v_c}, \text{ and Kill}(b, c) = \text{'c' otherwise.} \quad (1)$$

We present a pseudo code of the entire Rotate-and-Kill process in Algorithm 1.

Note 1. Since $I_{b,c}$ is undefined for $(b,c) = (t,t)$, the value of $\text{Kill}(t,t)$ is unspecified. For convenience, we can define $\text{Kill}(t,t) = 'c'$. However, this is unnecessary, because we can prove that $(b,c) \neq (t,t)$ throughout the process. Suppose in some iteration $(b,c) = (t,t)$. Then, in the previous iteration, $(b,c) = (t-1,t)$ and $\text{Kill}(b,c) = 'b'$. For $(b,c) = (t-1,t)$, however, we have $c = b+1$ and so $I_{b,c} = v_b$, hence $v_a > I_{b,c}$ in the distance to $\overrightarrow{v_b v_c}$, which means $\text{Kill}(b,c) = 'c'$. Contradiction.

2.2 Analysis of the Kill function

Function Kill defined in (1) clearly satisfies ②. Lemma 6 states that it also satisfies ①.

Lemma 6. Assume $b \in \{s, \dots, t\}$, $c \in \{t, \dots, r\}$, $(b,c) \neq (t,t)$, and v_a is defined as in (1).

1. If $v_a \leq I_{b,c}$ in the distance to $\overrightarrow{v_b v_c}$, then $(v_b, v_{c+1}), \dots, (v_b, v_r)$ are dead.
2. If $v_a > I_{b,c}$ in the distance to $\overrightarrow{v_b v_c}$, then $(v_{b+1}, v_c), \dots, (v_t, v_c)$ are dead.

We first give some observations and then use them to prove Lemma 6.

Definition 7. For edges $e_i \neq e_j$, we state that e_i is *chasing* e_j , denoted by $e_i \prec e_j$, if ℓ_i intersects ℓ_j and the intersecting point lies between e_i and e_j clockwise. For example, in Figure 4 (b), e_{j-1} is chasing e_j and e_{k-1} but not e_k , whereas e_k is chasing e_{j-1} but not e_j .

Observation 8. 1. Fix v_j and v_k ($j \neq k$). If there is a vertex v_i on the right of $\overrightarrow{v_j v_k}$ such that v_j, v_k are stable in $\triangle v_i v_j v_k$, then $v_i \in \mathcal{R}_{j,k}$. (Throughout, assume $\mathcal{R}_{j,k}$ contains its boundary.)

2. A pair (v_j, v_k) is dead if $\mathcal{R}_{j,k}$ does not intersect P .
3. A pair (v_j, v_k) is dead if $e_k \prec e_j$.
4. A pair (v_j, v_k) is dead if there exists a point A in P which lies on the right of $\overrightarrow{v_j v_k}$ and is further than $K_{j,k}$ in the distance to $\overrightarrow{v_j v_k}$. (If $K_{j,k} = \infty$, there could be no such A .)

Proof. Recall the four rays r_1, r_2, r'_1, r'_2 used in Definition 5. See Figure 4.

1. Since v_j needs to be stable, v_i must lie in the wedge bounded by r'_1 and r'_2 . Since v_k needs to be stable, v_i must lie in the wedge bounded by r_1 and r_2 . Together, v_i must lie in $\mathcal{R}_{j,k}$.

2. Assume $\mathcal{R}_{j,k}$ does not intersect P . Then, due to part 1 of this observation, there is no vertex v_i on the right of $\overrightarrow{v_j v_k}$ such that v_j, v_k are stable in $\triangle v_i v_j v_k$ (otherwise $\mathcal{R}_{j,k}$ contains v_i and hence intersects P). The nonexistence of such v_i implies that (v_j, v_k) is dead by the definition of dead.

```

1   $(a, b, c) \leftarrow (r, s, t);$       //  $\triangle v_r v_s v_t$  is 3-stable.
2  repeat
3    while  $v_{a+1} > v_a$  in the distance to  $\overrightarrow{v_b v_c}$  do  $a \leftarrow a + 1$  ;
4    Output  $\triangle v_a v_b v_c$  if it is 3-stable and output  $\triangle v_{a+1} v_b v_c$  if it is 3-stable ;
5    if  $v_a \leq I_{b,c}$  in the distance to  $\overrightarrow{v_b v_c}$  then  $b \leftarrow b + 1$  ;
6    else  $c \leftarrow c + 1$  ;
7  until  $(b, c) = (t, r);$ 

```

Algorithm 1: The Rotate-and-Kill process for finding all 3-stable triangles.

3. Assume $e_k \prec e_j$. We first argue that $\mathcal{R}_{j,k}$ does not intersect P . This holds obviously when $j = k + 1$; see Figure 4 (e). We assume $j \neq k + 1$ in the following.

First, observe that (i) $\mathcal{R}_{j,k}$ does not contain v_k . This is because the wedge bounded by r_1, r_2 cannot contain v_k . (This wedge contains v_k only when $k = j + 1$. Yet $e_k \prec e_j$ implies that $k \neq j + 1$.)

Second, observe that (ii) $\mathcal{R}_{j,k}$ does not intersect $P \setminus \{v_k\}$. Since $e_k \prec e_j$ and $j \neq k + 1$, rays r'_1, r'_2 are on the left of e_k (except for the originate v_k of r'_1, r'_2). So, the wedge bounded by r'_1, r'_2 is on the left of e_k (except for v_k). Therefore, this wedge, including $\mathcal{R}_{j,k}$, does not intersect $P \setminus \{v_k\}$.

Together, $\mathcal{R}_{j,k}$ does not intersect P . Hence (v_j, v_k) is dead according to part 2.

4. Suppose to the opposite that (v_j, v_k) is not dead but $\triangle v_i v_j v_k$ is 3-stable for some vertex v_i . By part 1 of this observation, v_i is contained in $\mathcal{R}_{j,k}$. By the definition of $\mathcal{R}_{j,k}$ (see Figure 4 (a)), this means v_i is not further than $K_{j,k}$ in the distance to $\overrightarrow{v_j v_k}$. However, by the assumption, we know A is further than $K_{j,k}$ in the distance to $\overrightarrow{v_j v_k}$. Therefore, A is further than v_i in the distance to $\overrightarrow{v_j v_k}$. This means that v_i is not stable in $\triangle v_i v_j v_k$. Contradictory. \square

Proof of Lemma 6. 1. If e_b is not chasing e_c , we get $e_{c+1} \prec e_b, \dots, e_r \prec e_b$, which implies that $(v_b, v_{c+1}), \dots, (v_b, v_r)$ are dead (by Observation 8 part 3). Therefore, we only need to consider the case that $e_b \prec e_c$, as shown in Figure 5 (a). Assume $v_a \leq I_{b,c}$ in the distance to $\overrightarrow{v_b v_c}$.

Let v_{c^*} denote the last vertex in the sequence v_c, v_{c+1}, \dots, v_r so that $e_b \prec e_{c^*}$ or $e_b \parallel e_{c^*}$. We know that $e_{c^*+1} \prec e_b, \dots, e_r \prec e_b$, which implies that $(v_b, v_{c^*+1}), \dots, (v_b, v_r)$ are dead (by Observation 8 part 3). It remains to prove that $(v_b, v_{c+1}), \dots, (v_b, v_{c^*})$ are also dead.

Let l denote the unique line at $I_{b,c}$ that is parallel to $\overrightarrow{v_b v_c}$. We state two facts about l .

(i) Polygon P lies in the (closed) half-plane delimited by l and containing v_b, v_c .

(ii) $\mathcal{R}_{b,c+1}, \dots, \mathcal{R}_{b,c^*}$ lie in the (open) half-plane delimited by l and not containing v_b, v_c .

Combining the two facts, no one in $\mathcal{R}_{b,c+1}, \dots, \mathcal{R}_{b,c^*}$ intersects P , which implies that $(v_b, v_{c+1}), \dots, (v_b, v_{c^*})$ are dead (by Observation 8 part 2). We prove facts (i) and (ii) in the following.

Proof of (i). By assumption, $v_a \leq I_{b,c}$ in the distance to $\overrightarrow{v_b v_c}$. However, v_a has the largest distance among all vertices of P that lie on the right of $\overrightarrow{v_b v_c}$. Together, we get fact (i).

Proof of (ii). For convenience, we shall introduce another region $\mathcal{Q}_{j,k}$ for each pair (v_j, v_k) such that $j \neq k, j + 1 \neq k$, and $e_j \prec e_k$. Recall $H_{j,k}, I_{j,k}, J_{j,k}$ in Definition 5. See Figure 4 (a) and (b). Region $\mathcal{Q}_{j,k}$ is defined as the wedge bounded by $\overrightarrow{J_{j,k} I_{j,k}}, \overrightarrow{J_{j,k} H_{j,k}}$ and containing $\mathcal{R}_{j,k}$.

As illustrated by Figure 5 (b), we have $\mathcal{Q}_{b,c} \supseteq \mathcal{Q}_{b,c+1}$. Similarly, we have $\mathcal{Q}_{b,c+1} \supseteq \mathcal{Q}_{b,c+2} \supseteq \dots \supseteq \mathcal{Q}_{b,c^*}$, which implies that $\mathcal{R}_{b,c+1}, \dots, \mathcal{R}_{b,c^*}$ lie in $\mathcal{Q}_{b,c+1}$. So to prove (ii) reduces to show $\mathcal{Q}_{b,c+1} \subseteq \phi$, where ϕ denotes the (open) half-plane delimited by l and not containing v_b, v_c .

As v_b, v_c, v_{c+1} lie in clockwise order, v_{c+1} is on the right of $\overrightarrow{v_b v_c}$. Further since $\overrightarrow{I_{b,c} J_{b,c+1}}$ is a translate of $\overrightarrow{v_c v_{c+1}}$ and $l \parallel v_b v_c$, we get $J_{b,c+1} \in \phi$. Thus, $\mathcal{Q}_{b,c+1} \subseteq \phi$, as $J_{b,c+1}$ is the apex of $\mathcal{Q}_{b,c+1}$.

2. Assume $v_a > I_{b,c}$ in the distance to $\overrightarrow{v_b v_c}$. This assumption implies that $I_{b,c} \neq \infty$. Hence $e_b \prec e_c$, as shown in Figure 5 (c). Let l and ϕ be the same as above. Let D be the intersecting point between $\overrightarrow{v_c v_{c+1}}$ and l . Let $d_{j,k}(X)$ denote the distance from X to $\overrightarrow{v_j v_k}$ for any vertex pair (v_j, v_k) such that $j \neq k$. We claim two inequalities: (i) $d_{b+1,c}(v_a) > d_{b+1,c}(D)$ and (ii) $d_{b+1,c}(D) = d_{b+1,c}(K_{b+1,c})$.

Since $v_a > I_{b,c}$ in the distance to $\overrightarrow{v_b v_c}$, we get $v_a \in \phi$. Since P is convex, v_a lies in the (closed) half-plane delimited by $\overrightarrow{v_c v_{c+1}}$ and containing P . Together, they imply (i). Since both $v_{b+1} K_{b+1,c}$ and $v_c D$ are translates of $v_b I_{b,c}$, region $v_{b+1} K_{b+1,c} D v_c$ is a parallelogram, which implies (ii).

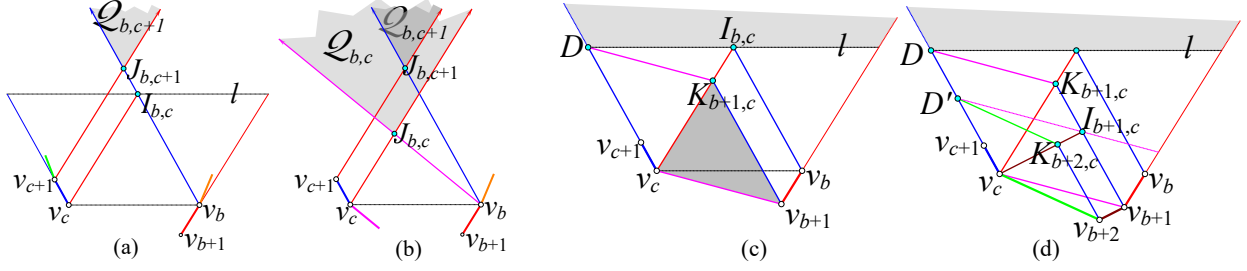


Figure 5: Illustration of the proof of Lemma 6.

Combining inequalities (i) and (ii), $d_{b+1,c}(v_a) > d_{b+1,c}(K_{b+1,c})$. This implies that (v_{b+1}, v_c) is dead (by Observation 8 part 4). Next, we argue that (v_{b+2}, v_c) is also dead. Applying Observation 8 part 4, it is enough to prove the following inequality (iii): $d_{b+2,c}(v_a) > d_{b+2,c}(K_{b+2,c})$. The proof of this inequality is illustrated in Figure 5 (d). Briefly, we can prove that $d_{b+2,c}(v_a) > d_{b+2,c}(D) > d_{b+2,c}(D') = d_{b+2,c}(K_{b+2,c})$. The proof is almost a copy of the proofs of (i) and (ii) and hence is omitted. Furthermore, by induction, $(v_{b+1}, v_c), (v_{b+2}, v_c), \dots, (v_t, v_c)$ are all dead. \square

3 Find all F-3-stable triangles in $O(n)$ time

This section finds **all** F-3-stable triangles based on Rotate-and-Kill, assuming we are given r, s, t such that $\triangle e_r e_s e_t$ is F-3-stable. We state some basic observations and lemmas first.

An edge pair (e_b, e_c) is *dead* if there is no edge e_a such that $\triangle e_a e_b e_c$ is F-3-stable.

Observation 9. *Given $b \in \{s, \dots, t\}$ and $c \in \{t, \dots, r\}$, at least one of the following holds.*

- (I) $(e_b, e_{c+1}), \dots, (e_b, e_r)$ are dead. (II) $(e_{b+1}, e_c), \dots, (e_t, e_c)$ are dead.

Observation 9 is a counterpart of Observation 4. It directly follows from Lemma 2 part 2.

Observation 10. *$\text{area}(\triangle e_i e_j e_k)$ is finite if and only if: $e_i \prec e_j, e_j \prec e_k$ and $e_k \prec e_i$.*

For each edge e_i , denote by D_i the clockwise first vertex with the furthest distance to ℓ_i , and denote by D_i^* the clockwise last vertex with the furthest distance to ℓ_i ($D_i = D_i^*$ in most cases).

Definition 11. For (e_b, e_c) such that $e_b \prec e_c$, denote by $\mathbf{a}_{b,c}$ the edge e_x in e_{c+1}, \dots, e_{b-1} such that $\text{area}(\triangle e_x e_b e_c)$ is minimized. To be specific, if there are multiple edges that minimize $\text{area}(\triangle e_x e_b e_c)$, the first edge in e_{c+1}, \dots, e_{b-1} that minimizes $\text{area}(\triangle e_x e_b e_c)$ is denoted by $\mathbf{a}_{b,c}$. If $\text{area}(\triangle e_a e_b e_c)$ are infinite for all $a \in \{c+1, \dots, b-1\}$ (this occurs if $D_b^* = D_c$), let $\mathbf{a}_{b,c}$ be the previous edge of D_c .

Lemma 12 (A unimodality of $\text{area}(\triangle e_a e_b e_c)$). *Given (e_b, e_c) such that $e_b \prec e_c$ and $D_b^* \neq D_c$, $\text{area}(\triangle e_a e_b e_c)$ is unimodal for $e_a \in [D_b^* \circ D_c]$. Specifically, let e_y denote the next edge of D_b^* , e_z denote the previous edge of D_c , and assume $\mathbf{a}_{b,c} = e_x$ (observe that $x \in \{y, \dots, z\}$). Then,*

1. $\text{area}(\triangle e_a e_b e_c)$ strictly decreases when a goes from y to x ; and
2. $\text{area}(\triangle e_a e_b e_c)$ strictly increases when a goes from $x+1$ to z .

Lemma 13 (Bi-monotonicity of $\mathbf{a}_{b,c}$). *Denote by $E = \{e_{c+1}, \dots, e_{b-1}\}$ in the following claims. 1. Assume $e_b \prec e_c, e_b \prec e_{c+1}$. Notice that $\mathbf{a}_{b,c}$ and $\mathbf{a}_{b,c+1}$ lie in E according to Definition 11. We claim that $\mathbf{a}_{b,c}, \mathbf{a}_{b,c+1}$ lie in clockwise order non-strictly in E . 2. Assume $e_b \prec e_c, e_{b+1} \prec e_c$. Notice that $\mathbf{a}_{b,c}$ and $\mathbf{a}_{b+1,c}$ lie in E according to Definition 11. We claim that $\mathbf{a}_{b,c}, \mathbf{a}_{b+1,c}$ lie in clockwise order non-strictly in E .*

We are ready to describe our algorithm. See Algorithm 2. As in the case of finding all 3-stable triangles, we need a function Kill_F in the algorithm. This function must satisfy properties ① and ② (note that (I) and (II) in the description of ① now refer to (I) and (II) in Observation 9). The design of this function is crucial and is shown right below.

```

1  $(a, b, c) \leftarrow (r, s, t);$ 
2 repeat
3   Compute  $e_a = \mathbf{a}_{b,c}$  (recall  $\mathbf{a}_{b,c}$  in Definition 11);
4   Output  $\triangle e_a e_b v_c$  if it is F-3-stable and output  $\triangle e_{a+1} e_b e_c$  if it is F-3-stable;
5   if  $\text{Kill}_F(b, c) = 'b'$  then  $b \leftarrow b + 1;$ 
6   else  $c \leftarrow c + 1;$ 
7 until  $(b, c) = (t, r);$ 

```

Algorithm 2: The Rotate-and-Kill process for finding all F-3-stable triangles.

Theorem 14. *If Kill_F satisfies ① and ②, Algorithm 2 finds all F-3-stable triangles in $O(n)$ time.*

The easy proofs of Lemmas 12, 13 and Theorem 14 are deferred to subsection 3.3. (Hint: Lemmas 12 and 13 together imply that $\mathbf{a}_{b,c}$ can be computed in amortized $O(1)$ time.)

3.1 Description of the killing function Kill_F

We need several notations in order to introduce our killing function Kill_F . See Figure 6. Fix two rays r, r' originating at some point O and a hyperbola branch h asymptotic to r, r' . Take an arbitrary tangent line of h and assume it intersects r, r' at A, A' respectively. Then, $\text{area}(\triangle OA'A)$ is a constant. This area is called the *triangle-area* of h , denoted by $\text{area}(h)$.

Consider (v_k, e_j) where $e_j \notin \{e_{k-1}, e_k\}$. See Figure 7. If $e_j \prec e_k$, denote by $h_{k,j}$ the hyperbola branch asymptotic to ℓ_{k-1}, ℓ_k in p_{k-1} with triangle-area equal to $\text{area}(p_{k-1}^C \cap p_k \cap p_j)$. If $e_{k-1} \prec e_j$, denote by $h_{k,j}$ the hyperbola branch asymptotic to ℓ_{k-1}, ℓ_k in p_k with triangle-area equal to $\text{area}(p_{k-1} \cap p_k^C \cap p_j)$. (Note that $h_{k,j}$ is undefined sometimes, e.g., when $e_k \prec e_j$ and $e_j \prec e_{k-1}$.)

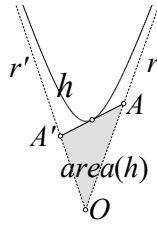


Figure 6: $\text{area}(h)$.

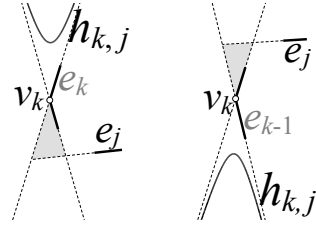


Figure 7: $h_{k,j}$.

Denote $\mathbf{U} = \{(b, c) \mid b \in \{s, \dots, t\}, c \in \{t, \dots, r\}\}$. Unless otherwise stated, assume hereafter in this section.

$$(b, c) \in \mathbf{U}, e_b, e_{b+1}, e_c, e_{c+1} \text{ are distinct, and } e_b \prec e_{c+1}. \quad (2)$$

See Figure 8. Let $G_{b,c}^+, H_{b,c}^+, G_{b,c}^-, H_{b,c}^-$ respectively denote $h_{c+1,b}, h_{c+1,b+1}, h_{b+1,c+1}, h_{b+1,c}$. (It is easy to check that $h_{c+1,b}, h_{c+1,b+1}, h_{b+1,c+1}, h_{b+1,c}$ are defined when (2) holds.)

Moreover, denote by $\ell_{b,c}^{GH}, \ell_{b,c}^{HG}, \ell_{b,c}^{GG}, \ell_{b,c}^{HH}$ the common tangent of $G_{b,c}^+, H_{b,c}^-$, the common tangent of $H_{b,c}^+, G_{b,c}^-$, the common tangent of $G_{b,c}^+, G_{b,c}^-$, and the common tangent of $H_{b,c}^+, H_{b,c}^-$, respectively.

See Figure 9 for examples (b, c are omitted when they are clear in context). Regard these common tangents as *directed*; the direction of a common tangent ℓ is from $\ell \cap \ell_{c+1}$ to $\ell \cap \ell_b$.

For any directed line ℓ , let $\theta[\ell]$ denote its direction, which is an angle in $[0, 2\pi)$, adopting the convention that $\theta[\vec{OA}]$ **increases when A rotates clockwise around O** .

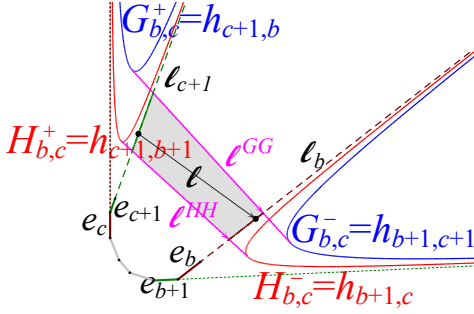


Figure 8: G^+, G^-, H^+, H^- .

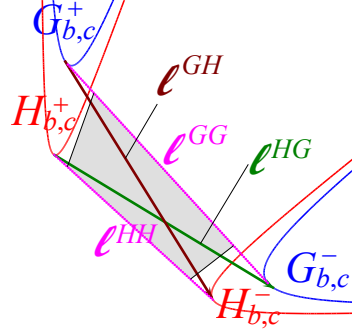


Figure 9: L^{GH}, L^{HG} .

Definition of Kill_F . Take $(b, c) \in \mathcal{U}$. If $b = c$ or $b + 1 = c$, define $\text{Kill}_F(b, c) = \text{'c'}$. If $e_b \prec e_{c+1}$ is not true, define $\text{Kill}_F(b, c) = \text{'b'}$. Otherwise, (2) holds. Choose some direction $\theta \in [\theta[\ell^{HG}], \theta[\ell^{GH}]]$ (specified below), and find any line $\ell_{b,c} = \overrightarrow{XY}$ with $\theta[\overrightarrow{XY}] = \theta$ and with the following property:

(P1) X lies strictly between $\ell^{GG} \cap \ell_{c+1}$ and $\ell^{HH} \cap \ell_{c+1}$, and Y lies strictly between $\ell^{GG} \cap \ell_b$ and $\ell^{HH} \cap \ell_b$. (A point A lies strictly between B, C if A is in segment BC and A neither equals B nor equals C .) (The existence of such a line is obvious and is formally stated in the next lemma.) Define

$$\text{Kill}_F(b, c) = \begin{cases} \text{'b'}, & \text{if } P \text{ lies on the right of } \ell_{b,c}; \\ \text{'c'}, & \text{Otherwise.} \end{cases} \quad (3)$$

Direction θ is a variable of our algorithm. Its value is updated in each iteration. Initially, $\theta \leftarrow \theta[\ell_{s,t}^{HG}]$. Subsequently, $\theta \leftarrow \begin{cases} \theta, & \text{if } \theta \in [\theta[\ell_{b,c}^{HG}], \theta[\ell_{b,c}^{GH}]]; \\ \theta[\ell_{b,c}^{HG}], & \text{otherwise.} \end{cases}$

Lemma 15. For any $\theta \in [\theta[\ell^{HG}], \theta[\ell^{GH}]]$, we can compute in constant time a directed line $\ell = \overrightarrow{XY}$ with $\theta[\ell] = \theta$ and with the aforementioned property (P1). Moreover, for any line ℓ satisfying (P1), the following hold: If P lies on the right of ℓ , condition (I) holds. Otherwise, condition (II) holds.

Lemma 16. Let θ_1, θ_2 be the opposite directions of e_{s+1}, e_r . Assume $[\theta_1, \theta_2] \subset [0, 2\pi)$ without loss of generality. The variable θ defined above increases (non-strictly) within the range $[\theta_1, \theta_2]$ during the algorithm.

Theorem 17. The function Kill_F satisfies ① and ②.

Theorem 17 is easily built on the Lemma 15 and Lemma 16. Lemma 16 is very challenging to prove and it is crucial for proving property ②. Due to space limit, we show the proofs of Theorem 17, Lemma 15, and Lemma 16 in subsection 3.2.

Combining Theorem 17 and 14, we find all F-3-stable triangles in $O(n)$ time.

3.2 Analysis of the Kill function Kill_F introduced in subsection 3.1

We first prove Theorem 17 and then prove Lemma 15 and Lemma 16.

Proof of Theorem 17. Property ① states that for any $(b, c) \in U$, $\text{Kill}_F(b, c)$ returns ‘b’ only if (I) $(e_b, e_{c+1}), \dots, (e_b, e_r)$ are dead, and ‘c’ only if (II) $(e_{b+1}, e_c), \dots, (e_t, e_c)$ are dead.

When $b = c$ or $b + 1 = c$, $\text{Kill}_F(b, c)$ returns ‘c’ by definition. Moreover, we have $(b, c) \in \{(t, t), (t-1, t), (t, t+1)\}$, hence condition (II) holds trivially. When $e_b \prec e_{c+1}$ is not true, $\text{Kill}_F(b, c)$ returns ‘b’ by definition. In this case, e_{c+1}, \dots, e_r are chasing or parallel to e_b , which implies that $(e_b, e_{c+1}), \dots, (e_b, e_r)$ are dead (by Observation 10). Assume now $b \neq c, b + 1 \neq c$, and $e_b \prec e_{c+1}$. In other words, condition (2) holds. There are two cases: $\text{Kill}_F(b, c) = \text{‘b’}$, or $\text{Kill}_F(b, c) = \text{‘c’}$. When $\text{Kill}_F(b, c) = \text{‘b’}$, P is on the right of $\ell_{b,c}$, which implies condition (I) by Lemma 15. When $\text{Kill}_F(b, c) = \text{‘c’}$, P is not on the right of $\ell_{b,c}$, which implies condition (II) by Lemma 15.

Property ② states that $\text{Kill}_F(b, c)$ can be computed in amortized $O(1)$ time. Denote by ℓ_θ the tangent of P with direction θ and with P on its right. As θ increases monotonously (within $[0, 2\pi)$) during the algorithm (due to Lemma 16), ℓ_θ can be computed in amortized $O(1)$ time. Moreover, $\ell_{b,c}$ can be computed in $O(1)$ time (by Lemma 15). Therefore, it takes amortized $O(1)$ time to check whether ℓ_θ is on the right of $\ell_{b,c}$. Further since polygon P is on the right of $\ell_{b,c}$ if and only if ℓ_θ is on the right of $\ell_{b,c}$, function $\text{Kill}_F(b, c)$ in (3) can be computed in amortized $O(1)$ time. \square

The following observation follows from elementary knowledge of hyperbolas; proof omitted.

Intersects & avoids Assume h is a hyperbola branch (see Figure 6). If $h \cap p_a \neq \emptyset$, we state that p_a intersects h . If $h \cap (p_a \setminus \ell_a) = \emptyset$, we state that p_a avoids h .

Observation 18. See Figure 6. Let ϕ be the wedge bounded by r, r' and containing h . If $\text{area}(p_a \cap \phi) \geq \text{area}(h)$, then p_a intersects h . If $\text{area}(p_a \cap \phi) \leq \text{area}(h)$, then p_a avoids h .

Proof of Lemma 15. The first part of this lemma is rather obvious. See Figure 9 for an illustration. We can compute tangents ℓ^{GG} and ℓ^{HH} in constant time and then compute the intersecting points between these two tangents and the two extended lines ℓ_b, ℓ_{c+1} . It is then easy to find two points X, Y with $\theta(\overrightarrow{XY}) = \theta$ and with X, Y satisfying property (P1). Further details are omitted.

The “moreover” part is less obvious. Before proving it, we first prove the following facts.

1. If $p_a \in \{p_{c+2}, \dots, p_{b-1}\}$ intersects both $G_{b,c}^+$ and $G_{b,c}^-$, v_a or v_{a+1} is not on the right of ℓ^{GG} .
2. If $p_a \in \{p_{c+2}, \dots, p_{b-1}\}$ avoids both $H_{b,c}^+$ and $H_{b,c}^-$, P is on the right of ℓ^{HH} .
3. Assume $\triangle e_a e_b e_{c'}$ is F -3-stable for some $e_{c'} \in \{e_{c+1}, \dots, e_r\}$. Then,
 - (a) p_a intersects $G_{b,c}^+ = h_{c+1,b}$; (b) p_a intersects $G_{b,c}^- = h_{b+1,c+1}$; and (c) $a \in \{c+2, \dots, b-1\}$.
4. Assume $\triangle e_a e_b e_c$ is F -3-stable for some $e_b \in \{e_{b+1}, \dots, e_t\}$. Then,
 - (a) p_a avoids $H_{b,c}^+ = h_{c+1,b+1}$; (b) p_a avoids $H_{b,c}^- = h_{b+1,c}$; and (c) $a \in \{c+2, \dots, b-1\}$.

Proof of fact 1. See Figure 10 (a). We prove it by contradiction. Suppose v_a, v_{a+1} are both on the right of ℓ^{GG} . We discuss two cases distinguished by whether v_a or v_{a+1} is closer to ℓ^{GG} . If v_{a+1} is closer to ℓ^{GG} , it is easy to see that p_a cannot intersect $G_{b,c}^+$. If v_a is closer to ℓ^{GG} , it is easy to see that p_a cannot intersect $G_{b,c}^-$. Either way, p_a cannot intersect both $G_{b,c}^+$ and $G_{b,c}^-$.

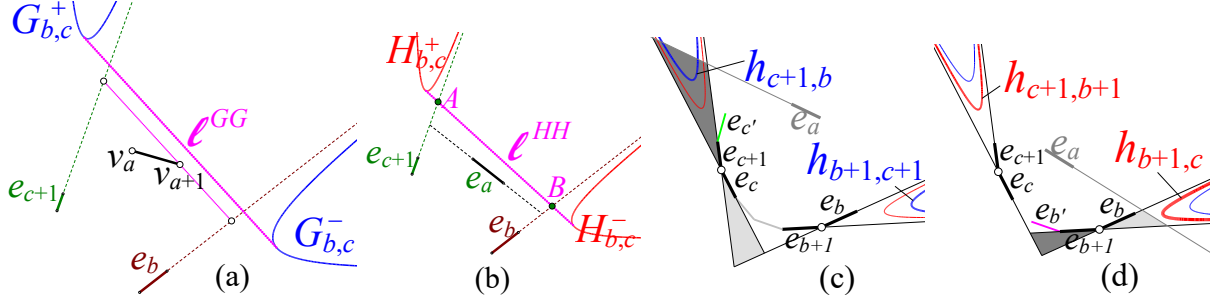


Figure 10: Illustration of the proof of Lemma 15.

Proof of fact 2. See Figure 10 (b). Assume p_a avoids $H_{b,c}^+$ and $H_{b,c}^-$. This means that both $H_{b,c}^+$ and $H_{b,c}^-$ lie on the left of ℓ_a . It follows that points $A = \ell^{HH} \cap \ell_{c+1}$ and $B = \ell^{HH} \cap \ell_b$ lie on the left of ℓ_a . Therefore, e_a, e_b, e_{c+1} are all on the right of $\overrightarrow{AB} = \ell^{HH}$. Thus, P lies on the right of ℓ^{HH} .

Proof of fact 3 (a). See Figure 10 (c). Because $e_{c'} \in \{e_{c+1}, \dots, e_r\}$ and is stable in $\Delta_{e_a e_b e_{c'}}$, following the unimodality stated in Lemma 12, $\text{area}(p_a \cap (p_c \cap p_{c+1}^C)) \geq \text{area}(p_b \cap (p_c^C \cap p_{c+1})) = \text{area}(h_{c+1,b})$. Applying Observation 18, this means p_a intersects $h_{c+1,b}$.

Proof of fact 3 (b). Because e_b is stable in $\Delta_{e_a e_b e_{c'}}$, $\text{area}(\Delta_{e_a e_b e_{c'}}) \geq \text{area}(\Delta_{e_a e_b e_{c+1}})$. In other words, $\text{area}(p_a \cap (p_b^C \cap p_{b+1})) \geq \text{area}(p_{c+1} \cap (p_b \cap p_{b+1}^C))$. It follows that $\text{area}(p_a \cap (p_b^C \cap p_{b+1})) \geq \text{area}(p_{c+1} \cap (p_b \cap p_{b+1}^C)) = \text{area}(h_{b+1,c+1})$. Applying Observation 18, this means p_a intersects $h_{b+1,c+1}$.

Proof of fact 3 (c). Since $c' \in \{c+1, \dots, r\}$ and $e_a, e_b, e_{c'}$ are in clockwise order, $a \in \{c+2, \dots, b-1\}$.

Proof of fact 4 (a). See Figure 10 (d). Because $e_{b'} \in \{e_{b+1}, \dots, e_t\}$ and is stable in $\Delta_{e_a e_{b'} e_c}$, following the unimodality stated in Lemma 12, $\text{area}(p_a \cap (p_b^C \cap p_{b+1})) \leq \text{area}(p_c \cap (p_b \cap p_{b+1}^C)) = \text{area}(h_{b+1,c})$. Applying Observation 18, this means p_a avoids $h_{b+1,c}$.

Proof of fact 4 (b). Because e_c is stable in $\Delta_{e_a e_{b'} e_c}$, $\text{area}(\Delta_{e_a e_{b'} e_c}) \leq \text{area}(\Delta_{e_a e_{b'} e_{c+1}})$. In other words, $\text{area}(p_a \cap (p_c \cap p_{c+1}^C)) \leq \text{area}(p_{b+1} \cap (p_c^C \cap p_{c+1}))$. It follows that $\text{area}(p_a \cap (p_c \cap p_{c+1}^C)) \leq \text{area}(p_{b+1} \cap (p_c^C \cap p_{c+1})) = \text{area}(h_{c+1,b+1})$. Applying Observation 18, this means p_a avoids $h_{c+1,b+1}$.

Proof of fact 4 (c). First, because $e_a, e_{b'}, e_c$ lie in clockwise order, $a \in \{c+1, \dots, b'-1\}$. Since $\Delta_{e_a e_{b'} e_c}$ is F-3-stable, $e_c \prec e_a$. However, edges $e_b, \dots, e_{b'-1}$ are chasing e_c , so they do not contain e_a . Therefore, $a \in \{c+1, \dots, b-1\}$. Because $e_b \prec e_{c+1}$, we have $e_{b'} \prec e_{c+1}$. However, $e_a \prec e_{b'}$ because $\Delta_{e_a e_{b'} e_c}$ is F-3-stable. Therefore, $a \neq c+1$. Altogether, $a \in \{c+2, \dots, b-1\}$.

We are ready to prove the “moreover” part. Assume P is on the right of ℓ . Then, P must be on the right of ℓ^{GG} . According to fact 1, this implies that *no one in $\{p_{c+2}, \dots, p_{b-1}\}$ intersects both $G_{b,c}^+$ and $G_{b,c}^-$* . Further by applying fact 3, $(e_b, e_{c+1}), \dots, (e_b, e_r)$ are dead, i.e., condition (I) holds.

Assume in the following P is not on the right of ℓ . Then, P is not on the right of ℓ^{HH} . According to fact 2, *no one in $\{p_{c+2}, \dots, p_{b-1}\}$ avoids both $H_{b,c}^+$ and $H_{b,c}^-$* . Further by applying fact 4, $(e_{b+1}, e_c), \dots, (e_t, e_r)$ are dead, i.e., condition (II) holds. \square

Proof of Lemma 16 Recall θ_1, θ_2 in Lemma 16. Our proof of Lemma 16 applies the following two observations.

Observation 19. When (2) holds, $[\theta[\ell_{b,c}^{HG}], \theta[\ell_{b,c}^{GH}]] \subset [\theta_1, \theta_2]$.

Observation 20. Assume we were given (b, c) in some iteration and (b', c') in a later iteration, both (b, c) and (b', c') satisfying condition (2), then $\theta[\ell_{b',c'}^{GH}] \geq \theta[\ell_{b,c}^{HG}]$.

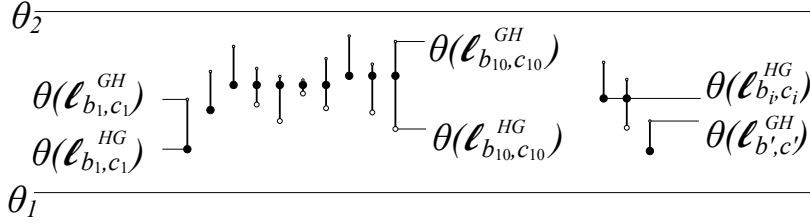


Figure 11: Illustration of the proof of Lemma 16.

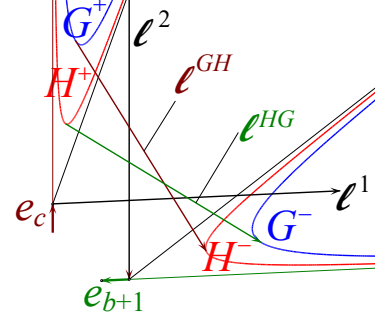


Figure 12: Observation 19

Proof of Lemma 16. See Figure 11 for an illustration. Assume we have visited m pairs $(b_1, c_1), \dots, (b_m, c_m)$ satisfying condition (2) thus far in the Rotate-and-Kill process, and we are at the beginning of another iteration (b', c') satisfying (2). Currently, θ equals to $\theta[\ell_{b_i, c_i}^{HG}]$ for some $i \leq m$. Therefore, $\theta \leq \theta[\ell_{b', c'}^{GH}]$ according to Observation 20. After visiting (b', c') , according to the formula
$$\theta \leftarrow \begin{cases} \theta, & \text{if } \theta \in [\theta[\ell_{b', c'}^{HG}], \theta[\ell_{b', c'}^{GH}]]; \\ \theta[\ell_{b', c'}^{HG}], & \text{otherwise.} \end{cases}, \theta \text{ either increases (if } \theta < \theta[\ell_{b', c'}^{HG}]) \text{ or remains unchanged (if } \theta \in [\theta[\ell_{b', c'}^{HG}], \theta[\ell_{b', c'}^{GH}]]).$$
 Further by Observation 19, θ increases within $[\theta_1, \theta_2]$ during the algorithm.

(The lemma fails if Observation 20 is not true; see the right part of Figure 11 for an example.) \square

Proof of Observation 19. 1. See Figure 12. Let $\ell_{b,c}^1$ be the line at v_{c+1} with the opposite direction to e_{b+1} , and $\ell_{b,c}^2$ be the line at v_{b+1} with the opposite direction to e_c . Clearly, $\ell_{b,c}^1$ intersects $G_{b,c}^-$ but not $H_{b,c}^+$, whereas $\ell_{b,c}^2$ intersect $G_{b,c}^+$ but not $H_{b,c}^-$. On the other hand, $\ell_{b,c}^{HG}$ is tangent to $G_{b,c}^-$ and $H_{b,c}^+$, whereas $\ell_{b,c}^{GH}$ is tangent to $G_{b,c}^+$ and $H_{b,c}^-$. Altogether, we can deduce that $[\theta[\ell_{b,c}^{HG}], \theta[\ell_{b,c}^{GH}]] \subset [\theta[\ell_{b,c}^1], \theta[\ell_{b,c}^2]]$. However, $[\theta[\ell_{b,c}^1], \theta[\ell_{b,c}^2]] \subset [\theta[\ell_{s,t}^1], \theta[\ell_{t,r}^2]] = [\theta_1, \theta_2]$. So $[\theta[\ell_{b,c}^{HG}], \theta[\ell_{b,c}^{GH}]] \subset [\theta_1, \theta_2]$. \square

Proof of Observation 20. Let $A = \ell_{b+1} \cap \ell_{c+1}, B = \ell_{b'} \cap \ell_{c'}$.

First, consider the case where $b' > b$ and $c' > c$. See Figure 13. Denote

$$M^- = \begin{cases} v_{b'+1}, & b' = b+1; \\ \ell_{b+1} \cap \ell_{b'}, & b' \geq b+2 \end{cases} \text{ and } M^+ = \begin{cases} v_{c'+1}, & c' = c+1; \\ \ell_{c+1} \cap \ell_{c'}, & c' \geq c+2. \end{cases}$$

Denote the reflections of A around M^-, M^+ by A^-, A^+ respectively. Denote the reflections of B around M^-, M^+ by B^-, B^+ respectively. Let $\ell = \overrightarrow{A^+ A^-}$ and $\ell' = \overrightarrow{B^+ B^-}$.

We state three equalities or inequalities which together imply the claimed inequality.

$$(i) \theta[\ell_{b,c}^{HG}] \leq \theta[\ell]. \quad (ii) \theta[\ell] = \theta[\ell']. \quad (iii) \theta[\ell'] \leq \theta[\ell_{b', c'}^{GH}].$$

By the definition of ℓ and ℓ' , we have $\theta[\ell] = \theta[\overrightarrow{M^+ M^-}] = \theta[\ell']$, thus equality (ii) holds.

Proof of (i): This reduces to showing that (i.1) ℓ intersects $H_{b,c}^+$ and (i.2) $G_{b,c}^-$ is on the left of ℓ . Now, let us focus on the objects shown in Figure 13 (e). Notice that A, v_{c+1}, M^+, A^+ lie in this order in line ℓ_{c+1} . Further since $|AM^+| = |A^+ M^+|$, we know $|A^+ v_{c+1}| > |Av_{c+1}|$. Thus the area of $h \cap (p_c \cap p_{c+1}^C)$, where h denotes the half-plane parallel to ℓ_{b+1} that admits A^+ on its boundary and contains v_{c+1} , is larger than the area of the (yellow) triangle $p_{b+1} \cap p_c^C \cap p_{c+1}$, which equals $\text{area}(h_{c+1, b+1})$. So the triangle area bounded by ℓ_c, ℓ_{c+1} and ℓ is even larger than $\text{area}(h_{c+1, b+1})$. By Observation 18, this means ℓ intersects $h_{c+1, b+1}$, i.e. (i.1) holds.

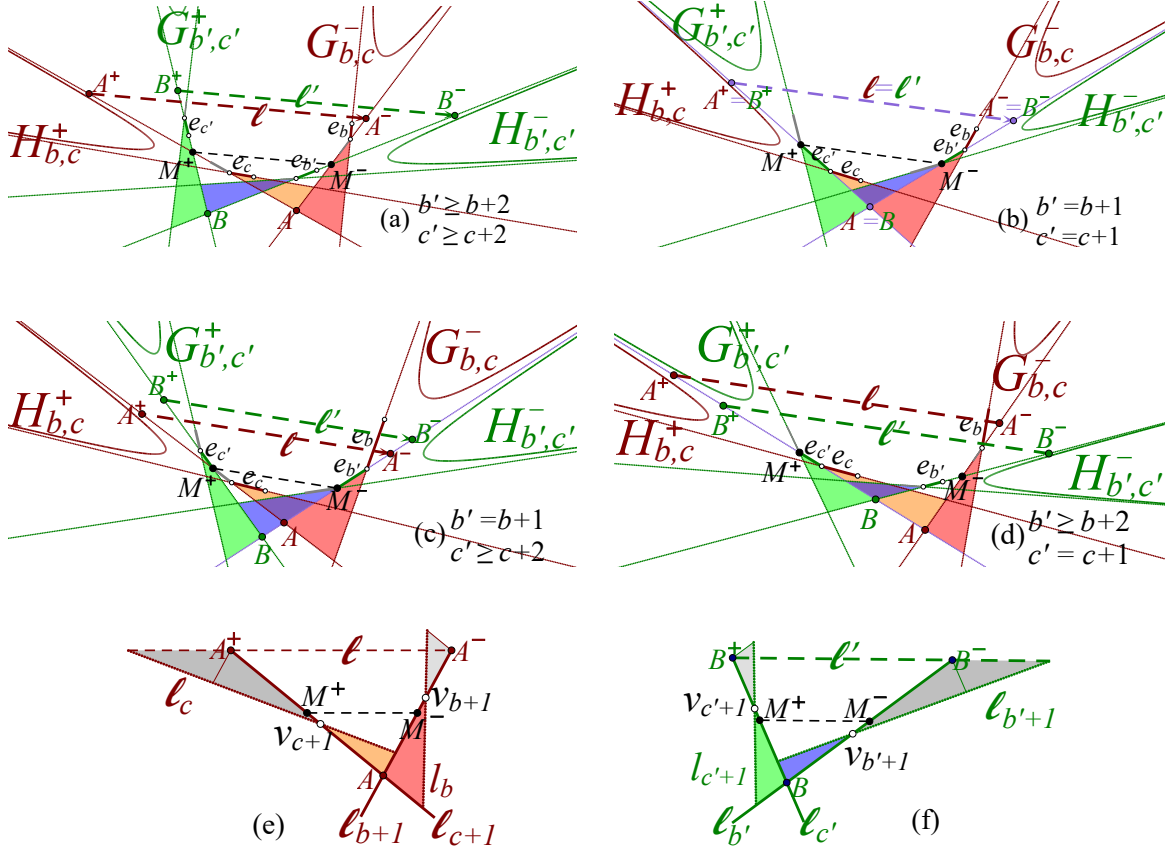


Figure 13: Proof of Observation 20 part I.

Assume A, M^-, v_{b+1}, A^- lie in this order in ℓ_{b+1} (otherwise the order would be A, M^-, A^-, v_{b+1} , which is easier). Similarly, the area bounded by ℓ_b, ℓ_{b+1} and ℓ is smaller than $\text{area}(h_{b+1, c+1})$, which by Observation 18 means that $h_{b+1, c+1}$ is on the left of ℓ , i.e. (i.2) holds.

Proof of (iii): This reduces to showing that (iii.1) ℓ' intersects $H_{b', c'}^-$ and (iii.2) $G_{b', c'}^+$ is on the left of ℓ' . See Figure 13 (f); they are symmetric to (i.1) and (i.2) respectively; proof omitted.

In the following, assume $b = b'$ or $c = c'$. We discuss four subcases.

Case 1 $b' = b+1, c' = c$. See Figure 14 (a). Notice that $H_{b, c}^+ = G_{b', c'}^+$. Denote by A^- be the reflection of A around v_{b+1} and B^- the reflection of B around $v_{b'+1}$. Let ℓ be the tangent line of $H_{b, c}^+$ passing through A^- , and ℓ' the tangent line of $G_{b', c'}^+$ passing through B^- . We argue that (i) $\theta[\ell_{b, c}^{HG}] \leq \theta[\ell]$ and (iii) $\theta[\ell'] \leq \theta[\ell_{b', c'}^{GH}]$ still hold in this case. They follow from the observations that the triangles with light color in the figure are smaller than their opposite triangles with dark color, which is because $|Bv_{b'+1}| = |B^-v_{b'+1}|$ and $|Av_{b+1}| = |A^-v_{b+1}|$. Clearly, A, B, B^-, A^- lie in this order in ℓ_{b+1} , thus $\theta[\ell] < \theta[\ell']$. Altogether, $\theta[\ell_{b, c}^{HG}] \leq \theta[\ell_{b', c'}^{GH}]$.

Case 2 $b' = b, c' = c+1$. See Figure 14 (b); symmetric to Case 1; proof omitted.

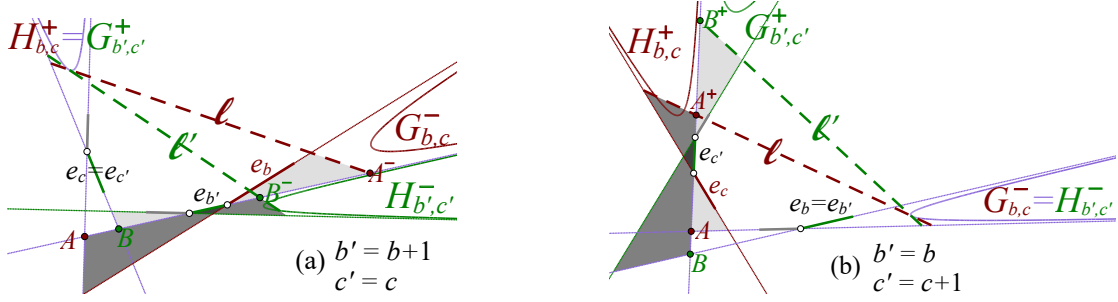


Figure 14: Proof of Observation 20 part II.

Case 3 $b' \geq b+2, c' = c$. **Hint:** This case is more difficult because $G_{b',c'}^+$ is now “below” $H_{b,c}^+$ as shown in Figure 15 (a); the following proof contains several more tricks.

Let A^-, B^- be the reflection of A, B around M^- respectively and ℓ be the tangent line of $H_{b,c}^+$ that passes through A^- , and ℓ' the tangent line of $G_{b',c'}^+$ that passes through B^- . As in the previous cases, (i) and (iii) hold and thus it reduces to showing that $\theta[\ell'] > \theta[\ell]$.

See Figure 15 (b). Make a parallel line ℓ'' of ℓ at B^- , which intersects ℓ_c, ℓ_{c+1} at B_1, B_2 respectively. It reduces to showing that the area bounded by $\ell'', \ell_c, \ell_{c+1}$, namely $\text{area}(\triangle v_{c+1}B_1B_2)$, is smaller than the area bounded by $\ell', \ell_c, \ell_{c+1}$. The latter equals $\text{area}(G_{b',c'}^+) = \text{area}(\triangle v_{c+1}BX)$, where $X = \ell_{c+1} \cap \ell_{b'}$. Let X^- be the reflection of X around M^- . Assume the parallel line of ℓ at X^- intersects ℓ_c, ℓ_{c+1} at X_1, X_2 respectively. Let $D = \ell_{b+1} \cap \ell_c$, and E be the point on ℓ_c so that $XE \parallel AD$. Clearly, $\text{area}(\triangle v_{c+1}B_1B_2) < \text{area}(\triangle v_{c+1}X_1X_2)$ and $\text{area}(\triangle v_{c+1}BX) > \text{area}(\triangle v_{c+1}EX)$. So it further reduces to proving that (I) $\text{area}(\triangle v_{c+1}X_1X_2) < \text{area}(\triangle v_{c+1}EX)$.

Assume ℓ intersects ℓ_c, ℓ_{c+1} at A_1, A_2 . We know (a) $\text{area}(\triangle v_{c+1}A_1A_2) = \text{area}(\triangle v_{c+1}DA)$ since ℓ is tangent to $H_{b,c}^+$, and so (b): $|v_{c+1}A_2| < |v_{c+1}A_1|$. Since segment A^-X^- is a translate of XA , (c) $|AX| = |A_2X_2|$. Combining (b) with (c), $|A_2X_2|/|v_{c+1}A_2| > |AX|/|v_{c+1}A_1|$, so (d) $|v_{c+1}X_2|/|v_{c+1}A_2| < |v_{c+1}X|/|v_{c+1}A_1|$. Further since $X_1X_2 \parallel A_1A_2$ whereas $XE \parallel AD$, we have (e) $|v_{c+1}X_1|/|v_{c+1}A_1| < |v_{c+1}E|/|v_{c+1}D|$. Therefore, (f) $\text{area}(\triangle v_{c+1}X_1X_2)/\text{area}(\triangle v_{c+1}A_1A_2) < \text{area}(\triangle v_{c+1}EX)/\text{area}(\triangle v_{c+1}DA)$. Combining (a) and (f) results (I).

Case 4 $b' = b, c' \geq c+2$. Symmetric to Case 3; proof omitted.

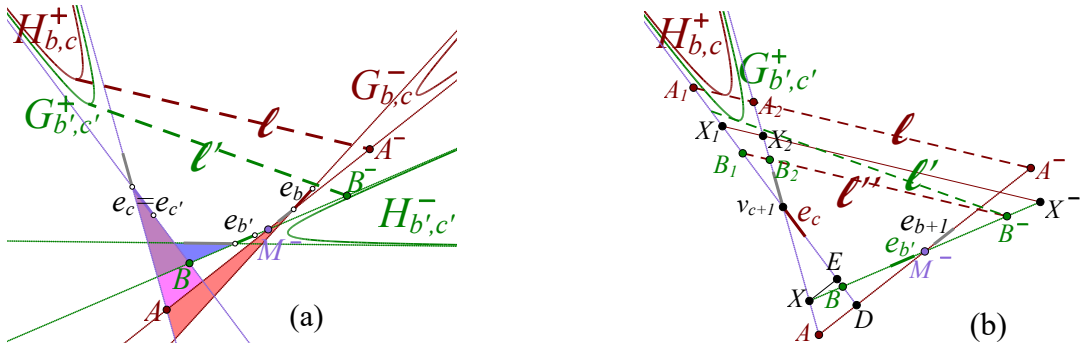


Figure 15: Proof of Observation 20 part III.

□

3.3 Proofs of Lemma 12, Lemma 13, and Theorem 14

Proof of Lemma 12. For each edge pair (e_i, e_j) such that $e_i \nparallel e_j$, let $O_{i,j}$ be the intersecting point between ℓ_i and ℓ_j . We classify the edges in $[D_b^* \circ D_c]$ into two categories: e_a is *negative* if $|O_{a,c}v_{a+1}| \leq |O_{a,b}v_{a+1}|$ and *positive* otherwise; see Figure 16. We have three observations.

- (i) If e_a is positive, its clockwise next edge e_{a+1} must also be positive.
- (ii) If e_a, e_{a+1} are both negative, $\text{area}(\triangle_{e_{a+1}e_b e_c}) < \text{area}(\triangle_{e_a e_b e_c})$.
- (iii) If e_a, e_{a+1} are both positive, $\text{area}(\triangle_{e_{a+1}e_b e_c}) > \text{area}(\triangle_{e_a e_b e_c})$.

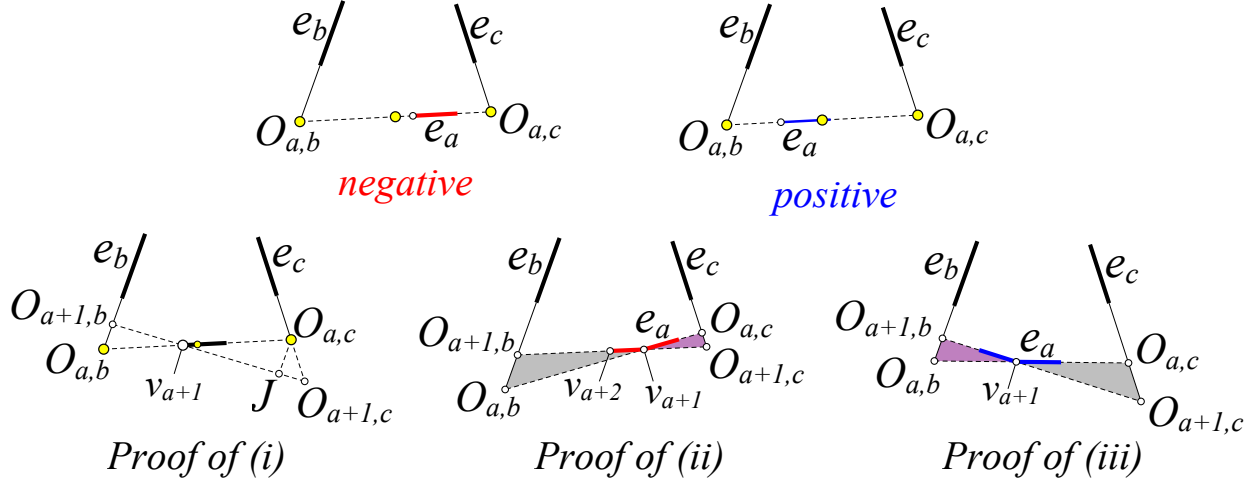


Figure 16: Illustration of the proof of Lemma 12

Proof of (i): Make a line at $O_{a,c}$ parallel to ℓ_b and assume it intersects ℓ_{a+1} at J . Since e_a is positive, $|O_{a,c}v_{a+1}| > |O_{a,b}v_{a+1}|$. It implies that $|Jv_{a+1}| > |O_{a+1,b}v_{a+1}|$. Therefore, $|O_{a+1,c}v_{a+1}| > |O_{a+1,b}v_{a+1}|$. Furthermore, $|O_{a+1,c}v_{a+2}| > |O_{a+1,b}v_{a+2}|$, i.e., e_{a+1} is positive.

Proof of (ii): Because e_a, e_{a+1} are negative, $|O_{a,c}v_{a+1}| \leq |O_{a,b}v_{a+1}|$ and $|O_{a+1,c}v_{a+1}| < |O_{a+1,b}v_{a+1}|$. Therefore, $|O_{a,c}v_{a+1}| \cdot |O_{a+1,c}v_{a+1}| < |O_{a,b}v_{a+1}| \cdot |O_{a+1,b}v_{a+1}|$. In other words, $\triangle_{v_{a+1}O_{a,c}O_{a+1,c}}$ is smaller than $\triangle_{v_{a+1}O_{a,b}O_{a+1,b}}$, i.e., $\text{area}(\triangle_{e_{a+1}e_b e_c}) < \text{area}(\triangle_{e_a e_b e_c})$.

Proof of (iii): Because e_a is positive, $|O_{a,c}v_{a+1}| > |O_{a,b}v_{a+1}|$ and $|O_{a+1,c}v_{a+1}| > |O_{a+1,b}v_{a+1}|$ (use the proof of (i)). Therefore, $|O_{a,c}v_{a+1}| \cdot |O_{a+1,c}v_{a+1}| > |O_{a,b}v_{a+1}| \cdot |O_{a+1,b}v_{a+1}|$, i.e. $\triangle_{v_{a+1}O_{a,c}O_{a+1,c}}$ is larger than $\triangle_{v_{a+1}O_{a,b}O_{a+1,b}}$, i.e., $\text{area}(\triangle_{e_{a+1}e_b e_c}) > \text{area}(\triangle_{e_a e_b e_c})$.

Next, we prove this lemma from observations (i)–(iii). Assume e_{p-1} is negative and e_p is positive (the case where all edges are positive or all edges are negative is easier and can be proved similarly). Applying (i), e_y, \dots, e_{p-1} are negative whereas e_p, \dots, e_z are positive. Denote $s_a = \text{area}(\triangle_{e_a e_b e_c})$.

As e_y, \dots, e_{p-1} are negative, applying (ii), we get (A): $s_y > s_{y+1} > \dots > s_{p-1}$.

As e_p, \dots, e_z are positive, applying (iii), we get (B): $s_p < s_{p+1} < \dots < s_z$.

Together, x equals either $p-1$ or p . By definition of x , we also have (C): $s_{x-1} > s_x$.

No matter x equals $p-1$ or p , we obtain the following from formulas (A), (B), and (C):

1. s_a **strictly** decreases when a goes from y to x ; and
2. s_a **strictly** increases when a goes from $x+1$ to z . □

Next, we prove an observation, which is preliminary to the proof of Lemma 13 and Lemma 2.

Observation 21. 1. Assume $e_a, e_b, e_{b'}, e_c, e_{c'}$ are distinct and lie in clockwise order (see Figure 17 (a)). Suppose $\text{area}(\triangle e_a e_{b'} e_c)$ and $\text{area}(\triangle e_a e_b e_{c'})$ are both finite – this means $e_a \prec e_{b'}, e_{b'} \prec e_{c'}, e_c \prec e_a$. Then, $\text{area}(\triangle e_a e_{b'} e_c) \leq \text{area}(\triangle e_a e_b e_c)$ implies that $\text{area}(\triangle e_a e_{b'} e_c) < \text{area}(\triangle e_a e_b e_{c'})$.

2. Assume $e_a, e_{a'}, e_b, e_{b'}, e_c$ are distinct and lie in clockwise order (see Figure 17 (b)). Suppose $\text{area}(\triangle e_a e_{b'} e_c)$ and $\text{area}(\triangle e_{a'} e_{b'} e_c)$ are both finite – this means $e_a \prec e_{b'}, e_{b'} \prec e_c, e_c \prec e_{a'}$. Then, $\text{area}(\triangle e_a e_{b'} e_c) \leq \text{area}(\triangle e_{a'} e_{b'} e_c)$ implies that $\text{area}(\triangle e_a e_{b'} e_c) < \text{area}(\triangle e_{a'} e_b e_c)$.

Proof of Observation 21. We only prove part 1; the proof of part 2 is similar and is omitted.

See Figure 17 (a). By the assumption, $\text{area}(\triangle e_a e_{b'} e_{c'})$ is finite. Assume $\text{area}(\triangle e_a e_b e_{c'})$ is also finite (hence $e_b \prec e_{c'}$), otherwise it is trivial that $\text{area}(\triangle e_a e_{b'} e_{c'}) < \text{area}(\triangle e_a e_b e_{c'})$.

Assume ℓ_b intersects $\ell_a, \ell_c, \ell_{c'}$ at X, X', X'' and $\ell_{b'}$ intersects $\ell_a, \ell_c, \ell_{c'}$ at Y, Y', Y'' , respectively. Let $O = \ell_b \cap \ell_{b'}$. Because $\text{area}(\triangle e_a e_{b'} e_c) \leq \text{area}(\triangle e_a e_b e_c)$, $\text{area}(\triangle OXY) \leq \text{area}(\triangle OX'Y')$. Hence $\text{area}(\triangle OXY) < \text{area}(\triangle OX''Y'')$, i.e. $\text{area}(\triangle e_a e_{b'} e_{c'}) < \text{area}(\triangle e_a e_b e_{c'})$. \square

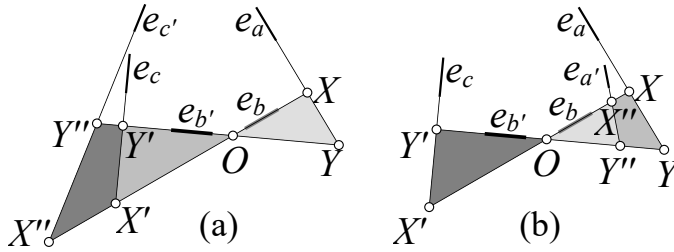


Figure 17: Illustration of Observation 21.

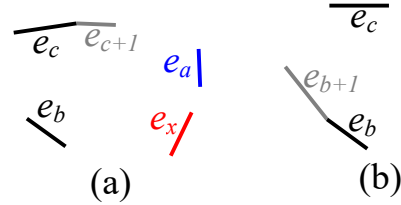


Figure 18: Proof of Lemma 13.

Proof of Lemma 13. 1. First, assume $D_b^* = D_c$. In this case, $a_{b,c}$ is the previous edge of D_c (by definition). If $D_{c+1} = D_c = D_b^*$, edges $a_{b,c}, a_{b,c+1}$ are both equal to the previous edge of D_c . If $D_{c+1} \neq D_c$, edge $a_{b,c+1}$ lies in $[D_b^* \circ D_{c+1}] = [D_c \circ D_{c+1}]$ and hence lies after $a_{b,c}$ (clockwise).

Assume $D_b^* \neq D_c$. Let $e_x = a_{b,c}$ and take e_a in $[D_b^* \circ v_x]$. See Figure 18 (a). As $a_{b,c} = e_x$, $\text{area}(\triangle e_x e_b e_c) < \text{area}(\triangle e_a e_b e_c)$. Applying Observation 21, $\text{area}(\triangle e_x e_b e_{c+1}) < \text{area}(\triangle e_a e_b e_{c+1})$. Therefore, $a_{b,c+1} \neq e_a$. This means $a_{b,c+1}$ lies in $[v_x \circ D_{c+1}]$ and hence equals or lies after $a_{b,c}$.

2. When $D_b^* = D_c$, it is trivial that $D_{b+1}^* = D_c$. Therefore, in this case both $a_{b,c}$ and $a_{b+1,c}$ equal to the previous edge of D_c . Next, assume that $D_b^* \neq D_c$. Let $e_x = a_{b,c}$. Similar as in the above case, we shall prove that $a_{b+1,c} \neq e_a$ for any e_a in $[D_b^* \circ v_x]$. See Figure 18 (b).

If it holds that e_a is not chasing e_{b+1} , we can get $a_{b+1,c} \neq e_a$ immediately as $\text{area}(\triangle e_a e_{b+1} e_c)$ is infinite in this case. (To make it rigorous, we need to show that $a_{b+1,c} \neq e_a$ even if $D_{b+1}^* = D_c$. In that case, $a_{b+1,c}$ is defined as the previous edge of D_c , which is in $[v_x \circ D_c]$ and cannot be e_a .)

Assume now $e_a \prec e_{b+1}$. Because $a_{b,c} = e_x$, $\text{area}(\triangle e_x e_b e_c) < \text{area}(\triangle e_a e_b e_c)$. Applying Observation 21, $\text{area}(\triangle e_x e_{b+1} e_c) < \text{area}(\triangle e_a e_{b+1} e_c)$. It follows that $a_{b+1,c} \neq e_a$. \square

Proof of Theorem 14. Correctness. Recall the proof of correctness in section 2. That proof can easily be adapted to show the correctness of Algorithm 2.

Running time. Because e_b, e_c move clockwise during the Rotate-and-Kill process, $a_{b,c}$ moves clockwise by the bi-monotonicity of $a_{b,c}$ (Lemma 13) and thus can be computed in amortized $O(1)$ time using the unimodality of $\text{area}(\triangle e_a e_b e_c)$ (Lemma 12). Checking whether an all-flush triangle

$\triangle e_a e_b e_c$ is F-3-stable (not necessarily) reduces to checking if e_a, e_b, e_c are stable in this triangle, which takes $O(1)$ time due to the unimodality in Lemma 12. Computing $\text{Kill}_F(b, c)$ takes amortized $O(1)$ time according to property ②. Altogether, Algorithm 2 runs in $O(n)$ time. \square

4 Find one 3-stable and one F-3-stable triangle in $O(n)$ time

forw-stable. v_i is *back-stable* in $\triangle v_i v_j v_k$ if $\text{area}(\triangle v_i v_j v_k) \geq \text{area}(\triangle v_{i-1} v_j v_k)$ (or $i - 1 = k$).

back-stable. v_i is *forw-stable* in $\triangle v_i v_j v_k$ if $\text{area}(\triangle v_i v_j v_k) \geq \text{area}(\triangle v_{i+1} v_j v_k)$ (or $i + 1 = j$).

We define *back-stable* and *forw-stable* for v_j and v_k similarly (note v_i, v_j, v_k in clockwise order). Observe that if v_i is back-stable and forw-stable, it is stable in $\triangle v_i v_j v_k$. (This follows from a unimodality of function $d(X)$ for $X \in [v_j \circlearrowleft v_k]$ where $d(X)$ denotes the distance from X to $\overleftarrow{v_j v_k}$.)

Our algorithm for finding one 3-stable triangle consists of two steps, as shown in the following.

Step 1. Find the largest area triangle $\triangle v_r v_s v_t$ with $r = 1$. See the pseudo code in Algorithm 3.

```

1  $r = 1, s = 2, t = 3, k = 3$ ;
2 for  $j = 2$  to  $n - 1$  do
3   if  $k = j$  then  $k \leftarrow k + 1$ ;
4   while  $v_k$  is not forw-stable in  $\triangle v_r v_j v_k$  do  $k \leftarrow k + 1$  ;
5   if  $\text{area}(\triangle v_r v_j v_k) > \text{area}(\triangle v_r v_s v_t)$  then  $(s, t) \leftarrow (j, k)$ ;
6 end
```

Algorithm 3: Step 1 of our algorithm for finding a 3-stable triangle.

After Line 4, v_k will be the vertex with the largest distance to $\overleftarrow{v_i v_j}$ among all vertices on the right of $\overleftarrow{v_i v_j}$, and thus $\triangle v_r v_j v_k$ will be the triangle with the largest area among all those triangles rooted at v_r, v_j . Further since we try every j at the for-loop, Algorithm 3 finds the largest area triangle with one corner at v_1 . Obviously, this algorithm runs in $O(n)$ time.

Step 2. This step is shown in Algorithm 4 and its analysis is given by the following lemma.

Lemma 22. 1. Initially (namely, at the beginning of Algorithm 4), v_s, v_t are stable in $\triangle v_r v_s v_t$.

2. If v_r is not forw-stable initially, v_r, v_s, v_t will be stable after the while-loop (beginning at Line 2).

3. If v_r is not back-stable initially, v_r, v_s, v_t will be stable after the while-loop (beginning at Line 10).

4. The algorithm terminates in $O(n)$ steps.

Proof. 1. Initially, because $\triangle v_r v_s v_t$ is the largest triangle with $r = 1$, v_s, v_t are stable in $\triangle v_r v_s v_t$.

2. Obviously, a corner is forw-stable or back-stable. When v_r is not forw-stable, it must be back-stable. Therefore, v_r, v_s, v_t are back-stable before entering the while-loop (beginning at Line 2).

We then argue that v_r, v_s, v_t are back-stable throughout the loop. This follows from two facts:

(i) A back-stable corner (e.g. the one at v_r) remains back-stable when we change another corner (e.g. the one at v_s or v_t) forwardly (e.g. $s \leftarrow s + 1$ or $t \leftarrow t + 1$). This is due to Observation 23 below.

```

Input:  $r, s, t$  output by step 1.
1 if  $v_r$  is not forw-stable (in  $\triangle v_r v_s v_t$ ; which is omitted in the following) then
2   while  $v_r$  is not forw-stable do
3      $r \leftarrow r + 1$  ;
4     repeat
5       while  $v_s$  is not forw-stable do  $s \leftarrow s + 1$ ;
6       while  $v_t$  is not forw-stable do  $t \leftarrow t + 1$ ;
7     until none of the above two conditions hold;
8   end
9 end
10 else while  $v_r$  is not back-stable do
11    $r \leftarrow r - 1$ ;
12   repeat
13     while  $v_s$  is not back-stable do  $s \leftarrow s - 1$ ;
14     while  $v_t$  is not back-stable do  $t \leftarrow t - 1$ ;
15   until none of the above two conditions hold;
16 end
17 ;

```

Algorithm 4: Step 2 of our algorithm for finding a 3-stable triangle.

(ii) Upon the execution of $r \leftarrow r + 1$ at Line 3, it holds that v_r is not forw-stable, which means v_{r+1} is back-stable in $\triangle v_{r+1} v_s v_t$. Therefore, after increasing r , the new v_r itself is back-stable. Similarly, v_s is back-stable after $s \leftarrow s + 1$ (Line 5) and v_t is back-stable after $t \leftarrow t + 1$ (Line 6).

On the other hand, according to the conditions of Line 2 and Line 10, it is obvious that v_r, v_s, v_t are forw-stable after the while-loop. Therefore, v_r, v_s, v_t are stable after the while-loop (beginning at Line 2). (This applies the trivial fact that *a corner is stable when it is forw-stable and back-stable.*)

3. The part is symmetric to part 2; proof omitted. (We need the following fact which is symmetric to (i): *A forw-stable corner remains forw-stable when we change another corner backwardly.*)

4. As the area of $\triangle v_r v_s v_t$ increases at every change of r, s, t , the algorithm terminates eventually. Because r, s, t can only increase throughout whereas r cannot return to 1 (otherwise it implies a triangle with a corner at v_1 whose area is larger than the triangle given by Step 1, contradiction), the total number of changes of r, s, t is bounded by $O(n)$; namely, the algorithm has $O(n)$ steps. \square

The following observation is a counterpart of Observation 21. Its trivial proof is omitted.

Observation 23. (a) Assume $v_a, v_b, v_{b'}, v_c, v_{c'}$ are distinct and lie in clockwise order. Then, $\text{area}(\triangle v_a v_{b'} v_c) \geq \text{area}(\triangle v_a v_b v_c)$ implies that $\text{area}(\triangle v_a v_{b'} v_{c'}) > \text{area}(\triangle v_a v_b v_{c'})$.

(b) Assume $v_a, v_{a'}, v_b, v_{b'}, v_c$ are distinct and lie in clockwise order. Then, $\text{area}(\triangle v_a v_{b'} v_c) \geq \text{area}(\triangle v_a v_b v_c)$ implies that $\text{area}(\triangle v_{a'} v_{b'} v_c) > \text{area}(\triangle v_{a'} v_b v_c)$.

Extension. Our algorithm for finding a 3-stable triangle easily extends to finding a F-3-stable triangle. In the first step, we find the smallest area all-flush triangle $\triangle e_r e_s e_t$ with $r = 1$. Thus, we obtain r, s, t where e_s and e_t are stable in $\triangle e_r e_s e_t$. In the second step, if e_r is not stable, we adjust r, s, t using the strategy given in Algorithm 4 (of course, v_r, v_s, v_t should be modified to e_r, e_s, e_t).

Here, we define the concepts back-stable and forw-stable on edges of an all-flush triangle in the same manner. Assume that $\text{area}(\triangle e_i e_j e_k)$ is finite. We state that e_i is *back-stable* in $\triangle e_i e_j e_k$ if $\text{area}(\triangle e_i e_j e_k) \leq \text{area}(\triangle e_{i-1} e_j e_k)$ (or $i-1 = k$), and e_i is *forw-stable* in $\triangle e_i e_j e_k$ if $\text{area}(\triangle e_i e_j e_k) \leq \text{area}(\triangle e_{i+1} e_j e_k)$ (or $i+1 = j$). Obviously, (i) If e_i is back-stable and forw-stable in $\triangle e_i e_j e_k$, it is stable. (ii) e_i is back-stable or forw-stable in $\triangle e_i e_j e_k$. These facts follow from Lemma 12. Moreover, (iii) A back-stable edge (e.g. the one at e_r) remains back-stable when we change another edge (e.g. the one at e_s or e_t) forwardly (e.g. $s \leftarrow s+1$ or $t \leftarrow t+1$). This fact is due to Observation 21.

The analysis of the algorithm for finding a F-3-stable triangle is almost the same as that given in Lemma 22. (The three underlying facts (i), (ii), and (iii) are keys to the analysis.)

Remark 1. Our algorithm given in section 4 (denoted by Alg-One) is different from Alg-DS. First, step 1 of Alg-One sets the initial value of (r, s, t) differently from the initial value $(1, 2, 3)$ used by Alg-DS. Second, step 2 of Alg-One has two symmetric subroutines (one beginning at Line 2, and the other beginning at Line 10), whereas Alg-DS has only one. Moreover, Alg-One finds one 3-stable triangle but Alg-DS does not.

The only thing in common between Alg-One and Alg-DS is that they both contain steps 3–7 of Algorithm 4, yet this does not indicate that Alg-One originates from Alg-DS.

5 Find all G-3-stable triangles in $O(n)$ time

Above all, some G-3-stable triangles that are not 3-stable are shown in Figure 19.

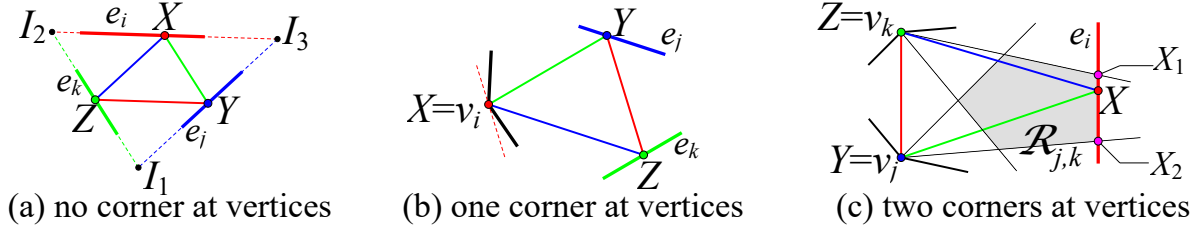


Figure 19: Some G-3-stable triangles that are not 3-stable.

Note 2. As shown by Figure 19 (c), the number of G-3-stable triangles could be infinite if an edge and a chord of P are parallel. In this case, the only two extremal triangle $\triangle X_1 Y Z$ and $\triangle X_2 Y Z$ are canonical. G-3-stable triangles shown in (a) and (b) and 3-stable triangles are also canonical.

Given r, s, t so that $\triangle v_r v_s v_t$ is 3-stable, in this section we design an algorithm for finding all (canonical) G-3-stable triangles. This algorithm generalizes the one for finding all 3-stable triangles.

For ease of discussion, call each edge or vertex of P a *unit*. Denote the $2n$ units $v_1, e_1, \dots, v_n, e_n$ by u_1, \dots, u_{2n} . Assume $u_{r'} = v_r, u_{s'} = v_s, u_{t'} = v_t$ (i.e., $r' = 2r - 1, s' = 2s - 1, t' = 2t - 1$). Denote

$$\mathcal{U}_{r,s,t} = \{(u_b, u_c) \mid b \in \{s', s' + 1, \dots, t'\}, c \in \{t', t' + 1, \dots, r'\}, (b, c) \notin \{(t' - 1, t'), (t', t')\}\}.$$

A unit pair (u_b, u_c) is *G-dead* if there is no G-3-stable $\triangle XYZ$ such that $Y \in u_b$ and $Z \in u_c$ (and that X, Y, Z lie in clockwise order). Be aware that we assume *the edges of P do not contain their endpoints*. Therefore, when we state $X \in e_i$, we disallow X to be equal to any endpoint of e_i . When we state $Y \in u_i$, we disallow Y to be equal to any endpoint of u_i if u_i is an edge.

Be aware that **G-dead is different from dead** for $(u_b, u_c) = (v_j, v_k)$. G-dead implies dead but the reverse is not true. For example, in Figure 19 (c), (v_j, v_k) is dead but not G-dead.

Finding all G-3-stable triangles (sketch). Using a Rotate-and-Kill process (which is shown in Algorithm 5), we find out *all the edge pairs and vertex pairs in $U_{r,s,t}$ that are not G-dead*. (There could be pairs of a vertex and an edge in $U_{r,s,t}$ that are not G-dead, but we do not need to find them out.) The function (oracle) for killing is Kill_G , whose description is given right below in (4).

Denote the set of unit pairs output by the above process by $\text{List}_{r,s,t}$, which contains $O(n)$ unit pairs. Using the same method, we compute two other set of unit pairs $\text{List}_{s,t,r}$ and $\text{List}_{t,r,s}$. Given $\text{List}_{r,s,t}$, $\text{List}_{s,t,r}$, $\text{List}_{t,r,s}$, we then compute all the G-3-stable triangles. This last step is not difficult (by observing that if $\triangle X_1 X_2 X_3$ is G-3-stable, it has a pair of neighboring pairs X_i, X_{i+1} which lie in two vertices simultaneously or lie in two edges simultaneously, and the vertex pair or edge pair containing X_i, X_{i+1} belongs to $\text{List}_{r,s,t} \cup \text{List}_{s,t,r} \cup \text{List}_{t,r,s}$). See the algorithm in subsection 5.3.

Description of Kill_G . Recall Definition 5 for $H_{j,k}, I_{j,k}, J_{j,k}, K_{j,k}$. For each $(u_b, u_c) \in U_{r,s,t}$, define

$$\text{Kill}_G(b, c) = \begin{cases} \text{'b'}, & (u_b, u_c) = (v_j, v_k) \text{ and } v_a \leq I_{j,k}; \\ \text{'c'}, & (u_b, u_c) = (v_j, v_k) \text{ and } v_a > I_{j,k}; \\ \text{'b'}, & (u_b, u_c) = (e_{j-1}, e_{k-1}) \text{ and } v_a \leq H_{j,k}; \\ \text{'c'}, & (u_b, u_c) = (e_{j-1}, e_{k-1}) \text{ and } v_a > H_{j,k}; \\ \text{'b'}, & (u_b, u_c) = (v_j, e_{k-1}) \text{ and } v_a < J_{j,k}; \\ \text{'c'}, & (u_b, u_c) = (v_j, e_{k-1}) \text{ and } v_a \geq J_{j,k}; \\ \text{'b'}, & (u_b, u_c) = (e_{j-1}, v_k) \text{ and } v_a \leq K_{j,k}; \\ \text{'c'}, & (u_b, u_c) = (e_{j-1}, v_k) \text{ and } v_a > K_{j,k}, \end{cases} \quad (4)$$

where v_a denotes the vertex on the right of $\overrightarrow{v_j v_k}$ furthest to $\overleftarrow{v_j v_k}$, and where “ $X < Y$ ” means that X is closer than Y to $\overleftarrow{v_j v_k}$ (and “ $\leq, >, \geq$ ” are defined similarly). Definition (4) generalizes (1).

Note 3. In the vertex-edge case “ $(u_b, u_c) = (v_j, e_{k-1})$ ” the condition is “ $<$ ” or “ \geq ”, whereas in the other three cases it is “ \leq ” or “ $>$ ”. This is not a typo although it looks like one for the readers.

An illustration of Algorithm 5 by a concrete example can be found in appendix A.1.

Analysis of Algorithm 5

The following lemma is crucial to the analysis of Algorithm 5. It is proved in the next subsections.

Lemma 24. Assume $(u_b, u_c) \in U_{r,s,t}$.

1. If $\text{Kill}_G(b, c) = \text{'b'}$, all the edges pairs and vertex pairs in $\{(u_b, u_{c+1}), \dots, (u_b, u_{r'})\}$ are G-dead.

```

1  $(b, c) \leftarrow (s', t'); \quad a \leftarrow r; \quad \text{List} \leftarrow \{(u_b, u_c)\};$ 
2 repeat
3   Let  $j$  be the index so that  $u_b \in \{v_j, e_{j-1}\}$  and  $k$  be the index so that  $u_c \in \{v_k, e_{k-1}\};$ 
4   Compute the vertex  $v_a$  on the right of  $\overrightarrow{v_j v_k}$  furthest to  $\overleftarrow{v_j v_k};$ 
5   if  $\text{Kill}_G(b, c) = \text{'b'}$  then  $b \leftarrow b + 1;$ 
6   else  $c \leftarrow c + 1;$ 
7    $\text{List} \leftarrow \text{List} \cup \{(u_b, u_c)\};$ 
8 until  $(b, c) = (t', r');$ 
```

Algorithm 5: Computing the edge pairs and vertex pairs in $U_{r,s,t}$ that are not G-dead.

2. If $\text{Kill}_G(b, c) = 'c'$, all the edges pairs and vertex pairs in $\{(u_{b+1}, u_c), \dots, (u_{t'}, u_c)\}$ are G-dead.

In fact, the following stronger statements hold (but these statements are neither used nor proved in this manuscript). 1. If $\text{Kill}_G(b, c) = 'b'$, all the unit pairs $(u_b, u_{c+1}), \dots, (u_b, u_{r'})$ are G-dead. 2. If $\text{Kill}_G(b, c) = 'c'$, all the unit pairs $(u_{b+1}, u_c), \dots, (u_{t'}, u_c)$ are G-dead.

Theorem 25. *In $O(n)$ time, Algorithm 5 computes a set of $O(n)$ unit pairs, namely List, which contains all the edge pairs and vertex pairs in $\mathcal{U}_{r,s,t}$ that are not G-dead.*

Proof. Because $\triangle v_r v_s v_t = \triangle u_{r'} u_s u_{t'}$ is 3-stable, $(u_{t'}, u_{r'})$ is not G-dead. This implies that the algorithm eventually arrives at a state with $(b, c) = (t', r')$, at which it terminates. Upon termination, each edge pair and vertex pair in $\mathcal{U}_{r,s,t}$ that is not G-dead is in List, as a corollary of Lemma 24.

(To be rigorous, we also need to prove that $(b, c) \notin \{(t' - 1, t'), (t', t')\}$ throughout the process. This easily follows from the fact that $\text{Kill}_G(t' - 2, t') = 'c'$, which is implicitly shown in Note 1.)

Throughout Algorithm 5, indices b, c and hence j, k increase monotonously. This implies that v_a can be computed in $O(1)$ amortized time. Therefore, computing $\text{Kill}_G(b, c)$ only takes $O(1)$ amortized time. So, Algorithm 5 runs in $O(n)$ time. \square

5.1 Preliminaries for proving Lemma 24

Observation 26. *Assume $\triangle XYZ$ is G-3-stable (X, Y, Z in clockwise order). Recall Figure 19.*

1. If X, Y, Z lie in e_i, e_j, e_k respectively (recall that we disallow X to be equal to any endpoint of e_i when we state that X_i lies in e_i), then e_i, e_j, e_k are distinct and in clockwise order and X, Y, Z are respectively the midpoints of $I_2 I_3, I_3 I_1$, and $I_1 I_2$, where I_1, I_2, I_3 respectively denote the intersecting point between ℓ_j, ℓ_k , and that between ℓ_k, ℓ_i , and that between ℓ_i, ℓ_j .

2. If X lies at a vertex v_i and Y, Z lie in e_j, e_k respectively, then v_i, e_j, e_k are in clockwise order, and e_j cannot admit v_i as an endpoint (otherwise Y cannot be stable) and e_k cannot admit v_i as an endpoint (otherwise Z cannot be stable), and Y is the unique point in e_j such that $v_i Y \parallel e_k$, and Z is the unique point in e_k such that $v_i Z \parallel e_j$.

3. If X lies in e_i and Y, Z lie at vertices v_j, v_k respectively, then e_i, v_j, v_k are in clockwise order and $v_j v_k \parallel e_i$ (otherwise X cannot be stable). Moreover, X lies in $X_1 X_2$ – the intersecting segment of e_i and $\mathcal{R}_{j,k}$. In this case, the area of $\triangle X' v_j v_k$ is a constant for any X' in $X_1 X_2$.

Proof. 1. See Figure 19 (a). Since X, Y, Z are stable, $XY \parallel e_k, YZ \parallel e_i$ and $ZX \parallel e_j$. So, $|I_2 X| : |X I_3| = |I_1 Y| : |Y I_3| = |I_1 Z| : |Z I_2| = |I_3 X| : |X I_2|$. Hence $|I_3 X| = |X I_2|$, so $X = (I_2 + I_3)/2$. Similarly, $Y = (I_3 + I_1)/2$ and $Z = (I_1 + I_2)/2$.

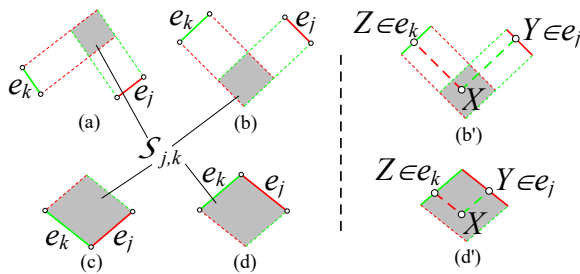


Figure 20: Illustration of the definition of $\mathcal{S}_{j,k}$.

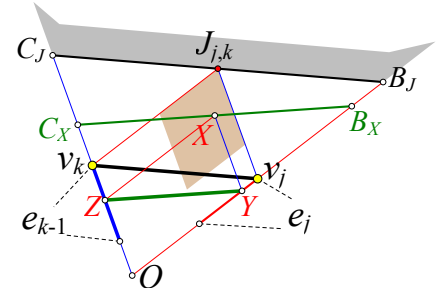


Figure 21: Proof of Observation 28 part 3

Part 2 is trivial. The proof of part 3 is similar to that of Observation 8 part 1. \square

Definition 27. For each edge pair (e_j, e_k) , define $\mathcal{S}_{j,k}$ as the intersecting region of two strips: The first strip is bounded by the two lines parallel to e_k at the two endpoints of e_j respectively. The second strip is bounded by the two lines parallel to e_j at the two endpoints of e_k respectively. See Figure 20 (a)-(d). Regard that $\mathcal{S}_{j,k}$ does **not** contain its boundaries. Note that $\mathcal{S}_{j,k} = \emptyset$ if $e_j \parallel e_k$.

Observation 28. 1. Given two distinct edges e_j, e_k and assume that there is a $\triangle XYZ$ with $Y \in e_j, Z \in e_k$, and $X \in \partial P$, where Y, Z are stable, then X must lie in $\mathcal{S}_{j,k}$.

2. A pair (e_j, e_k) is G-dead if (1) $\mathcal{S}_{j,k}$ does not intersect P or (2) $e_k \prec e_j$.
3. A pair (e_j, e_{k-1}) is G-dead if there exists some point A in P which lies on the right of $\overrightarrow{v_j v_k}$ such that $A \geq J_{j,k}$ in the distance to $\overleftarrow{v_j v_k}$.
4. A pair (v_j, v_k) is G-dead if (1) $\mathcal{R}_{j,k}$ does not intersect P or (2) $e_k \prec e_j$ or (3) there exists some point A in P which lies on the right of $\overrightarrow{v_j v_k}$ such that $A > K_{j,k}$ in the distance to $\overleftarrow{v_j v_k}$.

Proof. 1. Since $Y \in e_j$ is stable, we get $XZ \parallel e_j$. So X lies in the aforementioned strip parallel to e_j . Since $Z \in e_k$ is stable, we get $XY \parallel e_k$. So X lies in the aforementioned strip parallel to e_k .

2. When $\mathcal{S}_{j,k}$ does not intersect P , there is no G-3-stable $\triangle XYZ$ such that Y, Z are restricted to e_j, e_k respectively according to part 1 of this observation; namely, (e_j, e_k) is G-dead.

Next, suppose that $e_k \prec e_j$ yet (e_j, e_k) is not G-dead. Then, there is a G-3-stable $\triangle XYZ$ such that $Y \in e_j$ and $Z \in e_k$. We require that X, Y, Z lie in clockwise order. However, X, Y, Z lie in counterclockwise order since (i) $X \in \mathcal{S}_{j,k}$ (by part 1) and (ii) $e_k \prec e_j$; see Figure 20 (b') and (d').

3. Suppose (e_j, e_{k-1}) is not G-dead. It implies a G-3-stable $\triangle XYZ$ with $Y \in e_j$ and $Z \in e_{k-1}$; see Figure 21. We claim that $A > X$ in the distance to $\overleftarrow{Y Z}$ (and hence X is not stable in $\triangle XYZ$).

Make a parallel line of YZ at X . Assume that it intersects ℓ_j, ℓ_{k-1} at B_X, C_X , respectively. Make a parallel line of $v_j v_k$ at $J_{j,k}$. Assume that it intersects ℓ_j, ℓ_{k-1} at B_J, C_J , respectively. Let ϕ be the closed region on the right of $\overrightarrow{B_J C_J}$, the right of e_j , and the right of e_{k-1} . Let $O = \ell_j \cap \ell_{k-1}$.

Following the assumption that $A \in P$ and $A \geq J_{j,k}$ in the distance to $\overleftarrow{v_j v_k}$, point A lies in ϕ . Observe that $|OB_X| = 2|OY| < 2|Ov_j| = |OB_J|$ and $|OC_X| = 2|OZ| < 2|Ov_k| = |OC_J|$. Therefore, any point in ϕ (in particular, point A) is further than X in the distance to $\overleftarrow{Y Z}$. So the claim holds.

4. Observation 8 states that (v_j, v_k) is dead under cases (1)-(3). In fact, using the proof of Observation 8, we can obtain the stronger result that states (v_j, v_k) is G-dead under these cases. \square

5.2 Proof of Lemma 24

According to the definition of Kill_G in (4), proving Lemma 24 reduces to proving the following $4 \times 2 = 8$ arguments. (Assume $j \in [s, t]$, $k \in [t, r]$, and $j \neq k$ in the following.)

- VV1: if $v_a \leq I_{j,k}$, $(v_j, v_{k'})$ is G-dead for $k' \in [k+1, r]$.
- VV2: if $v_a > I_{j,k}$, $(v_{j'}, v_k)$ is G-dead for $j' \in [j+1, t]$.
- EE1: if $v_a \leq H_{j,k}$, $(e_{j-1}, e_{k'})$ is G-dead for $k' \in [k, r-1]$.
- EE2: if $v_a > H_{j,k}$, $(e_{j'}, e_{k-1})$ is G-dead for $j' \in [j, t-1]$.
- VE1: if $v_a < J_{j,k}$, $(v_j, v_{k'})$ is G-dead for $k' \in [k, r]$.
- VE2: if $v_a \geq J_{j,k}$, $(e_{j'}, e_{k-1})$ is G-dead for $j' \in [j, t-1]$.
- EV1: if $v_a \leq K_{j,k}$, $(e_{j-1}, e_{k'})$ is G-dead for $k' \in [k, r-1]$.
- EV2: if $v_a > K_{j,k}$, $(v_{j'}, v_k)$ is G-dead for $j' \in [j, t]$.

Note that EE1 and EE2 are respectively contained by EV1 and VE2 (using $K_{j,k} > H_{j,k} > J_{j,k}$).

In the proof of Lemma 6, some vertex pairs are proved dead under certain cases, and it is easy to see that these vertex pairs are actually G-dead therein. Therefore, the proof of Lemma 6 can be borrowed to prove VV1 and VV2 without much change.

Note that VE1 is almost contained by VV1. The only claim in VE1 not covered by VV1 is the following: (i) (v_j, v_k) is G-dead when $v_a < J_{j,k}$. Note that EV2 is almost contained by VV2. The only claim in EV2 not covered by VV2 is the following: (ii) (v_j, v_k) is G-dead when $v_a > K_{j,k}$. We leave the proofs of claims (i) and (ii) as exercises for the reader (they should already be obvious), and we prove EV1 and VE2 in the following to complete the proof of Lemma 24.

Proof of EV1. First, we argue that (e_{j-1}, e_k) is G-dead. Note that $\mathcal{S}_{j-1,k} = \emptyset$ if $e_{j-1} \parallel e_k$. Therefore, (e_{j-1}, e_k) is G-dead when $e_{j-1} \parallel e_k$ or $e_k \prec e_{j-1}$ (applying Observation 28 part 2). Assume $e_{j-1} \prec e_k$ in the following. See Figure 22 (a). Let l be the line at $K_{j,k}$ that is parallel to $v_j v_k$, and let ϕ denote the (closed) half-planes delimited by l and containing $v_j v_k$. Following the assumption that $v_a \leq K_{j,k}$, polygon P is contained in ϕ . Moreover, $\mathcal{S}_{j-1,k}$ clearly is disjoint with ϕ . Together, $\mathcal{S}_{j-1,k}$ does not intersect P , and thus (e_{j-1}, e_k) is G-dead (due to Observation 28 part 2). The same argument applies to any pair $(e_{j-1}, e_{k'})$ where $k' \in [k, r-1]$. \square

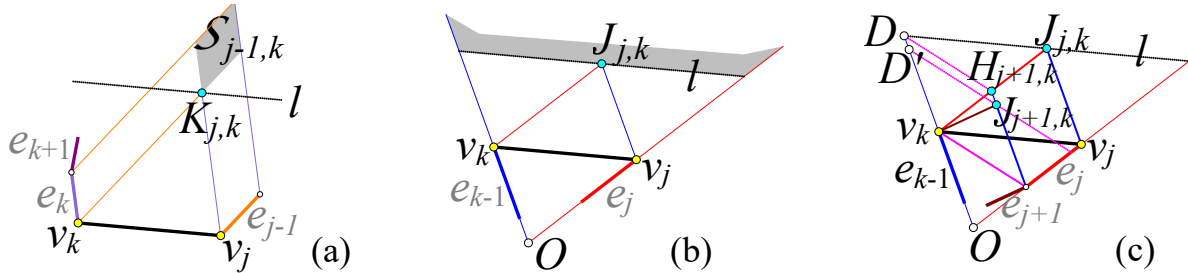


Figure 22: Illustration of the proofs of EV1 and VE2.

Proof of VE2. Because $v_a \geq J_{j,k}$, we get $J_{j,k} \neq \infty$ and $e_j \prec e_{k-1}$. See Figure 22 (b). Let $d_{j,k}(X)$ denote the distance from X to $\overrightarrow{v_j v_k}$ for any pair (v_j, v_k) such that $j \neq k$. Let l be the line at $J_{j,k}$ that is parallel to $v_j v_k$. Denote by ϕ the closed half-plane delimited by l and not containing v_b, v_c .

Since $v_a \geq J_{j,k}$, pair (e_j, e_{k-1}) is G-dead (due to Observation 28 part 3).

See Figure 22 (c). Denote by D the intersecting point between l and ℓ_{k-1} . Make a parallel line of $v_{j+1}v_k$ at $J_{j+1,k}$, and denote its intersecting point with ℓ_{k-1} by D' . Since $v_a \geq J_{j,k}$, point v_a lies in ϕ . Since that $v_a \in P$, this point also lies in p_{k-1} . Together, we obtain that $d_{j+1,k}(v_a) \geq d_{j+1,k}(D)$. Moreover, it is clear that $d_{j+1,k}(D) = d_{j+1,k}(H_{j+1,k}) > d_{j+1,k}(J_{j+1,k})$. Altogether, we get $d_{j+1,k}(v_a) > d_{j+1,k}(J_{j+1,k})$, which implies that (e_{j+1}, e_{k-1}) is G-dead (due to Observation 28 part 3). By induction, we can see $(e_{j'}, e_{k-1})$ is G-dead for $j' \in [j, t-1]$. \square

5.3 Computing all G-3-stable triangles from $\text{List}_{r,s,t}$, $\text{List}_{s,t,r}$, $\text{List}_{t,r,s}$

Suppose we are given r, s, t such that $\triangle v_r v_s v_t$ is 3-stable. Suppose $\text{List}_{r,s,t}$, $\text{List}_{s,t,r}$, $\text{List}_{t,r,s}$ are preprocessed. We show how to find all canonical G-3-stable triangles in the following.

Recall Note 2 for canonical G-stable triangles. Henceforth, for convenience, we abuse the notation a little so that a **G-3-stable triangle** refers to a **canonical G-3-stable triangle**.

Denote by $Q_{r,s,t}$ the set of G-3-stable $\triangle XYZ$ where $Y \in [v_s \circ v_t]$ and $Z \in [v_t \circ v_r]$, and where neither Y nor Z or both of them lie at vertices of P (and X, Y, Z lie in clockwise order).

Observation 29. $Q_{r,s,t} \cup Q_{s,t,r} \cup Q_{t,r,s}$ contains all the G-3-stable triangles.

Proof. Take any G-3-stable triangle $\triangle XYZ$. It has two corners which both lie at vertices of P or both lie in edges of P . Without loss of generality, assume that Y and Z are such a pair of corners. By Lemma 2 part 3, $\triangle XYZ$ interleaves $\triangle v_r v_s v_t$. Therefore, there are three possibilities: 1. $Y \in [v_s \circ v_t]$ and $Z \in [v_t \circ v_r]$. In this case, $\triangle XYZ \in Q_{r,s,t}$. 2. $Y \in [v_t \circ v_r]$ and $Z \in [v_r \circ v_s]$. In this case, $\triangle XYZ \in Q_{s,t,r}$. 3. $Y \in [v_r \circ v_s]$ and $Z \in [v_s \circ v_t]$. In this case, $\triangle XYZ \in Q_{t,r,s}$. \square

Denote $Q = Q_{r,s,t}$ and $\text{List} = \text{List}_{r,s,t}$. We show how to compute Q from List in the following, and we can compute $Q_{s,t,r}$ from $\text{List}_{s,t,r}$ and compute $Q_{t,r,s}$ from $\text{List}_{t,r,s}$ using the same method.

Consider the vertex (or two vertices) with the largest distance to $\overrightarrow{v_j v_k}$ on the right of $\overrightarrow{v_j v_k}$. If there is only one such vertex, we define it to be $A_{j,k}$ and $A_{j,k}^*$. Otherwise, there are two such vertices. The (clockwise) first one is defined to be $A_{j,k}$ and the last one is defined to be $A_{j,k}^*$.

Observation 30. Assume that $\triangle XYZ$ is G-3-stable, where $Y \in u_b, Z \in u_c$. We claim that $X \in [A_{j,k} \circ A_{j,k}^*]$ if $(u_b, u_c) = (v_j, v_k)$, and that $X \in [A_{j,k} \circ A_{j+1,k+1}^*]$ if $(u_b, u_c) = (e_j, e_k)$.

Proof. We only show the proof of the second claim, as the first claim is trivial. Suppose $(u_b, u_c) = (e_j, e_k)$ yet $X \notin [A_{j,k} \circ A_{j+1,k+1}^*]$. First, notice that $e_j \prec e_k$. This follows from Observation 28 part 2 and the fact that (e_j, e_k) is not G-dead. Next, there are two symmetric cases: $X \in [v_{k+1} \circ A_{j,k}]$ or $X \in [A_{j+1,k+1}^* \circ v_j]$. Without loss of generality, assume the first case occurs.

See Figure 23 (a). Denote by ϕ_1 the half-plane at X which is parallel to $v_j v_k$ and does not contain $v_j v_k$. Denote by ϕ_2 the half-plane at X which is parallel to YZ and does not contain YZ . By the definition of $A_{j,k}$, it lies in ϕ_1 . This implies that $A_{j,k} \in \phi_2$ since YZ intersects $v_j v_k$ whereas X lies between v_{k+1} and $A_{j,k}$. It follows that X is not stable in $\triangle XYZ$. Contradictory. \square

Our first algorithm for computing Q is given in Algorithm 6 (some details of this algorithm are elaborated below). The correctness of Algorithm 6 follows from Observation 30.

- 1 Compute $A_{j,k}$ and $A_{j,k}^*$ for each vertex pair $(v_j, v_k) \in \text{List}$;
- 2 **foreach** vertex pair $(v_j, v_k) \in \text{List}$ and unit u_i in $[A_{j,k} \odot A_{j,k}^*]$ **do** Output all G-3-stable triangle $\triangle XYZ$ such that $X \in u_i, Y \in v_j$ and $Z \in v_k$;
- 3 Compute $A_{j,k}$ and $A_{j+1,k+1}^*$ for each edge pair $(e_j, e_k) \in \text{List}$;
- 4 **foreach** edge pair $(e_j, e_k) \in \text{List}$ and unit u_i in $[A_{j,k} \odot A_{j+1,k+1}^*]$ **do** Output all G-3-stable triangle $\triangle XYZ$ such that $X \in u_i, Y \in e_j$ and $Z \in e_k$;

Algorithm 6: Compute Q from List (the first naive algorithm).

Running time analysis. According to Algorithm 5, the pairs $(u_{b_1}, u_{c_1}), \dots, (u_{b_m}, u_{c_m})$ in List has a monotonicity property that b_1, \dots, b_m are increasing (non-strictly) and so as c_1, \dots, c_m . Therefore, if (v_j, v_k) is taken over all vertex pairs in List in order, $A_{j,k}$ and $A_{j,k}^*$ move in clockwise and thus can be computed in amortized $O(1)$ time. Therefore, Line 1 costs $O(n)$ time. So as Line 3.

Following Observation 26, given any three units u_i, u_b, u_c , we can compute in $O(1)$ time all the (canonical) G-3-stable triangles with corners restricted to these units respectively. So Lines 2 and 4 both take $O(1)$ time. Therefore, the total running time of Algorithm 6 is $O(T)$, where

$$T = \sum_{(v_j, v_k) \in \text{List}} |A_{j,k} \odot A_{j,k}^*| + \sum_{(e_j, e_k) \in \text{List}} |A_{j,k} \odot A_{j+1,k+1}^*|, \quad (5)$$

where $|X \odot Y|$ denotes the number of vertices in $[X \odot Y]$.

The first term of T is easily bounded by $O(n)$ using the monotonicity property of List. However, the second term of T could be $\Omega(n^2)$ in the worst case! Assume $(e_j, e_k), \dots, (e_j, e_{k'})$ are $\Omega(n)$ edge pairs in List. Assume $A_{j,k} = \dots = A_{j,k'} = v_a$ and $A_{j+1,k+1}^* = \dots = A_{j+1,k'+1}^* = v_{a'}$ and there are $\Omega(n)$ units in $[v_a \odot v_{a'}]$. See Figure 23 (b). In this case, the second term of T would be $\Omega(n^2)$.

In the remaining part of this section, we optimize Algorithm 6 by a batch technique.

Lemma 31. 1. For $(e_j, e_k), \dots, (e_j, e_{k'}) \in \text{List}$, we can use a batch to find all G-3-stable $\triangle XYZ$ where $Y \in e_j$ and Z lies in some edge in $e_k, \dots, e_{k'}$, in $O(k' - k + |A_{j,k} \odot A_{j+1,k'+1}^*|)$ time.

2. For $(e_j, e_k), \dots, (e_{j'}, e_k) \in \text{List}$, we can use a batch to find all G-3-stable $\triangle XYZ$ where $Z \in e_k$ and Y lies in some edge in $e_j, \dots, e_{j'}$, in $O(j' - j + |A_{j,k} \odot A_{j'+1,k+1}^*|)$ time.

Proof. 1. For each $e_h \in \{e_k, \dots, e_{k'}\}$, let Ans_h be the set of G-3-stable $\triangle XYZ$ with $Y \in e_j$ and $Z \in e_h$. Make two parallel lines of e_j at the two endpoints of e_h , as shown in Figure 23 (c). This defines a stripe ϕ_h . Assume ϕ_h does not contain its boundaries. Denote $\rho = [A_{j,k} \odot A_{j+1,k'+1}^*]$.

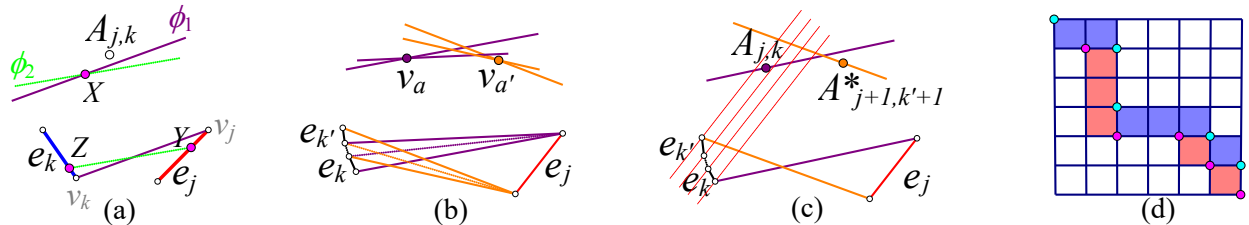


Figure 23: (a) illustrates Observation 30. (b) illustrates that the running time of Algorithm 6 could be $\Omega(n^2)$; see an explanation right below. (c) and (d) illustrate the batch technique given below.

For each $\triangle XYZ \in \text{Ans}_h$, we have (i) $X \in \phi_h$ and (ii) $X \in \rho$. Fact (i) is because $XZ \parallel e_j$, whereas fact (ii) comes from Observation 30. Based on these two facts, computing Ans_h reduces to enumerating all the units in ρ that intersect ϕ_h . Therefore, computing $\text{Ans}_k, \dots, \text{Ans}_{k'}$ reduces to enumerating all the units in ρ that intersect $\phi_k, \dots, \phi_{k'}$ respectively.

Since the stripes $\phi_k, \dots, \phi_{k'}$ do not overlap and has a monotonicity property (to prove this, we need to apply the fact that $e_j \prec e_k, \dots, e_j \prec e_{k'}$. Note that Ans_h is empty if e_j is not chasing e_h ; without loss of generality, we can assume that $e_j \prec e_k, \dots, e_j \prec e_{k'}$), enumerating the aforementioned units only take $O(k' - k + |A_{j,k} \circ A_{j+1,k'+1}^*|)$ time. Therefore, part 1 holds.

The proof of part 2 is symmetric to the proof of part 1 and is thus omitted. \square

Optimize Algorithm 6 to $O(n)$ time (using the batches mentioned in Lemma 31). We change Lines 4 and 4 to the following scheme with multiple rounds. In round one, take the first edge pair in List and take as many edge pairs in List as long as they are still in the same row. Handle the edge pairs taken in this round (which are in a row) by a batch. In round two, take the next edge pair in List and take as many edge pairs in List as long as they are still in the same column. Handle the edge pairs taken in this round (which are in a column) by a batch. Repeat these two rounds alternatively until all edge pairs in List are handled. See an illustration in Figure 23 (d). Following Lemma 31, the total running time of the odd rounds can be bounded by $O(n)$, so as the total running time of the even rounds. Therefore, the overall running time is $O(n)$.

As a summary, we can compute all the G-3-stable triangles in $O(n)$ time.

A connection between the G-3-stable and the minimum enclosing triangle. Assume $T = \triangle xyz$ is a locally minimum area triangle among the triangles enclosing P . It is proved in [17] (and rediscovered in many places) that *the midpoint of each side of T touches P* . Therefore, X, Y, Z lie in ∂P , where Z, X, Y denote the midpoints of the three sides xy, yz, zx of T .

Moreover, X, Y, Z are all stable in $\triangle XYZ$, because $\triangle xyz$ contains P , $yz \parallel YZ$, $zx \parallel ZX$, and $xy \parallel XY$. Therefore, $\triangle XYZ$ is G-3-stable. (Yet it may not be canonical; see Note 2. However, if it is not canonical, we can find a canonical one with the same area).

Further since it is easy to compute x, y, z in $O(1)$ time from X, Y, Z , finding the locally minimum triangles enclosing P reduces to computing the (canonical) G-3-stable triangles.

6 Find the all-flush triangle with the minimum perimeter

We give some preliminaries first.

Observation 32. Assume rays r_1, r_2 originate from point A , and r_2 is on the right of r_1 ; see Figure 24. Assume circle O is tangent to r_1 and r_2 at points J, K respectively. Let \widehat{JK} denote the arc starting from J and counterclockwise to K . Consider any segment BC that connects r_1 and r_2 .

1. If BC is tangent to \widehat{JK} , the perimeter of $\triangle ABC$ equals $2|AJ|$.
2. If BC lies below \widehat{JK} as shown in Figure 24, the perimeter of $\triangle ABC$ is smaller than $2|AJ|$.
3. Otherwise, the perimeter of $\triangle ABC$ is larger than $2|AJ|$.

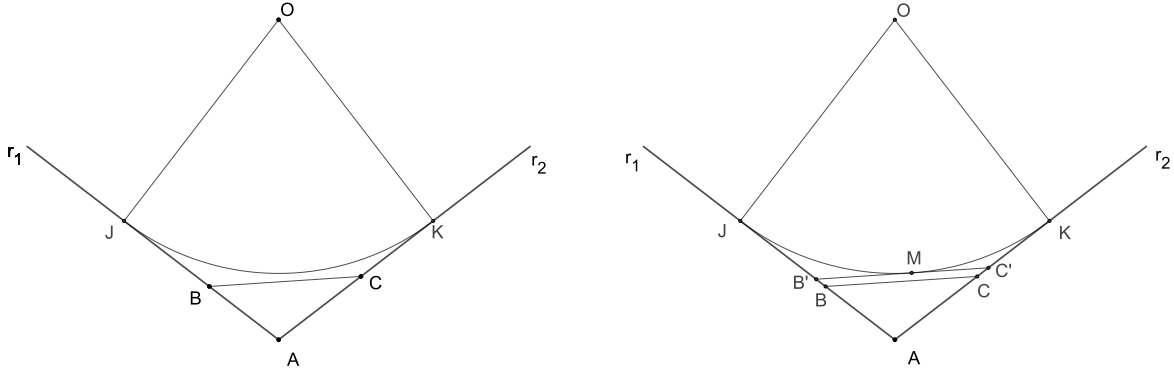


Figure 24: Illustration of Observation 32

Proof. We only prove the first claim. The other claims follow from the first one immediately.

Consider any segment $B'C'$ tangent to \widehat{JK} (see the right picture of Figure 24 for example). The perimeter of $\triangle AB'C'$ equals $(|AB'| + |B'M|) + (|MC'| + |C'A|) = |AJ| + |AK| = 2|AJ|$. \square

Observation 33. Assume rays r_1, r_2 originate from point A , and r_2 is on the right of r_1 ; assume moreover that point G is on the right of r_1 and on the left of r_2 ; see Figure 25. We claim that there exists a unique circle O tangent to r_1, r_2 such that the arc \widehat{JK} passes through G , where J denotes the tangent point of circle O and r_1 , and where K denotes the tangent point of circle O and r_2 .

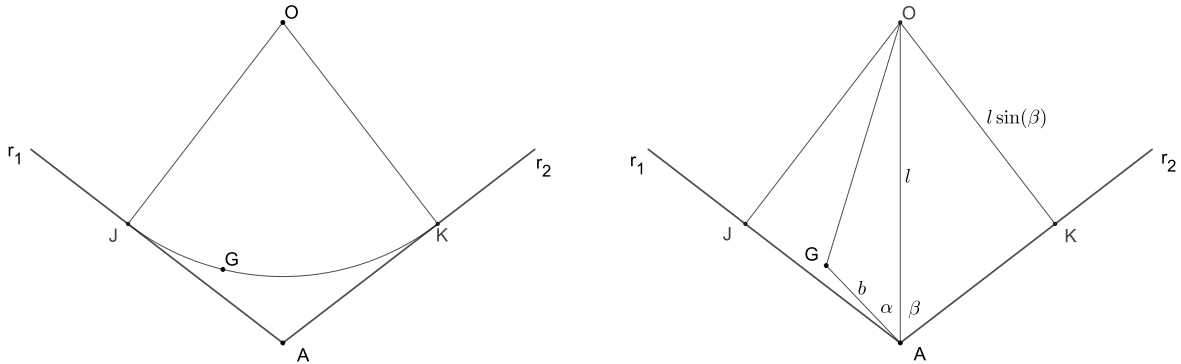


Figure 25: Illustration of Observation 33

Proof. First, we argue that there cannot be more than one such circles. We prove it by contradiction. Suppose that O_1, O_2 are two such circles. Let B_1C_1 be the segment connecting r_1, r_2 which is tangent to O_1 at G . Let B_2C_2 be the segment connecting r_1, r_2 which is tangent to O_2 at G .

Be aware that B_2C_2 is different from B_1C_1 (otherwise $O_1 = O_2$). Since B_1C_1 the tangent line of O_1 at G , segment B_2C_2 cuts the circle O_1 . Applying Observation 32, $\triangle AB_2C_2$ has a larger perimeter than $\triangle AB_1C_1$. Since B_2C_2 the tangent line of O_2 at G , segment B_1C_1 cuts the circle O_2 . Applying Observation 32, $\triangle AB_1C_1$ has a larger perimeter than $\triangle AB_2C_2$. Contradiction.

Next, we argue that there exists at least one circle O satisfying the requirement.

See the right picture of Figure 25. Let α, β denote the angle as shown in the figure and let $b = |AG|$, which are fixed by the assumption. As circle O must be tangent to r_1, r_2 , point O lies on the bisector of r_1, r_2 , and hence its position can be specified by the length $l = |OA|$. It reduces to showing that there exists a number $l > 0$ so that $OK = OG$ and $\angle AOG < \angle AOK$.

According to the requirement $OK = OG$, we get $OK^2 = OG^2$, namely, $l^2 \sin^2 \beta = b^2 + l^2 - 2bl \cos \alpha$. In other words, $\cos^2 \beta \cdot l^2 - 2b \cos \alpha \cdot l + b^2 = 0$. One solution to this equation is

$$l = b \cdot \left(\cos \alpha + \sqrt{\cos^2 \alpha - \cos^2 \beta} \right) / \cos^2 \beta. \quad (6)$$

For this particular l , we have $OK = OG$ and it remains to be shown that $\angle AOG < \angle AOK$. Because $\alpha < \beta$, we have $\frac{\cos \alpha}{\cos \beta} > \frac{\sin \alpha}{\sin \beta}$. So, $\frac{l \cos \beta}{b} > \frac{\sin \alpha}{\sin \beta}$ (applying (6)). So $\cos \beta > \frac{b \sin \alpha}{l \sin \beta}$. Further since $\frac{\sin \angle AOG}{b} = \frac{\sin \alpha}{l \sin \beta}$, we get $\sin \angle AOG = \frac{b \sin \alpha}{l \sin \beta} < \cos \beta = \sin \angle AOK$. So, $\angle AOG < \angle AOK$. \square

6.1 Unimodality and bi-monotonicity

Let $M_A(B, C)$ denote the unique point M on BC such that $|AB| + |BM| = |AC| + |CM|$.

Observation 34. Let r_1, r_2, G be the same as Observation 33. Let BC be the segment connecting r_1, r_2 , passing through G , and tangent to the circle O mentioned in Observation 33; see Figure 26.

Consider another segment $B'C'$ connecting r_1, r_2 and passing through G . Let $M' = M_A(B', C')$.

If C' is between A, C , point M' is to the left of G (namely, B', M', G, C' lie in order).

If B' is between A, B , point M' is to the right of G (namely, B', G, M', C' lie in order).

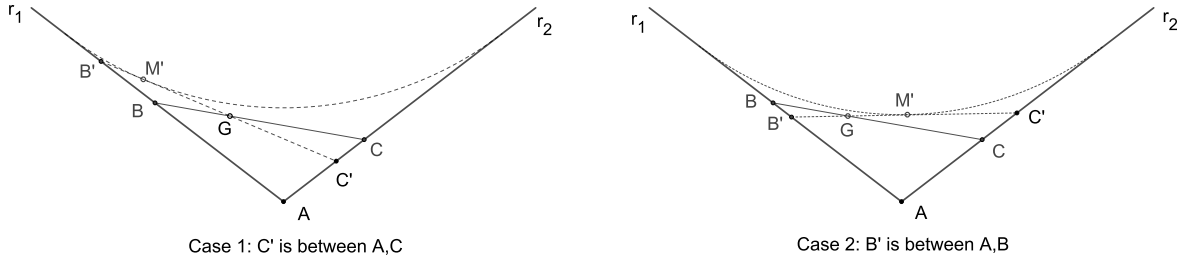


Figure 26: Illustration of Observation 34

Proof. We only show the proof of the first case. The proof of the other case is symmetric.

Because BC is tangent to the circle O defined in Observation 34, whereas $B'C'$ cuts circle O , $\triangle ABC$ has a smaller perimeter than $\triangle AB'C'$ (due to Observation 32). Build the circle O' tangent

to r_1, r_2 and $B'C'$, a part of which is drawn as the dotted arc (see the left part of Figure 26). Since $\triangle ABC$ has a smaller perimeter than $\triangle AB'C'$, segment BC lies below the arc (by Observation 32). Therefore, GC' is below the arc. It follows that the tangent point M' is between B' and G . \square

Observation 35. *Let $r_1, r_2, G, B, C, B', C'$ be the same as Observation 34. see Figure 26.*

The perimeter of $\triangle AB'C'$ grows if we move B' along r_1 away from A starting at B (meanwhile move C' along the opposite direction of r_2 so that $B'C'$ passes through the fixed point G).

The perimeter of $\triangle AB'C'$ grows if we move C' along r_2 away from A starting at C (meanwhile move B' along the opposite direction of r_1 so that $B'C'$ passes through the fixed point G).

Proof. We only show the proof of the claim on B' . The proof of the claim on C' is symmetric.

Suppose there is another segment $B''C''$ connecting r_1, r_2 , passing through G , with $|AB''| > |AB'| > |AB|$. We shall prove the following (x): $\triangle AB''C''$ has a larger perimeter than $\triangle AB'C'$.

Let O' be the circle tangent to r_1, r_2 and $B'C'$. By Observation 34, the tangent point M' of segment $B'C'$ and circle O' is on the left of G , as shown in the left picture of Figure 26. It follows that $B''C''$ cuts circle O' . Further due to Observation 32, we obtain the argument (x) above. \square

Lemma 36 (Unimodality of $\text{perimeter}(\triangle e_i e_j e_k)$). *Fix two indices i, j such that $e_i \prec e_j$. Let E be the set of e_k such that $e_k \prec e_i$ and $e_j \prec e_k$, which is obviously an interval of edges. We claim that the perimeter of $\triangle e_i e_j e_k$ is unimodal when e_k is taken over the edges in E in clockwise. More precisely, for $e_{k-1}, e_k, e_{k+1} \in E$, we claim that it cannot occur that*

$$\text{perimeter}(\triangle e_i e_j e_k) \geq \text{perimeter}(\triangle e_i e_j e_{k-1}) \text{ and } \text{perimeter}(\triangle e_i e_j e_k) \geq \text{perimeter}(\triangle e_i e_j e_{k+1}). \quad (7)$$

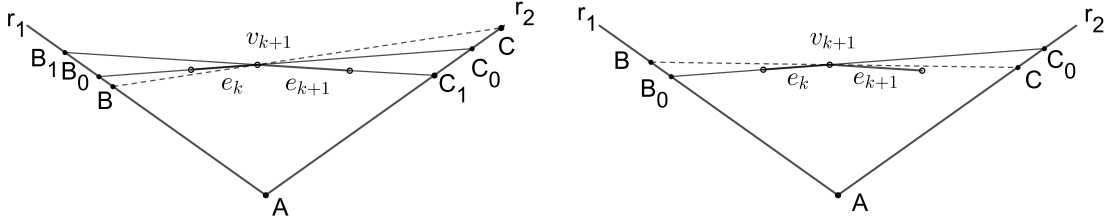


Figure 27: Illustration of the proof of Lemma 36

Proof. Let r_1, r_2 be the rays containing e_j, e_i respectively as shown in Figure 27. Assume ℓ_k intersect r_1, r_2 at B_0, C_0 respectively, and ℓ_{k+1} intersect r_1, r_2 at B_1, C_1 respectively.

This lemma follows from the following three facts immediately.

1. If $\text{perimeter}(\triangle e_i e_j e_k) \geq \text{perimeter}(\triangle e_i e_j e_{k+1})$, point $M_A(B_0, C_0)$ is on the right of v_{k+1} .
2. If $\text{perimeter}(\triangle e_i e_j e_k) \geq \text{perimeter}(\triangle e_i e_j e_{k-1})$, point $M_A(B_0, C_0)$ is on the left of v_k .
3. Point $M_A(B_0, C_0)$ cannot be on the right of v_{k+1} and on the left of v_k .

Fact 3 is trivial. Fact 2 is symmetric to Fact 1. We prove Fact 1 in the following.

Choose $G = v_{k+1}$ and let BC be the segment connecting r_1, r_2 that is tangent to the circle O given in Observation 33. First, we argue that $|AC| < |AC_0|$. Suppose to the opposite that $|AC| \geq |AC_0|$, as shown in the left picture of Figure 27. We obtain from Observation 35 that $\triangle AB_1C_1$ has a larger perimeter than $\triangle AB_0C_0$, namely, $\text{perimeter}(\triangle e_i e_j e_k) < \text{perimeter}(\triangle e_i e_j e_{k+1})$.

Next, observe the right picture of Figure 27, where $|AC| < |AC_0|$. Since $|AC_0| > |AC|$, we obtain from Observation 34 that $M_A(B_0, C_0)$ is on the right of v_{k+1} . \square

Definition 37. For any two indices i, j such that $e_i \prec e_j$, denote by $\text{opt}_{i,j}$ the index k in set $\{k \mid e_j \prec e_k, e_k \prec e_i\}$ which minimizes $\text{perimeter}(\triangle e_i e_j e_k)$. Be aware that there could be two consecutive indices which minimize $\text{perimeter}(\triangle e_i e_j e_k)$ according to the unimodality of $\text{perimeter}(\triangle e_i e_j e_k)$ (Lemma 36); in this case, we denote by $\text{opt}_{i,j}$ the first index between the two indices.

Lemma 38 (Bi-monotonicity of $\text{opt}_{i,j}$). *It holds that $\text{opt}_{i+1,j} \geq \text{opt}_{i,j}$ and $\text{opt}_{i,j+1} \geq \text{opt}_{i,j}$.*

Note: $\text{opt}_{i+1,j}$ and $\text{opt}_{i,j}$ are in the interval $[j+1, i]$. The inequality $\text{opt}_{i+1,j} \geq \text{opt}_{i,j}$ means that $\text{opt}_{i+1,j} = \text{opt}_{i,j}$ or $\text{opt}_{i+1,j}$ is after $\text{opt}_{i,j}$ when we enumerate indices in $[j+1, i]$ from $j+1$ to i . The inequality $\text{opt}_{i,j+1} \geq \text{opt}_{i,j}$ has a similar meaning. (Similar to Lemma 13.)

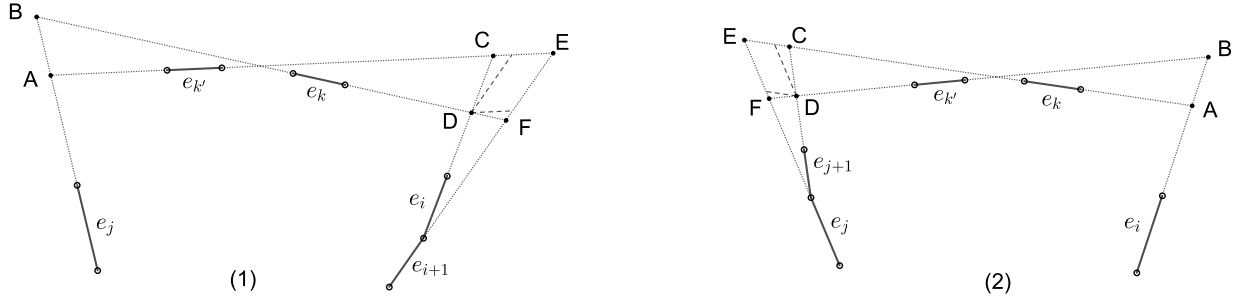


Figure 28: Illustration of Lemma 38

Proof. First, we prove $\text{opt}_{i+1,j} \geq \text{opt}_{i,j}$. Suppose to the opposite that $\text{opt}_{i+1,j} = k' < k = \text{opt}_{i,j}$, as shown in Figure 28 (1).

Because $\text{opt}_{i,j} = k > k'$, we know $|AB| + |BD| < |AC| + |CD|$.

Observe that $|CD| + |DF| < |CE| + |EF|$ by the triangle inequality (see dashed line).

Summing up, we get $|AB| + |BD| + |DF| < |AC| + |CE| + |EF|$; i.e., $|AB| + |BF| < |AE| + |EF|$; i.e. $\text{perimeter}(\triangle e_{i+1} e_j e_k) < \text{perimeter}(\triangle e_{i+1} e_j e_{k'})$, contradicting with $\text{opt}_{i+1,j} = k'$.

Next, we prove $\text{opt}_{i,j+1} \geq \text{opt}_{i,j}$. Suppose to the opposite that $\text{opt}_{i,j+1} = k' < k = \text{opt}_{i,j}$, as shown in Figure 28 (2).

Because $\text{opt}_{i,j} = k > k'$, we know $|AE| + |EF| < |AB| + |BF|$.

Observe that $|CD| + |DF| < |CE| + |EF|$ by the triangle inequality (see dashed line).

Summing up, $|AE| + |CD| + |DF| < |AB| + |BF| + |CE|$; i.e., $|AC| + |CD| < |AB| + |BD|$; i.e. $\text{perimeter}(\triangle e_i e_{j+1} e_k) < \text{perimeter}(\triangle e_i e_{j+1} e_{k'})$, contradicting with $\text{opt}_{i,j+1} = k'$. \square

Definition 39. We say e_i is *stable* in $\triangle e_i e_j e_k$ if $\text{perimeter}(\triangle e_i e_j e_k)$ cannot be reduced by changing e_i . We state that $\triangle e_i e_j e_k$ is a *3-stable triangle*, if e_i, e_j, e_k are all stable in $\triangle e_i e_j e_k$.

Lemma 40. *The 3-stable triangles are pairwise interleaving.*

Proof. Suppose $T_1 = \triangle e_i e_j e_k$ and $T_2 = \triangle e_r e_s e_t$ are 3-stable triangles that are not interleaving. As they are not interleaving, sets $\{e_i, e_j, e_k\}$ and $\{e_r, e_s, e_t\}$ share at most one common element. Therefore, there are two essentially different cases (as shown in Figure 29):

Case 1. $e_t, e_r, e_i, e_j, e_s, e_k$ are distinct and lie in clockwise order.

Case 2. $e_t, e_r, e_i, e_j = e_s, e_k$ are distinct and lie in clockwise order.

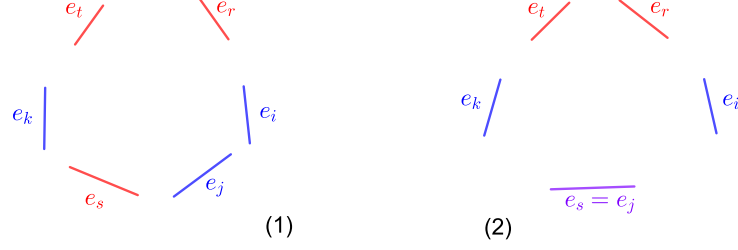


Figure 29: Illustration of the proof of Lemma 40

Because e_i is stable in $\triangle e_i e_j e_k$, we have $\text{perimeter}(\triangle e_i e_j e_k) \leq \text{perimeter}(\triangle e_r e_j e_k)$. This further implies that $\text{perimeter}(\triangle e_i e_s e_t) < \text{perimeter}(\triangle e_r e_s e_t)$. A proof of this implication is basically the same as the proof of the bi-monotonicity of $\text{opt}_{i,j}$ (Lemma 38) and is omitted.

As e_i is better than e_r for (e_s, e_t) , edge e_r is not stable in $\triangle e_r e_s e_t$. Contradiction. \square

6.2 Key lemmas for designing the killing function

Observation 41. Assume $e_c \prec e_a$. Assume e_b, e_{b+1} are chased by e_a and are chasing e_c . Circle O is tangent to ℓ_b, ℓ_{b+1} , and ℓ_c on the right of e_c and left of e_b, e_{b+1} ; see Figure 30.

$\text{perimeter}(\triangle e_a e_b e_c) = \text{perimeter}(\triangle e_a e_{b+1} e_c) \Leftrightarrow \ell_a$ is tangent to O .

$\text{perimeter}(\triangle e_a e_b e_c) < \text{perimeter}(\triangle e_a e_{b+1} e_c) \Leftrightarrow \ell_a$ is disjoint with O .

$\text{perimeter}(\triangle e_a e_b e_c) > \text{perimeter}(\triangle e_a e_{b+1} e_c) \Leftrightarrow \ell_a$ cuts O .

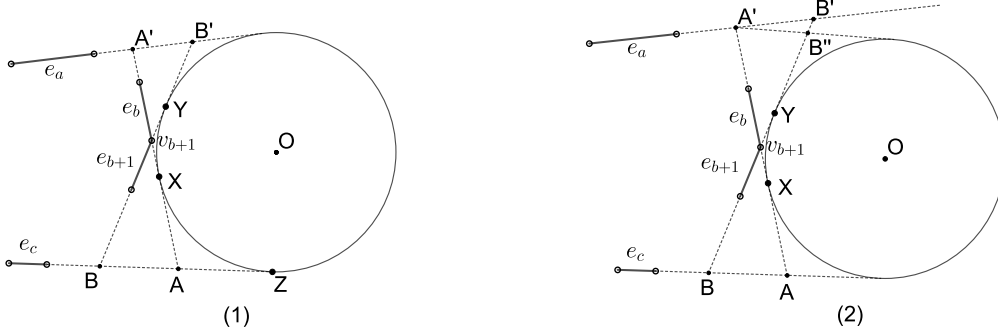


Figure 30: Illustration of the proof of Observation 41

Proof. First, assume that ℓ_a is tangent to O , as shown in Figure 30 (1).

Observe that $|BA| + |AX| = |BA| + |AZ| = |BZ| = |BY| = |Bv_{b+1}| + |Xv_{b+1}|$.

Therefore, $|BA| + |Av_{b+1}| = |BA| + |AX| + |Xv_{b+1}| = |Bv_{b+1}| + 2|Xv_{b+1}|$.

Therefore, $2|Xv_{b+1}| = |BA| + |Av_{b+1}| - |Bv_{b+1}|$. Similarly, $2|Yv_{b+1}| = |A'B'| + |B'v_{b+1}| - |A'v_{b+1}|$.

Further since $|Xv_{b+1}| = |Yv_{b+1}|$, we get $|BA| + |Av_{b+1}| - |Bv_{b+1}| = |A'B'| + |B'v_{b+1}| - |A'v_{b+1}|$. In other words, $|AB| + |AA'| = |A'B'| + |BB'|$, namely, $\text{perimeter}(\triangle e_a e_b e_c) = \text{perimeter}(\triangle e_a e_{b+1} e_c)$.

Next, assume that ℓ_a is disjoint with O , as shown in Figure 30 (2).

Make a tangent line of O at point A' (other than ℓ_b) and denote its intersection with ℓ_{b+1} by B'' . From the above analysis we have $|A'B''| + |BB''| = |AB| + |AA'|$. By the triangle inequality, we have $|A'B'| + |B'B''| > |A'B''|$. Therefore, $|A'B'| + |B'B| = |A'B'| + |B'B''| + |BB''| > |A'B''| + |BB''| = |AB| + |AA'|$. It follows that $\text{perimeter}(\triangle e_a e_b e_c) < \text{perimeter}(\triangle e_a e_{b+1} e_c)$.

Similarly, we get $\text{perimeter}(\triangle e_a e_b e_c) > \text{perimeter}(\triangle e_a e_{b+1} e_c)$ when ℓ_a cuts circle O . \square

Definition 42. For $b \neq c$, denote by $O_{b,c}$ the circle tangent to e_b, e_{b+1}, e_c on the right of e_c and on the left of e_b, e_{b+1} . (It is the circle O introduced in Observation 41; see Figure 30.)

Observation 43. Assume $e_b \prec e_{c+1}$ and assume that $e_b, e_{b+1}, \dots, e_{c+1}$ have at least five edges. See Figure 31. Consider any edge $e_a \in \{e_{c+2}, e_{c+3}, \dots, e_{b-1}\}$. We claim that

1. If ℓ_a intersects circle $O_{c,b+2}$, it also intersects circle $O_{c,b+1}$.
2. If ℓ_a intersects circle $O_{b+1,c}$, it also intersects circle $O_{b,c}$.

To be clear, “intersects” means “cuts or is tangent to”.

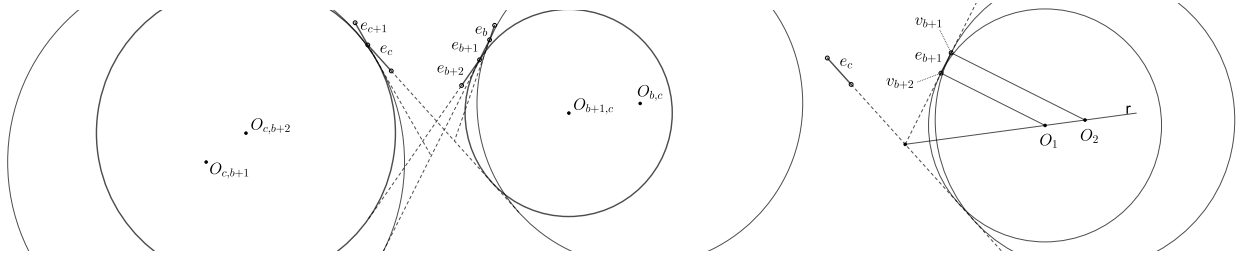


Figure 31: Illustration of the proof of Observation 43

Proof. The proof to the first claim is rather trivial, and can be obtained by slightly modifying the proof of Lemma 38 (the bi-monotonicity of opt); so we omit it.

To prove the second claim, we construct two auxiliary circles O_1, O_2 which are both tangent to ℓ_c and ℓ_{b+1} , as shown in the right part of Figure 31. Point O_1 is on the perpendicular line of ℓ_{b+1} at v_{b+2} , and point O_2 is on the perpendicular line of ℓ_{b+1} at v_{b+1} . We point out three facts:

- a. If ℓ_a intersects circle O_1 , it also intersects circle O_2 (trivial proof omitted).
- b. If ℓ_a intersects circle $O_{b+1,c}$, it also intersects circle O_1 .
- c. If ℓ_a intersects circle O_2 , it also intersects circle $O_{b,c}$.

Combine these three facts, we obtain the second claim of this lemma.

Denote by r the ray originating from the intersection of ℓ_{b+1} and ℓ_c and is toward O_1, O_2 . Imagine a process where e_{b+2} rotates in counterclockwise around v_{b+2} until it lies on ℓ_{b+1} . Point $O_{b+1,c}$ would move along r (get further from the origin of r) and arrive O_1 , which implies fact b.

The proof of fact c is similar to that of fact b (but rotate e_b around v_{b+1} in clockwise). \square

Lemma 44. Assume $e_b \prec e_{c+1}$ and $e_{b+1} \prec e_c$ as shown in Figure 32. We claim that

1. If $\triangle e_{b'} e_c e_a$ is 3-stable for some $e_{b'} \in \{e_{b+1}, \dots, e_{c-1}\}$ and $e_a \in \{e_{c+2}, \dots, e_{b-1}\}$, then ℓ_a intersects $O_{c,b+1}$ and $O_{b,c}$ (i.e. the two small circles in the figure).
2. If $\triangle e_b e_{c'} e_a$ is 3-stable for some $e_{c'} \in \{e_{c+1}, \dots, e_{b-1}\}$ and $e_a \in \{e_{c+2}, \dots, e_{b-1}\}$, then ℓ_a avoids $O_{b,c+1}$ and $O_{c,b}$ (i.e. the two big circles in the figure).

To be clear, “avoid” means “is disjoint with or tangent to”.

Proof of Claim 1. Suppose $\triangle e_{b'}e_ce_a$ is 3-stable.

Because e_c is stable in $\triangle e_{b'}e_ce_a$, $\text{perimeter}(\triangle e_{b'}e_ce_a) \leq \text{perimeter}(\triangle e_{b'}e_{c+1}e_a)$. Applying Observation 41, ℓ_a intersects $O_{c,b'}$. Applying Observation 43.1, ℓ_a also intersects $O_{c,b'-1}, \dots, O_{c,b+1}$.

Because $e_{b'}$ is stable in $\triangle e_{b'}e_ce_a$, $\text{perimeter}(\triangle e_{b'}e_ce_a) \leq \text{perimeter}(\triangle e_{b'-1}e_ce_a)$. Applying Observation 41, ℓ_a intersects $O_{b'-1,c}$. Applying Observation 43.2, ℓ_a also intersects $O_{b'-2,c}, \dots, O_{b,c}$. \square

Proof of Claim 2. Suppose $\triangle e_be_{c'}e_a$ is 3-stable.

Because e_b is stable in $\triangle e_be_{c'}e_a$, $\text{perimeter}(\triangle e_be_{c'}e_a) \leq \text{perimeter}(\triangle e_{b+1}e_{c'}e_a)$. Applying Observation 41, ℓ_a avoids $O_{b,c'}$. It follows (from an observation symmetric to Observation 43.1) that ℓ_a also avoids $O_{b,c'-1}, \dots, O_{b,c+1}$.

Because $e_{c'}$ is stable in $\triangle e_be_{c'}e_a$, $\text{perimeter}(\triangle e_be_{c'}e_a) \leq \text{perimeter}(\triangle e_be_{c'-1}e_a)$. Applying Observation 41, ℓ_a avoids $O_{c'-1,b}$. It follows (from an observation symmetric to Observation 43.2) that ℓ_a also avoids $O_{c'-2,b}, \dots, O_{c,b}$. \square

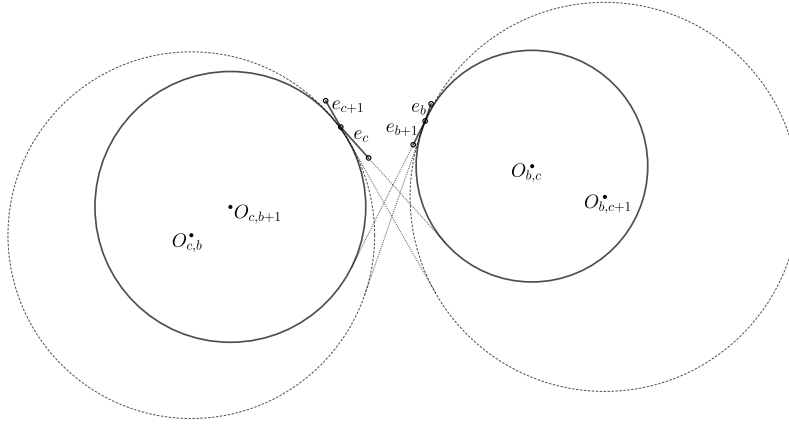


Figure 32: Illustration of two key lemmas: Lemma 44 and Lemma 45

We state that (e_i, e_j) is *dead* if there is no e_k such that $\triangle e_ie_je_k$ is 3-stable.

Lemma 45. Assume $e_b \prec e_{c+1}$ and $e_{b+1} \prec e_c$ as shown in Figure 32. We claim that

1. $(e_{b+1}, e_c), (e_{b+2}, e_c), \dots$ are dead if it holds that

$$\text{none of } \ell_{c+2}, \dots, \ell_{b-1} \text{ intersects } O_{c,b+1} \text{ and } O_{b,c}, \quad (8)$$

- and 2. $(e_b, e_{c+1}), (e_b, e_{c+2}), \dots$ are dead if it holds that

$$\text{none of } \ell_{c+2}, \dots, \ell_{b-1} \text{ avoids } O_{b,c+1} \text{ and } O_{c,b}. \quad (9)$$

Proof. 1. Suppose some $(e_{b'}, e_c)$ in the list $(e_{b+1}, e_c), \dots$ is not dead. Clearly, $e_{b'} \in \{e_{b+1}, \dots, e_{c-1}\}$.

Because $(e_{b'}, e_c)$ is not dead, there exists e_a such that $\triangle e_a e_{b'} e_c$ is 3-stable. Be aware that $e_c \prec e_a$. Therefore $e_a \in \{e_{c+1}, \dots, e_{b-1}\}$. Moreover, $e_a \prec e_{b'}$ and so $e_a \neq e_{c+1}$. Together, $e_a \in \{e_{c+2}, \dots, e_{b-1}\}$. Applying Lemma 44, ℓ_a intersects $O_{c,b+1}$ and $O_{b,c}$. Contradictory.

2. Suppose some $(e_b, e_{c'})$ in the list $(e_b, e_{c+1}), \dots$ is not dead. Clearly, $e_{c'} \in \{e_{c+1}, \dots, e_{b-1}\}$.

Because $(e_b, e_{c'})$ is not dead, there exists $\triangle e_a e_b e_{c'}$ which is 3-stable. Clearly, $e_a \in \{e_{c'+1}, \dots, e_{b-1}\}$ and hence $e_a \in \{e_{c+2}, \dots, e_{b-1}\}$. Applying Lemma 44, ℓ_a avoids $O_{b,c+1}$ and $O_{c,b}$. Contradictory. \square

Remark 2. To continue, we may try the strategy used in subsection 3.1: Define a common tangent of circles $O_{b,c}$, $O_{c,b}$, and a common tangent of circles $O_{b,c+1}$, $O_{c,b+1}$, and find a line l whose angle is between these two tangent lines and moreover, use the relation between l and P to determine that (8) or (9) holds. This is correct but we are not able to determine the relation between l and P in amortized $O(1)$ time. To determine the relation in such time, we must prove a monotonicity of the angles resembling the one given in Observation 20, but such a monotonicity does not hold here.

6.3 Designing an efficient killing functions

We state that (e_i, e_j) is *DEAD*, if there is no e_k such that $\triangle e_i e_j e_k$ has the minimum perimeter among all the all-flush triangles. Note that “dead” implies “DEAD”, but the reverse is false.

Lemma 46. Assume $e_b \prec e_{c+1}$ and $e_{b+1} \prec e_c$. See Figure 33. Denote by $g_{b,c}$ the common tangent of circles $O_{c,b}$, $O_{b,c+1}$ (that intersects the ray $\overrightarrow{v_c v_{c+1}}$). Denote by $h_{b,c}$ the common tangent of circles $O_{b,c}$, $O_{c,b+1}$ (that intersects the ray $\overrightarrow{v_c v_{c+1}}$). Denote $a = \text{opt}_{b,c}$. We claim that

1. If e_a is not (entirely) below line $h_{b,c}$, pairs $(e_{b+1}, e_c), (e_{b+2}, e_c), \dots$ are dead.
 2. If e_a is (entirely) below line $h_{b,c}$, pairs $(e_b, e_{c+1}), (e_b, e_{c+2}), \dots$ are DEAD.
- (In fact, we conjecture that these pairs are also dead. Yet we have no clue how to prove it.)

Following this lemma, we obtain the following killing function which is similar to (1).

$$\text{Kill}_p(b, c) = 'b' \text{ if } e_a \text{ is below } h_{b,c}, \text{ and } \text{Kill}_p(b, c) = 'c' \text{ otherwise.} \quad (10)$$

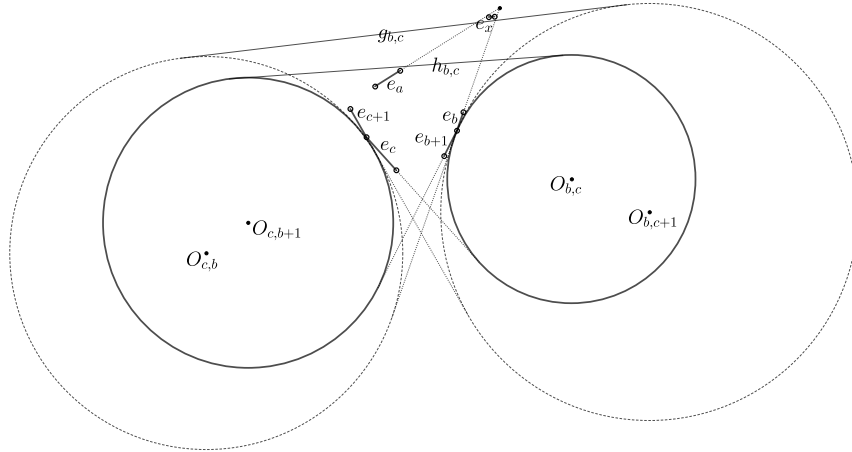


Figure 33: Illustration of our killing function

Proof of Claim 1. If e_a is not (entirely) below line $h_{b,c}$, none of $\ell_{c+2}, \dots, \ell_{b-1}$ can intersect both $O_{c,b+1}$ and $O_{b,c}$ (otherwise the convex polygon P is entirely below $h_{b,c}$ and so as e_a). It follows that $(e_{b+1}, e_c), (e_{b+2}, e_c), \dots$ are dead according to Lemma 45 claim 1. \square

We now proceed to the proof of Claim 2.

When e_a is below $h_{b,c}$, there could be some ℓ_x in $\{\ell_{c+2}, \dots, \ell_{b-1}\}$ which avoids $O_{b,c+1}$ and $O_{c,b}$; see Figure 33. So, condition (9) does not hold and hence we cannot apply Lemma 45 claim 2 directly. However, we can show that even if there is ℓ_x as mentioned above, $\triangle e_b e_{c'} e_x$ cannot be the minimum perimeter all-flush triangle for $e_{c'} \in \{e_{c+1}, \dots, e_{b-1}\}$, as $\triangle e_b e_c e_a$ has a smaller perimeter.

We state three inequalities for $\ell_x \in \{\ell_{c+2}, \dots, \ell_{b-1}\}$ that avoids circles $O_{b,c+1}$ and $O_{c,b}$.

$$\text{perimeter}(\triangle e_a e_b e_c) < \text{perimeter}(\triangle g e_b e_c), \quad (11)$$

$$\text{perimeter}(\triangle g e_b e_c) \leq \text{perimeter}(\triangle g e_b e_{c'}), \quad (12)$$

$$\text{perimeter}(\triangle g e_b e_{c'}) \leq \text{perimeter}(\triangle e_x e_b e_{c'}), \quad (13)$$

where g is short for $g_{b,c}$. Combining these inequalities, we prove Claim 2 as follows.

Proof of Claim 2. Suppose some pair $(e_b, e_{c'})$ in the list $(e_b, e_{c+1}), \dots$ is not DEAD. This means there is $\triangle e_x e_b e_{c'}$ which is (one of) the globally minimum solution (and hence is 3-stable). Clearly, $e_x \in \{e_{c'+1}, \dots, e_{b-1}\}$ and hence $e_x \in \{e_{c+2}, \dots, e_{b-1}\}$, whereas $e_{c'} \in \{e_{c+1}, \dots, e_{b-1}\}$. Applying Lemma 44, ℓ_x avoids $O_{b,c+1}$ and $O_{c,b}$. Then, applying the inequalities (11)-(13) above, $\text{perimeter}(\triangle e_a e_b e_c) < \text{perimeter}(\triangle e_x e_b e_{c'})$. So $\triangle e_x e_b e_{c'}$ is not the minimum. Contradiction. \square

Proof of (12). Since g is tangent to circle $O_{c,b}$, $\text{perimeter}(\triangle g e_b e_c) = \text{perimeter}(\triangle g e_b e_{c+1})$ due to Observation 41. By the unimodality of the perimeters (Lemma 36), $\text{perimeter}(\triangle g e_b e_c) = \text{perimeter}(\triangle g e_b e_{c+1}) < \text{perimeter}(\triangle g e_b e_{c+2}) < \dots$, which implies (12). \square

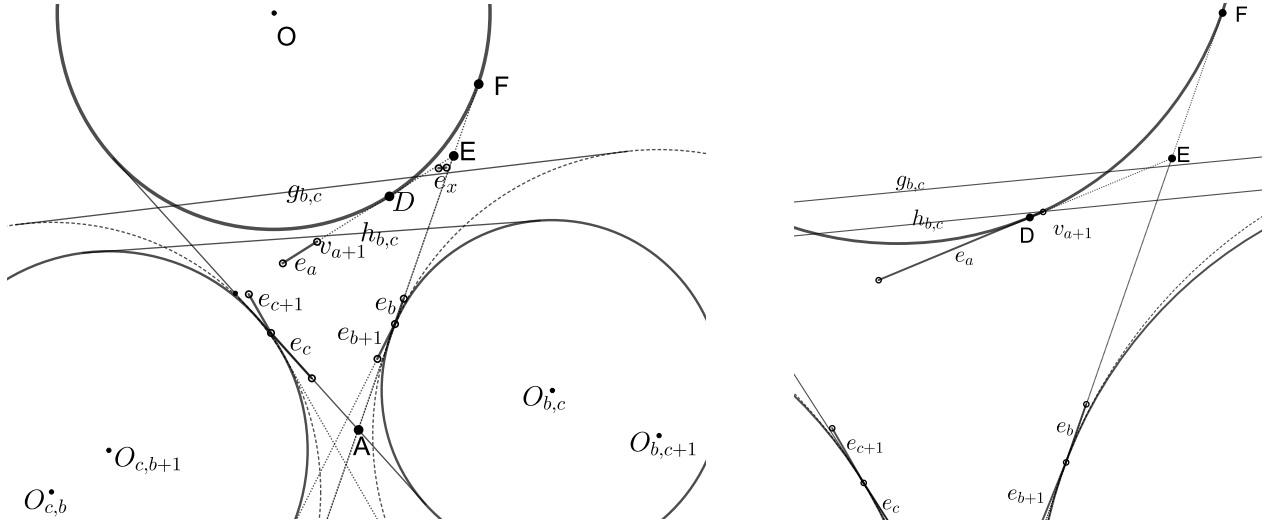


Figure 34: Illustration of the proof of (11)

Proof of (11). Construct a circle O tangent to ℓ_b, ℓ_c , and ℓ_a , on the right of e_b, e_c and the left of e_a ; see Figure 34. Applying Observation 32, it reduces to proving that line g cuts circle O . This further reduces to proving that O contains a point above g and a point below g .

Denote by D the tangent point of ℓ_a and circle O . Denote by F the tangent point of ℓ_b and circle O . As O contains D and F , it suffices to show that (i) F is above g and (ii) D is below g .

Proof of (i): Because ℓ_x avoids circles $O_{b,c+1}$ and $O_{c,b}$, edge e_x is above g . This means that the intersection of ℓ_a and ℓ_b , denoted by E , must be above g . Further since E lies on ℓ_a whereas circle O (including point F) is on the left of e_a , we see that F must also be above g .

Proof of (ii): Dividing ℓ_a at v_{a+1} returns two rays, one of which intersects ℓ_b ; denote it by r . We first show that D does not lie in r . Suppose to the opposite that D lies in r , as shown in the left part of Figure 34. Obviously, ℓ_{a+1} must be disjoint with circle O , which implies that

$\text{perimeter}(\triangle e_b e_c e_{a+1}) < \text{perimeter}(\triangle e_b e_c e_a)$ due to Observation 32, contradicting with $a = \text{opt}_{b,c}$. Therefore, D must lie in the ray at v_{a+1} toward v_a , as shown in the right part of Figure 34. Applying the assumption that e_a lies below $h_{b,c}$ whereas the intersection E is above g (proved above), the ray at v_{a+1} toward v_a , which contains point D , is below $h_{b,c}$. It follows that D is below g . \square

Proof of (13). If e_x is parallel to g , the inequality is trivial. Otherwise, there are two cases:

Case 1: v_x is closer to g than v_{x+1} , as shown in the left part of Figure 35. Denote by O' the circle tangent to $g, \ell_{c'}$, and ℓ_b (above g and on the right of $e_b, e_{c'}$). Build two parallel lines t, t' of e_x tangent to $O', O_{b,c+1}$ respectively. Since (1) v_x is closer to g than v_{x+1} and (2) $e_x \prec e_b$, extreme positions for t are ℓ_b and g . It follows that t intersects $O_{c,b}$. Similarly, t' also intersects $O_{c,b}$. So, all lines parallel to e_x between t and t' intersects $O_{c,b}$. Further since ℓ_x avoids $O_{c,b}$ and $O_{b,c+1}$, ℓ_x is above t , which implies that $\text{perimeter}(\triangle e_b e_{c'} g) < \text{perimeter}(\triangle e_b e_{c'} e_x)$ due to Observation 32.

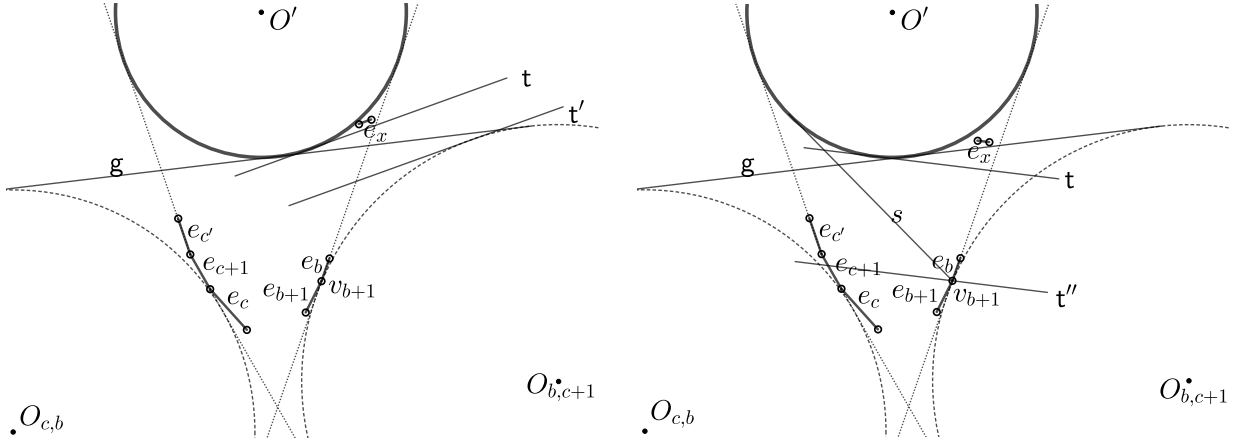


Figure 35: Illustration of the proof of (13)

Case 2: v_{x+1} is closer to g than v_x , as shown in the right part of Figure 35. Define O' and t the same as above. Denote by t'' the line at v_{b+1} which is parallel to e_x . Denote by s the tangent line of O' at v_{b+1} other than ℓ_b . Observe that s cuts circle $O_{b,c+1}$ (see Figure 36 for an easy illustration).

Imagine a line l rotates in clockwise around v_{b+1} , starting at the direction parallel to g . If l meets t'' later than s , line t'' has to cut O' . So, the parallel line ℓ_x of t'' (above t'') cuts or is above O' . If on the contrary l meets t'' earlier than s (as shown in the figure), t'' cuts $O_{b,c+1}$, and so does t , hence ℓ_x (which avoids $O_{b,c+1}$) can only be above t . In both subcases, it holds that ℓ_x cuts or is above O' . Applying Observation 32, this means $\text{perimeter}(\triangle e_b e_{c'} g) < \text{perimeter}(\triangle e_b e_{c'} e_x)$. \square

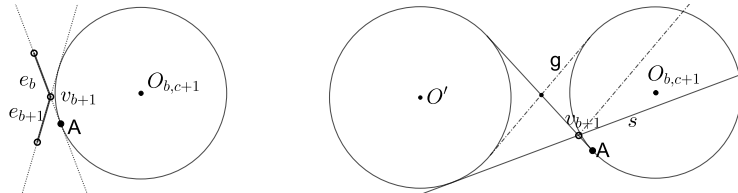


Figure 36: Illustration of an observation used in the proof of (13) (Case 2)

Remark 3. The proof of Lemma 46 is very similar to the proof of Lemma 6. Basically, for claim 1 it applies only the assumption that e_b, e_c (or, v_b, v_c in Lemma 6) are stable; but for claim 2 it applies the other assumption that e_a (or, v_a in Lemma 6) is stable as well.

7 Comparison of Alg-A to the previous Alg-CM and Alg-K

Outline of Alg-K [16]. Take any $\alpha \in [0, 2\pi)$. Kallus [16] proved that among those $\triangle ABC$ in which A, B, C lie in P 's boundary and $\theta[\overrightarrow{BC}] = \alpha$, there is a unique one with the maximum area, denoted by $T_\alpha = \triangle A_\alpha B_\alpha C_\alpha$. It is also proved that, when α increases, $A_\alpha, B_\alpha, C_\alpha$ will all move in clockwise around P 's boundary (non-strictly). Moreover, this rotating process of $A_\alpha, B_\alpha, C_\alpha$ can be simulated discretely; in $O(1)$ time we can jump from one “critical point” of $(\alpha, \triangle A_\alpha B_\alpha C_\alpha)$ to the next. Finally, the maximum area triangle can be found among $\{\triangle A_\alpha B_\alpha C_\alpha \mid \alpha \text{ is a critical point}\}$.

Outline of Alg-CM [8]. Chandran and Mount define the P -stable triangles (outside P) as follows. All sides of a P -stable triangle are touched by P . In particular, two of them (called *legs*) have their midpoints touched by P , whereas the remaining one is called the *base*. Moreover, one of the following holds: (1) The base is flushed with (i.e. contains an edge of) P . (2) One of the legs is flushed with an edge of P and has as its midpoint a vertex of this edge. See Figure 37 (a).

If such a triangle satisfies (1), it is called P -anchored. The P -anchored triangles were introduced earlier in [18], where it is proved that *they contain all the local minimums of enclosing triangles of P* . It is proved in [21] that the P -anchored triangles are “interspersing” (similar to interleaving). Using the Rotating-Caliper technique [26] with some clever algorithmic tricks, [21] computes the P -anchored triangles in linear time and thus find the minimum enclosing triangles.

Using some “more involved” (as said in [8]) observations, Chandran and Mount [8] compute all the P -stable triangles in linear time by the Rotating-Caliper technique, and show that *all the local maximums of triangles in P can be computed easily from P -stable triangles*. (It follows that Alg-CM computes all the maximum area triangles in P and all the minimum area triangles enclosing P .)

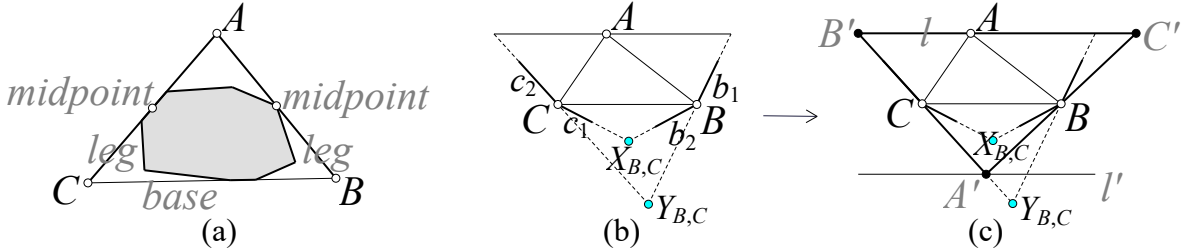


Figure 37: Equivalence between Alg-K and Alg-CM.

An equivalence between the triangles explored by the two algorithms. We find that the triangles explored by Alg-K are the same as the P -stable triangles explored by Alg-CM. Assume $T_\alpha = \triangle ABC$. See Figure 37 (b). Let b_1, b_2 be the two neighboring edges of B and c_1, c_2 be the two neighboring edges of C as shown in the figure. Assume the extended lines of b_2, c_1 intersect at point $X_{B,C}$ whereas the extended lines of b_1, c_2 intersect at point $Y_{B,C}$. Let $d(X)$ denote the distance from point X to \overrightarrow{BC} . It is easy to prove that the following are equivalent: (i) $\triangle ABC$ is the maximum area triangle with $\theta[\overrightarrow{BC}] = \alpha$; and (ii) $d(A) \in [d(X_{B,C}), d(Y_{B,C})]$ and A has the largest distance to \overrightarrow{BC} among all vertices on the right of \overrightarrow{BC} . As fact (i) holds, (ii) also holds. We now construct a triangle $\triangle A'B'C'$ outside P (see Figure 37 (c)). Let l be the line at A parallel to \overrightarrow{BC} and l' be its symmetric line with respect to \overrightarrow{BC} . Assume the extended line of c_2 intersects l, l' at points B', A' , respectively, and let C' be the symmetric point of A' with respect to B . Applying

fact (ii), P must be contained in $A'B'C'$, which implies that $A'B'C'$ is P -stable. Similarly, from a P -stable triangle $A'B'C'$, we can also construct $\triangle ABC$ satisfying (ii) and hence satisfying (i).

7.1 Experimental results

We implement Alg-A, Alg-K, and Alg-CM by *c++ programs*. The running times of these programs on seven randomly generated test cases are shown in Table 1, in which we also record the number of iterations required by each program. Download our implementations at GitHub [4]. **Our implementations of Alg-K and Alg-CM are based on comprehensive understanding of their algorithms, and the code optimizations in three programs are at the same level.**

	N	T(A)	T(K)	T(CM)	#(A)	#(K)	#(CM)
1	100035	0.0027	0.0157	0.0228	99878	455361	455178
2	1000000	0.0235	0.2001	0.2605	998511	4659599	4657908
3	1000000	0.0207	0.1673	0.2355	997681	4501969	4499593
4	999900	0.0241	0.2109	0.2950	998933	4658202	4657109
5	999900	0.0209	0.2110	0.2513	998203	5001147	4999500
6	1000000	0.0263	0.2319	0.2797	999673	4580226	4579936
7	1000000	0.0329	0.2283	0.2789	999968	4581191	4581150
Sum	6099835	0.1511	1.2652	1.6237	6092847	28437695	28430374

Table 1: A test on our implementations of Alg-A, Alg-K, and Alg-CM. In the table, symbol “T” denotes the running time, “#” denotes the number of iterations taken by the algorithm, and “N” denotes the total number of vertices in the test case (each test case consists of several polygons).

Running environment and experiment result. We run the experiment on Lenovo Notepad X1 Carbon (i7-8550U CPU, 8G RAM) with Win10 (64bit). We use VC++ compiler on release mode. (We also did an experiment using GCC compiler [4]. The result is similar.)

Our experiment shows that the running time of Alg-A is roughly **one eighth** of the running time of Alg-K, or **one tenth** of the running time of Alg-CM. (Moreover, the number of iterations required by Alg-CM and Alg-K is roughly **4.67** times that of Alg-A.)

On convex polygon generation. We generate all test cases in random. Specifically, three methods are applied: (1) Generate N random points in a disk and compute their convex hull. (Only test 1 is generated using this method) (2) Take n random points in an ellipse. (3) A clever and efficient method for generating convex polygons given in [29] (which is based on [27]).

Our seven test cases and our *C++ program* for generating them can be downloaded at [4]. Test 2 and Test 3 consist of 5000 polygons, each of which has 200 vertices; Test 4 and Test 5 consist of 3333 polygons, each of which has 300 vertices; Test 6 (Test 7, respectively) consists of 1000 (100, respectively) polygons, each of which has 1000 (10000, respectively) vertices.

As Alg-K and Alg-CM suffers from float issue, we give up polygons with > 10000 vertices.

Further notes. 1. We only calculate the time for computing the maximum area triangle and does not calculate the time for inputting the data. See *experiment.cpp* in [4]. 2. Theoretically, $\#(\text{Alg-K})$ equals $\#(\text{Alg-CM})$ (see last page). However, these two statistics are slightly different in our experiment; see Table 1. The difference is mainly due to the degenerate case (where a chord of P is parallel to an edge of P) and the float issue of both programs. Our implementations of Alg-K and Alg-CM have logical difference in handling degenerate cases.

7.2 A comparison of Alg-A, Alg-CM, and Alg-K

Alg-A has a smaller constant behind the asymptotic complexity $O(n)$ than others as mentioned in subsection 1.2.4. Moreover, Alg-A is more stable than the alternatives. During the iterations of Alg-CM, the coordinates of three corners and two midpoints of a P-stable triangle (see Figure 37) are maintained. These coordinates are computed somehow and their true values can differ from their values stored in the computer. Alg-CM uses an involved subroutine (far more complicated than ours given in Algorithm 1) to update the coordinates in each iteration, which accumulates the inaccuracy of coordinates. Even worse, this subroutine computes three angles and selects the smallest to decide how to proceed each time, and due to float issue it is possible to select a wrong angle when angles are close, which causes the subroutine performs incorrectly. The following comparison might be subjective, though we tried our best to be unbiased. (We refer the readers to a recent class note of Rote [22] for an excellent comparison from third-party.)

On difficulty of analysis. Comparing the description of the main part of Alg-A (the 7 lines in Algorithm 1) with that of Alg-CM (pages 9–10 of [8]), Alg-A is conceptually simpler. Alg-CM is claimed “involved” by its authors as it contains complicated subroutines for handling many subcases. Our proof is based on few prerequisite results – only the trivial pairwise interleaving property, whereas Alg-CM is built upon nontrivial results of [17, 18, 21].

On difficulty of implementation. We implement all the three known algorithms ² (see [4]). Alg-CM and Alg-K are respectively **3** times and **2** times longer in code length comparing to Alg-A. Implementing Alg-CM correctly is a real challenge and we spent roughly 4 to 5 days on doing this. The difficulties lies in: (1) degenerated cases are not discussed in [8] and (2) we have to put patches to the program multiple times to avoid all kinds of float issues.

²As far as we know, Alg-CM has not been implemented in history. An implementation of Alg-K was given by Kallus. However, to compare Alg-K with the other two alternatives, it is better to implement it by us instead of using the implementation of Kallus, so that the algorithms are implemented using similar programming techniques.

A Appendix

Note that in the following proof of Lemma 2, we apply Observation 21 stated in subsection 3.3.

Proof of the interleaving property stated in Lemma 2. The first claim is implied by the third, as 3-stable implies G-3-stable. So we only show the proof of claim 2 and claim 3.

2. Suppose $T_1 = \triangle e_i e_j e_k$ and $T_2 = \triangle e_r e_s e_t$ are F-3-stable triangles that are not interleaving. As they are not interleaving, sets $\{e_i, e_j, e_k\}$ and $\{e_r, e_s, e_t\}$ share at most one common element. First, consider the case where the two sets share one common edge, e.g., $e_j = e_s$. Without loss of generality, assume that $e_k, e_t, e_r, e_i, e_j = e_s$ are in clockwise order; see Figure 38 (a) (otherwise $e_t, e_k, e_i, e_r, e_j = e_s$ are in clockwise order and it is symmetric).

Because $\triangle e_i e_j e_k$ is F-3-stable, $\text{area}(\triangle e_i e_j e_k) \leq \text{area}(\triangle e_r e_j e_k)$. This implies that $\text{area}(\triangle e_i e_j e_t) < \text{area}(\triangle e_r e_j e_t)$ (due to Observation 21); i.e., $\text{area}(\triangle e_i e_s e_t) < \text{area}(\triangle e_r e_s e_t)$. It follows that e_r is not stable in $\triangle e_r e_s e_t$, which contradicts the assumption that $\triangle e_r e_s e_t$ is F-3-stable.

Second, consider the case where the above mentioned two sets share no common edges. In this case, since T_1 and T_2 are not interleaving, among $[v_{j+1} \cup v_k], [v_{k+1} \cup v_i]$ and $[v_{i+1} \cup v_j]$, there must be one boundary portion that contains no edge from $\{e_r, e_s, e_t\}$, whereas the others respectively contain one and two. (Note that e_r, e_s, e_t cannot be contained in the same portion. Otherwise $\triangle e_r e_s e_t$ is unbounded and hence not F-3-stable.) Without loss of generality, assume that $[v_{j+1} \cup v_k]$ and $[v_{k+1} \cup v_i]$ respectively contain $\{e_s\}$ and $\{e_t, e_r\}$, as shown in Figure 38 (b).

Because $\triangle e_i e_j e_k$ is F-3-stable, $\text{area}(\triangle e_i e_j e_k) \leq \text{area}(\triangle e_r e_j e_k)$. This implies that $\text{area}(\triangle e_i e_s e_k) < \text{area}(\triangle e_r e_s e_k)$ (due to Observation 21). To be rigorous, check that $\text{area}(\triangle e_i e_s e_k)$ is finite. This holds because $e_i \prec e_s$ (since $e_r \prec e_s$) and $e_s \prec e_k$ (since $e_s \prec e_t$) and $e_k \prec e_i$. Furthermore, it follows that $\text{area}(\triangle e_i e_s e_t) < \text{area}(\triangle e_r e_s e_t)$ (due to Observation 21 again). To be rigorous, check that $\text{area}(\triangle e_i e_s e_t)$ is finite. This holds because $e_i \prec e_s$ (since $e_r \prec e_s$) and $e_s \prec e_t$ and $e_t \prec e_i$ (since $e_k \prec e_i$). It follows that e_r is not stable in $\triangle e_r e_s e_t$, which contradicts the F-3-stable assumption.

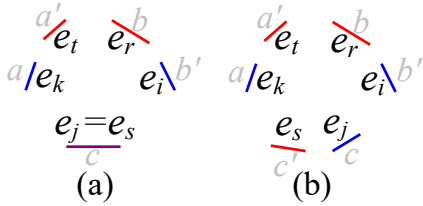


Figure 38: Proof of Lemma 2 part 2.

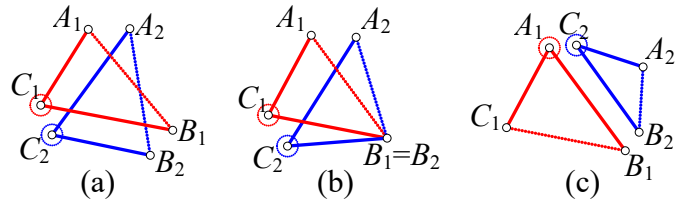


Figure 39: Proof of Lemma 2 part 3.

3. It reduces to showing that for any two triangles $\triangle A_1 B_1 C_1, \triangle A_2 B_2 C_2$ (with corners lying in ∂P) that do not interleave, at most one of them is G-3-stable. When the two triangles do not interleave, there are only three essentially different cases as shown in Figure 39:

Case 1. $A_1, A_2, B_1, B_2, C_2, C_1$ are different and lie in this order around ∂P . See Figure 39 (a). As $A_1 B_1$ intersects $A_2 B_2$, at most one of the following holds: (i) C_1 is stable in $\triangle A_1 B_1 C_1$; (ii) C_2 is stable in $\triangle A_2 B_2 C_2$. This means at most one of the two triangles is G-3-stable.

Case 2. $A_1, A_2, B_1, B_2, C_2, C_1$ lie in this order around ∂P and are distinct except $B_1 = B_2$. See Figure 39 (b). The proof of this case is the same as above.

Case 3. $C_1, A_1, C_2, A_2, B_2, B_1$ lie in this order around ∂P and are distinct or are distinct except that $B_1 = B_2$. See Figure 39 (c). At most one of the following holds: (i) A_1 is stable in $\triangle A_1 B_1 C_1$; (ii) C_2 is stable in $\triangle A_2 B_2 C_2$. This means at most one of the two triangles is G-3-stable. \square

Proof of Corollary 3. Assume the number of F-3-stable triangles is m . By Lemma 2, the F-3-stable triangles can be represented as $\triangle e_{a_1} e_{b_1} e_{c_1}, \dots, \triangle e_{a_m} e_{b_m} e_{c_m}$ where $e_{a_1}, \dots, e_{a_m}, e_{b_1}, \dots, e_{b_m}, e_{c_1}, \dots, e_{c_m}$ lie in clockwise order (in the non-strictly manner as in defining interleaving).

For each i ($1 \leq i \leq m$), denote δ_i to be

$$|\{a_1, a_1 + 1, \dots, a_i\}| + |\{b_1, b_1 + 1, \dots, b_i\}| + |\{c_1, c_1 + 1, \dots, c_i\}|,$$

where $|\cdot|$ indicates the size of the set here. We know $3 \leq \delta_1 < \delta_2 < \dots < \delta_m < n + 3$ and this means that $m \leq n$. Similarly, the number of 3-stable triangles is at most n . \square

A.1 An example of the Rotate-and-Kill process

Figure 40 demonstrates the Rotate-and-Kill process given in Algorithm 5.

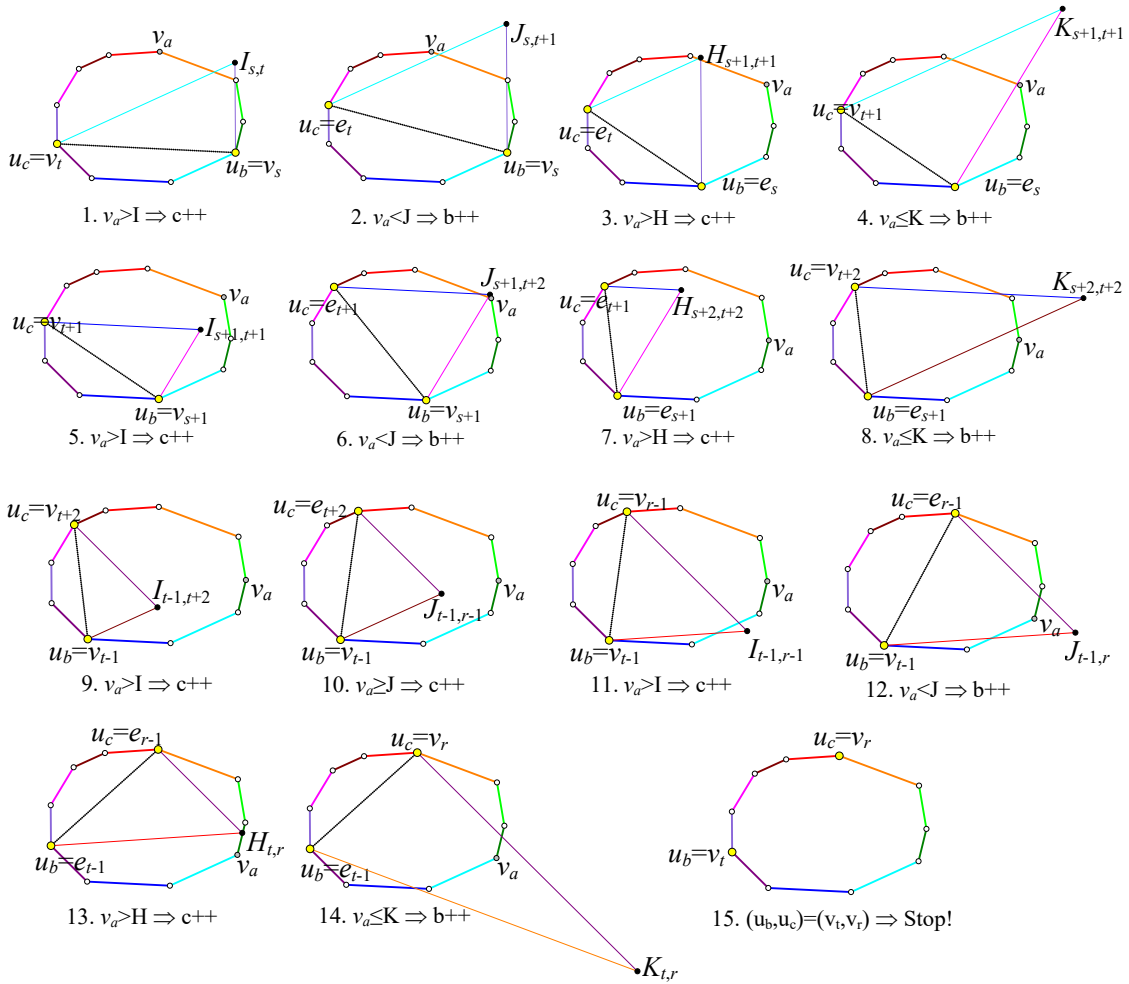


Figure 40: A demonstration of the Rotate-and-Kill process given in Algorithm 5.

A.2 Alg-DS may fail to find any 3-stable triangle

Suppose P is a regular hexagon, see Figure 41. Initially, Alg-DS visits $\triangle v_a v_b v_c = \triangle v_1 v_2 v_3$. See part (a) in the figure. Next, it increases c by 1 and visits $\triangle v_1 v_2 v_4$, because v_4 is better than v_3

when the other two corners are at v_1, v_2 . See (b). Now c can no longer be improved, so as b , and thus Alg-DS increases a by 1 and visits $\triangle v_2 v_3 v_4$, and $\triangle v_2 v_3 v_5$ subsequently. See (c) and (d). So on and so forth, it visits twelve triangles: $\triangle v_i v_{i+1} v_{i+2}$ and $\triangle v_i v_{i+1} v_{i+3}$ for each $i \in \{1, \dots, 6\}$. However, none of them are 3-stable. Instead, $\triangle v_i v_{i+2} v_{i+4}$ for $i \in \{1, \dots, 6\}$ are 3-stable. See (e).

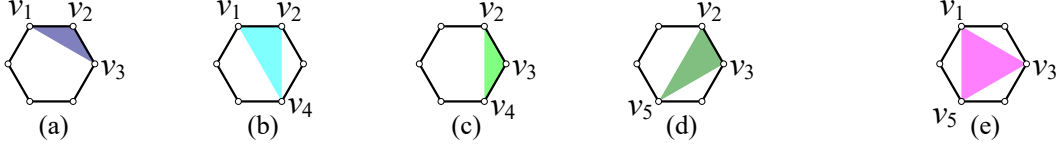


Figure 41: Algorithm of Dobkin and Snyder fails to find one 3-stable triangle.

Acknowledgement. We are sincerely grateful for Professor Zhiyi Huang, who took part in fruitful discussions.

References

- [1] A. Aggarwal, M. M. Klawe, S. Moran, P. Shor, and R. Wilber. Geometric applications of a matrix-searching algorithm. *Algorithmica*, 2(1-4):195–208, 1987.
- [2] A. Aggarwal and J. Park. Notes on searching in multidimensional monotone arrays. In *29th Symposium on Foundations of Computer Science*, pages 497–512, 1988. doi:10.1109/SFCS.1988.21966.
- [3] A. Aggarwal, B. Schieber, and T. Tokuyama. Finding a minimum-weight k -link path in graphs with the concave monge property and applications. *Discrete & Computational Geometry*, 12(1):263–280, 1994.
- [4] Anonymity. Implementation of three algorithms for finding the maximum area triangle in a convex polygon. <https://github.com/quantumTuringMachine/Rotate-and-Kill/>, 2021. [Online; accessed 12-July-2022].
- [5] B. Bhattacharya and A. Mukhopadhyay. *On the Minimum Perimeter Triangle Enclosing a Convex Polygon*, pages 84–96. Springer Berlin Heidelberg, 2003. doi:10.1007/978-3-540-44400-8_9.
- [6] J. E. Boyce, D. P. Dobkin, R. L. (Scot) Drysdale, III, and L. J. Guibas. Finding extremal polygons. In *14th Symposium on Theory of Computing*, pages 282–289, 1982.
- [7] P. Brass and H. Na. Finding the maximum bounded intersection of k out of n halfplanes. *Information Processing Letters*, 110(3):113 – 115, 2010.
- [8] S. Chandran and D. M. Mount. A parallel algorithm for enclosed and enclosing triangles. *International Journal of Computational Geometry & Applications*, 02(02):191–214, 1992. doi:10.1142/S0218195992000123.
- [9] J. S. Chang and C. K. Yap. A polynomial solution for potato-peeling and other polygon inclusion and enclosure problems. In *25th Symposium on Foundations of Computer Science*, pages 408–416, 1984. doi:10.1109/SFCS.1984.715942.

- [10] H.S. Chew and L.E. Holloway. Approximating state sets using circumscribing polyhedron with fewer facets. In *IEEE Southeastcon'99: Technology on the Brink of 2000*, pages 14–20, 1999.
- [11] D. P. Dobkin and L. Snyder. On a general method for maximizing and minimizing among certain geometric problems. In *20th Symposium on Foundations of Computer Science*, pages 9–17, Oct 1979. doi:10.1109/SFCS.1979.28.
- [12] R. Fleischer, K. Mehlhorn, G. Rote, E. Welzl, and C. Yap. Simultaneous inner and outer approximation of shapes. *Algorithmica*, pages 8:365–389, 1992.
- [13] M.J. Fonseca, A. Ferreira, and J.A Jorge. Generic shape classification for retrieval. In *Graphics Recognition. Ten Years Review and Future Perspectives (GREC'05)*, pages 291–299, 2006.
- [14] C. Gotsman and M. Werman. Recognition of affine planar curves using geometric properties. In *Shape in Picture. NATO ASI Series (Computer and Systems Sciences)*, 1994.
- [15] K. Jin. Maximal parallelograms in convex polygons - a novel geometric structure. *CoRR*, abs/1512.03897, 2015. URL: <http://arxiv.org/abs/1512.03897>.
- [16] Y. Kallus. A linear-time algorithm for the maximum-area inscribed triangle in a convex polygon. *CoRR*, abs/1706.03049, 2017. URL: <http://arxiv.org/abs/1706.03049>.
- [17] V. Klee. Facet centroids and volume minimization. *Studia Scientiarum Mathematicarum Hungarica*, 21:143–147, 1986.
- [18] V. Klee and M. C. Laskowski. Finding the smallest triangles containing a given convex polygon. *Journal of Algorithms*, 6(3):359 – 375, 1985. doi:10.1016/0196-6774(85)90005-7.
- [19] E. A. Melissaratos and D. L. Souvaine. Shortest paths help solve geometric optimization problems in planar regions. *SIAM Journal on Computing*, 21(4):601–638, 1992. doi:10.1137/0221038.
- [20] J. S. B. Mitchell and V. Polishchuk. Minimum-perimeter enclosures. *Information Processing Letters*, 107(3):120–124, 2008. doi:10.1016/j.ipl.2008.02.007.
- [21] J. O'Rourke, A. Aggarwal, S. Maddila, and M. Baldwin. An optimal algorithm for finding minimal enclosing triangles. *Journal of Algorithms*, 7(2):258 – 269, 1986. doi:http://dx.doi.org/10.1016/0196-6774(86)90007-6.
- [22] Günter Rote. The largest inscribed triangle and the smallest circumscribed triangle of a convex polygon: An overview of linear-time algorithms. <https://mycampus.imp.fu-berlin.de/x/w77mPE>, 2019. [Online; accessed 6-July-2020].
- [23] B. Schieber. Computing a minimum-weight k -link path in graphs with the concave monge property. In *6th Symposium on Discrete Algorithms*, pages 405–411. Society for Industrial and Applied Mathematics, 1995.
- [24] M.I. Shamos. *Computational geometry (PhD. Dissertation)*. Yale University, 1978.
- [25] A. Spillner, B.T. Nguyen, and V. Moulton. Computing phylogenetic diversity for split systems. *Transactions on Computational Biology and Bioinformatics*, 5(2):235–244, 2008.
- [26] G. Toussaint. Solving geometric problems with the rotating calipers. In *IEEE MELECON'83*, pages 10–02, 1983.

- [27] P. Valtr. Probability thatn random points are in convex position. *Discrete & Computational Geometry*, 13:637–643, 1995. doi:10.1007/BF02574070.
- [28] I. van der Hoog, V. Keikha, M Löffler, A. Mohades, and J. Urhausen. Maximum-area triangle in a convex polygon, revisited. *Information Processing Letters*, 161:105943, 2020. doi:10.1016/j.ip1.2020.105943.
- [29] S. Verdonschot. Generating random convex polygons. <https://cglab.ca/~sander/misc/ConvexGeneration/convex.html>, 2017. [Online; accessed 6-July-2020].
- [30] F. Vivien and N. Wicker. Minimal enclosing parallelepiped in 3d. *Computational Geometry*, 29(3):177–190, 2004. doi:10.1016/j.comgeo.2004.01.009.
- [31] Y. Zhou and S. Suri. Algorithms for a minimum volume enclosing simplex in three dimensions. *SIAM Journal on Computing*, 31(5):1339–1357, 2002. doi:10.1137/S0097539799363992.